ÇUKUROVA UNIVERSITY
INSTITUTE OF NATURAL AND APPLIED SCIENCES

PhD. THESIS

Serdar ŞAHİN

INVESTIGATION OF WAKE FLOW CHARACTERISTICS OF A SPLITTER PLATE WITH DIFFERENT POROSITY BEHIND A VERTICAL CYLINDER

DEPARTMENT OF MECHANICAL ENGINEERING

ADANA-2019

ÇUKUROVA UNIVERSITY
INSTITUTE OF NATURAL AND APPLIED SCIENCE

INVESTIGATION OF WAKE FLOW CHRACTERISTICS OF A SPLITTER PLATE WITH DIFFERENT PROSITY BEHIND A VERTICAL CYLINDER

Serdar ŞAHİN

PhD THESIS

DEPARTMENT OF MECHANICAL ENGINEERING

We certify that the thesis titled above was reviewed and approved for the award of degree of the Doctor of Philosophy by the board of jury on …/…/20….

…………………	…………………	…………………
Prof. Dr. Hüseyin AKILLI	Prof. Dr. Beşir ŞAHİN	Prof. Dr. Erol ARCAKLIOĞLU
SUPERVISOR	MEMBER	MEMBER
…………………	…………………	
Dr.Ögr.Üyesi Bengi ŞANLI	Dr.Ögr.Üyesi Tahir DURHASAN	
MEMBER	MEMBER	

This PhD Thesis was prepared in Mechanical Engineering Department of the Institute of Natural and Applied Science of Çukurova University.
Registration Number:

Prof. Dr. Mustafa GÖK
Director
Institute of Natural and Applied Science

ABSTRACT

Ph.D. THESIS

INVESTIGATION OF WAKE FLOW CHARACTERISTICS OF A SPLITTER PLATE WITH DIFFERENT POROSITY BEHIND A VERTICAL CYLINDER.

Serdar ŞAHİN

ÇUKUROVA UNIVERSITY
INSTITUTE OF NATURAL AND APPLIED SCIENCE
DEPARTMENT OF MECHANICAL ENGINEERING

Supervisor : Prof. Dr. Hüseyin AKILLI
Year 2019, Pages: 121
Jury : Prof. Dr. Beşir ŞAHİN
: Prof. Dr. Erol ARCAKLIOĞLU
: Assoc. Prof. Dr. Bengi ŞANLI
: Assoc. Prof. Dr. Tahir DURHASAN

Researcher studies on flow over bluff bodies for understanding wake flow physic and the cylinders are widely used for experiments due to their basic geometry and large number of technical applications like heat exchanger tubes, cooling systems for nuclear power plants, power transmission lines, chimney stacks, bridges, buildings, radio telescopes, power lines, offshore drilling rigs, underwater pipelines, marine cables etc.

Submerged hydrodynamics is a general term used to describe the hydrodynamics of floating or stationary structures that cause flow separation. A continuous flow causes periodic vortex fluctuations around the sinking object. When the vortex fluctuates behind the object, the drag force on the object increases and periodic forces are generated perpendicular to the flow direction on the object. These periodic forces cause structural vibrations and acoustic noise or resonance. At the same time vortexes increases the mixing behind the flow and in this way, the heat transfer also increases.

Learning to control the vortex fluctuations can reduce the noise level by increasing energy efficiency. In this study, it is aimed to examine passive flow behind the cylinder passively with different permeability separator plates, using particle imaged velocity measurement (PIV) technique. Experiments have been carried out at Cukurova University, Mechanical Engineering Department, Fluid Mechanics Laboratories. According to the results obtained, the effects of the permeability ratio β, the separator plate length, the distance between the plate cylinder and the separator plate cylinder axis, the effects on the vortex formation behind the cylinder and the turbulence statistics of the flow (Turbulence Kinetic Energy) have been revealed.

Keywords: PIV, Fluid, Splitter Plate, Porosity, Turbulence Kinetic Energy, TKE

ÖZ

DOKTORA TEZİ

DEĞİŞİK GEÇİRGENLİKLİ AYIRICI PLAKANIN DİKEY SİLİNDİR ARDIL AKIŞA ETKİSİNİN İNCELENMESİ

Serdar ŞAHİN

ÇUKUROVA ÜNİVERSİTESİ
FEN BİLİMLERİ ENSTİTÜSÜ
MAKİNE MÜHENDİSLİĞİ ANABİLİM DALI

Danışman: : Prof. Dr. Hüseyin AKILLI
Yıl 2019, Sayfa: 121
Jüri: : Prof. Dr. Beşir ŞAHİN
: Prof. Dr. Erol ARCAKLIOĞLU
: Dr.Ögr.Üyesi Bengi ŞANLI
: Dr.Ögr.Üyesi Tahir DURHASAN

Araştırmacılar, batmış küt cisimlerin ardıl akışlarının özelliklerini anlamak için çeşitli çalışmalar yürütmekte ve bu çalışmalarında basit geometrileri ve ısıl değiştiriciler, nükleer santrallerin soğutma sistemleri, güç aktarım hatları, bacalar, köprüler, radyo teleskopları, enerji nakil hatları, açık deniz petrol platformları, sualtı boru hatları, denizaltı kabloları gibi birçok farklı kullanım hattı olmasında ötürü, genellikle silindirler kullanmaktadırlar.

Batmış cisim hidrodinamiği, akış ayrışmasına sebep olan yüzen veya sabit yapılarının hidrodinamiğini anlatmak için kullanılan genel bir tanımdır. Sürekli bir akış, batmış cisim etrafında periyodik girdap dalgalanmalarına sebep olur. Cisim arkasında girdap dalgalanması olduğu vakit, cisim üzerindeki sürükleme kuvveti artar ve cisim üzerinde akış yönüne dik yönde periyodik kuvvetler oluşur. Bu periyodik kuvvetler yapısal titreşimlere ve akustik gürültüye veya rezonansa sebep olur. Girdap dalgalanması aynı zamanda akış ardındaki karışmayı artırır ve bu yolla ısı transferi de artar.

Girdap dalgalanmasını kontrol edebilmeyi öğrenmek, enerji verimliliğini artırarak, gürültü seviyesini düşürebilir. Bu çalışmada, silindir ardındaki daimî olmayan akışın, değişik geçirgenlikli ayırıcı plakalarla edilgen bir şekilde kontrolünün, parçacık görüntülemeli hız ölçme (PIV) tekniği kullanılarak incelenmesi amaçlanmaktadır. Deneyler, Çukurova Üniversitesi, Makine Mühendisliği Bölümü, Akışkanlar Mekaniği Laboratuvarlarında gerçekleştirilmiştir. Elde edilen sonuçlara göre, geçirgenlik oranı *β'nın*, ayırıcı plaka uzunluğunun, plaka silindir arasındaki mesafenin ve ayırıcı plakanın silindir ekseniyle yaptığı açının, silindir ardındaki girdap oluşumu üzerindeki etkileri ve akışın türbülans istatistikleri (Türbülans Kinetik Enerji) ortaya çıkartılmıştır.

Anahtar Kelimeler: PIV, Akışkan, Ayrıcı Plaka, Geçirgenlik, Türbülans Kinetik Enerji, TKE

EXTENDED ABSTRACT

Researcher studies on flow over bluff bodies for understanding wake flow physic and the cylinders are widely used for experiments due to their basic geometry and large number of technical applications like heat exchanger tubes, cooling systems for nuclear power plants, power transmission lines, chimney stacks, bridges, buildings, radio telescopes, power lines, offshore drilling rigs, underwater pipelines, marine cables etc.

Submerged hydrodynamics is a general term used to describe the hydrodynamics of floating or stationary structures that cause flow separation. A continuous flow causes periodic vortex fluctuations around the sinking object. When the vortex fluctuates behind the object, the drag force on the object increases and periodic forces are generated perpendicular to the flow direction on the object. These periodic forces cause structural vibrations and acoustic noise or resonance. At the same time vortexes increases the mixing behind the flow and in this way, the heat transfer also increases.

Learning to control the vortex fluctuations can reduce the noise level by increasing energy efficiency. In this study, it is aimed to examine passive flow behind the cylinder passively with different permeability separator plates, using particle imaged velocity measurement (PIV) technique. Experiments have been carried out at Cukurova University, Mechanical Engineering Department, Fluid Mechanics Laboratories. According to the results obtained, the effects of the permeability ratio β, the separator plate length, the distance between the plate cylinder and the separator plate cylinder axis, the effects on the vortex formation behind the cylinder and the turbulence statistics of the flow (Turbulence Kinetic Energy) have been revealed.

In fluid dynamics, turbulence kinetic energy (TKE) is the mean kinetic energy per unit mass associated with eddies in a turbulent flow. Physically, the turbulence kinetic energy is characterized by measured root-mean-square (RMS) velocity fluctuations. TKE can be produced by fluid shear, friction or buoyancy, or through external forcing at low-frequency eddy scales. Turbulence kinetic energy is then transferred down the turbulence energy cascade and is dissipated by viscous forces at the Kolmogorov scale. The value of TKE directly represents the strength

of the turbulence in the flow. Dimensionless Turbulence kinetic energy (TKE) is a measure of the intensity of the turbulence and can be calculated with the following equations:

$$TKE = \frac{1}{2}(u'^2 + v'^2 + w'^2)$$

İzotropik akış varsayıldığında, üçüncü dalgalı hız bileşeni (w'^2) 2 boyutlu bir yaklaşımla tahmin edilebilir (FENG & WANG, 2000). Üçüncü hız bileşeni şu hali alır:

$$w'^2 = \frac{u'^2 + v'^2}{2}$$

then TKE can be calculated with the following expression

$$TKE = \frac{3}{4}(u'^2 + v'^2) = \frac{3}{4}(< u'u' > + < v'v' >)$$

To define the effect of splitter plates with different porosities to flow structure in the wake region of a bare cylinder were investigated. For this purpose, peak value of turbulent kinetic energy and formation point of peak value of turbulent kinetic energy were compared due to bare cylinder case. 251 different cases are inspected by PIV system. Most valuable ones are evaluated in three different cases due to TKE formation: 1) Flow control of a circular cylinder by permeable splitter plate with different porosities and gap values. 2) Flow control of a circular cylinder by permeable splitter plate with different porosities and length values. 3) Flow control of a circular cylinder by permeable splitter plate with different porosities and angle values. The findings of these examinations are compiled under the following headings: a)Effect of gap b) Effect of Splitter Plate Length c) Effect of Splitter Plate Porosity d) Effect of Splitter Plate Angle

For parameterization, all dimensions diveded by cylinder diameter (D) and defined with “*” indice. Ccylinder diameter (D) is fixed to 60 mm. Height of the cylinder (h) fixed to 7D. The gap (l_g^*) between the base of the cylinder and the leading edge of the splitter plate have been ranged between 0.5 to 2. with 0.5 increment. The length of the splitter plate (l_s^*) have been ranged between 1 to 3 with 1 increment. The gap (l_g^{**}) between the base of the cylinder and rotation axis of splitter plate is defined and all rotation are based on this axis. The angle of the splitter plate has been ranged between 0^0-90^0 with 15^0 increments (0^0 /15^0 /30^0 /45^0 /60^0 /75^0 /90^0). Splitter plate thickness is chosen constant as 0.8 mm.

Effect Of Gap Between Splitter Plate and Base of Cylinder:

It is obviously seen that as the gap between splitter plate and the cylinder increase, turbulent kinetic energy reduced and as the gap between splitter plate and the cylinder increases, Formation point of the peak value of turbulent kinetic energy in the flow direction reduced. Flow control is achieved for the gap lg*=2 and β=0.7. The peak magnitude of TKE is reduced up to 35%, although the location of the peak magnitude of TKE is decreased compared to the bare cylinder for the gap lg*=2 and β=0.7.

It is obviously seen that as the splitter plate porosity (β) changes, turbulent kinetic energy is reduced. But a linear correlation is not observed.

Effect of Splitter Plate Length:

Three different the splitter plate length values (ls*=1, 2 and 3) were investigated and the splitter plate angle and the gap between splitter plate and cylinder were kept to constant during the experiments as lg*=1. As splitter plate length increase, turbulent kinetic energy reduced in all situation. Also, the formation point of the peak value of turbulent kinetic energy in the flow direction increased nearly in all situations except ls*=1, β=0.50, lg*=1 and ls*=1, β=0.70, lg*=1 situations. Flow control is achieved for the gap ls*=3 and β=0.3. The peak magnitude of TKE is reduced up to 42%, although the location of the peak magnitude of TKE is increased by 25%.

It is obviously seen that as the splitter plate porosity (β) changes, turbulent kinetic energy is reduced. But a linear correlation is not observed.

.

Effect of Splitter Plate Porosity:

The porosities of the splitter plate were taken as β=0.3, 0.5 and 0.7. Four different gaps where between the cylinder and the splitter plate (lg*=0.5, 1, 1.5 and 2) were investigated and the splitter plate angle and length were kept to constant during the experiments as ls*=1. The effect of the porosity is not observed in these investigations.

To define the porosity effect, TKE variation due to porosity values 0.3/0.5/0.7, with constant values of ls and lg, is investigated. The effect of splitter plate length is obviously seen in these investigations, but the effect of the porosity is not observed. The effect of the porosity is not observed in these investigations.

Seven different the splitter plate angle values (θ =0; 15; 30; 45; 60; 75; 90) and three different porosity values (β=0.30; 0.50; 0.70) were investigated and the splitter plate length (ls*) and the gap between splitter plate midpoint and cylinder (lg^{**}) were kept to constant during the experiments as ls*=1 and lg^{**}=1.5.

It is obviously seen that as the splitter plate porosity (β) changes, turbulent kinetic energy is reduced. But a linear correlation is not observed.

Effect of Splitter Plate Angle:

Seven different the splitter plate angle values (θ =0; 15; 30; 45; 60; 75; 90) and three different porosity values (β=0.30; 0.50; 0.70) were investigated and the splitter plate length (ls*) and the gap between splitter plate midpoint and cylinder (lg^{**}) were kept to constant during the experiments as ls*=1 and lg^{**}=1.5. It is observed that vortex formation delayed with increasing the splitter plate angle. As splitter plate angle increase, turbulent kinetic energy reduced in most situation. Also, the formation point of peak value of turbulent kinetic energy in the flow direction reduced nearly in all situations except θ =90, β=0.30 and θ =60, β=0.70 situations.

It is obviously seen that as the splitter plate angle (θ) changes, turbulent kinetic energy is reduced. For θ=30 degrees, TKE reducing is maximized. The effect of the splitter plate angle is obviously seen in these investigations, but the effect of the porosity is not observed.

Flow control is achieved for β=0.30 and $\theta=90^0$. The peak magnitude of TKE is reduced up to 28%, although the location of the peak magnitude of TKE is decreased by 4%.

It is obviously seen that as the splitter plate porosity (β) changes, turbulent kinetic energy is reduced. But a linear correlation is not observed.

ACKNOWLEDGEMENT

This work has been successful thanks to my family, who have never given up their support for me. I would like to thank all of them.

I offer my gratitude to my thesis advisor Prof. Dr. Hüseyin Akıllı for his predictions, advice and inexhaustible patience.

TABLE OF CONTENTS **PAGE**

LIST OF TABLES **PAGE**

LIST OF FIGURES **PAGE**

LIST OF ABBREVIATIONS

<u`u`>	: Streamwise Reynolds normal stress
<u`v`>	: Reynolds shear stress
<u>	: Streamwise velocity
<v`v`>	: Transverse Reynolds normal stress
CFD	: computational fluid dynamics
D	: cylinder diameter
F	: vortex shedding frequency
l_c	: length of the cylinder
l_g	: the gap between the base of the cylinder and the leading edge of the splitter plate
l_s	: length of the splitter plate
PIV	: particle image velocimetry
Re	: Reynolds Number
S_t	: Strouhal number
TKE	: Turbulent Kinetic Energy
x	: characteristic length
β	: porosity of splitter plate
θ	: angle of the splitter plate
μ	: dynamic viscosity
ρ	: density
ϑ	: kinematic viscosity

XXI

1. INTRODUCTION

Researcher studies on flow over bluff bodies for understanding wake flow physic and the cylinders are widely used for experiments due to their basic geometry and large number of technical applications like heat exchanger tubes, cooling systems for nuclear power plants, power transmission lines, chimney stacks, bridges, buildings, radio telescopes, power lines, offshore drilling rigs, underwater pipelines, marine cables, etc.

Bluff body hydrodynamics is a general term that may be used to describe the study of the hydrodynamics of floating and fixed structures that generate regions of separated flow. A steady flow causes periodic vortex shedding around the bluff body. When the vortex shedding occurs behind a body, drag on the body increases and the body suffers from the periodic force in the normal direction to the mainstream, and these periodic forces generate structural vibrations and acoustic noise or resonance. Also, the vortex shedding enhances mixing and by the way heat transfer behind the structure. In nature, most of the flows around bluff bodies have considerably shorter vertical dimensions than their length and these types of flows consider as shallow water. In nature wide rivers, lakes, shallow coastal waters, mountains may be characterized as shallow flow. Chen and Jirka (CHEN, D.; JIRKA, 1997) used a criterion for the shallow water, given as $\frac{\lambda}{h_w} \gg 1$, and main parameters are given in Figure 1.1.

Learning how to control vortex shedding may improve energy efficiency and noise reduction. There are two main categories of vortex control methods: Passive vortex control methods and active vortex control methods.

Passive vortex control methods modify the shape of the bluff body or attach additional geometries in the flow stream like surface protrusion (Favier, Dauptain, Basso, & Bottaro, 2009), control cylinder applications (Ozdil, 2013) and splitter plates (Roshko, 1954b).

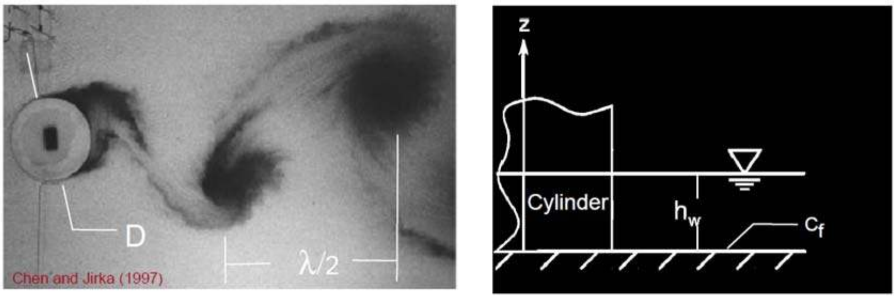

Figure 1.1. Shallow water parameters

Active vortex control method deploys an external energy in to the flow field like flow suction and blowing (Chen et al., 2013), feedback control (Fujisawa, 2001), electro-magnetic control (T. Weier, G. Gerbeth, G. Mutschke, E. Platacis, 1998), rotary oscillation of cylinder (E. Guilmineau, 2002), heating (Lecordier, J. C., L. Hamma, 1991), acoustics excitations (Blevins, 1985), plasma actuator (Tabatabaeian S., M. Mirzaei, A. Sadighzadeh, V. Damideh, Shadaram, 2015)

1.1. Vortex Formation around a circular cylinder

Research of flow pass around a circular cylinder can be traced back to 1752, date of D'Alembert research studies. In fluid dynamics, d'Alembert's paradox (or the hydrodynamic paradox) is a contradiction reached in 1768 by French mathematician Jean le Rond d'Alembert. D'Alembert proved that – for incompressible and inviscid potential flow – the drag force is zero on a body moving with constant velocity relative to the fluid.[(G.Grimberg, W.Pauls, & U.Frisch, 2008)] Zero drag is in direct contradiction to the observation of substantial drag on bodies moving relative to fluids, such as air and water; especially at high velocities corresponding with high Reynolds numbers.

According to scientific consensus, the occurrence of the paradox is due to the neglected effects of viscosity. In conjunction with scientific experiments, there were huge advances in the theory of viscous fluid friction during the 19th century. With respect to the paradox, this culminated in the discovery and description of thin boundary layers by Ludwig Prandtl in 1904. Even at very high Reynolds numbers, the thin boundary layers remain as a result of viscous forces. These viscous forces cause friction drag on streamlined objects, and for bluff bodies the additional result is flow separation and a low-pressure wake behind the object, leading to form drag. (Schlichting & Gersten, 2000)

Reynolds number is the ratio of inertial forces to viscous forces within a fluid which is subjected to relative internal movement due to different fluid velocities. Reynolds number is represented as:

$$R_e = \frac{\rho V x}{\mu} = \frac{V x}{\vartheta}$$

Where R_e is Reynolds number, ρ is density, V is freestream velocity, x is the characteristic length, μ is the dynamic viscosity and ϑ is the kinematic viscosity. For a circular cylinder x can be defined as D, the diameter of the cylinder. Hence the Reynolds number will be:

$$R_e = \frac{VD}{\vartheta}$$

The Reynolds number (Re) is an important dimensionless quantity in fluid mechanics used to help predict flow patterns in different fluid flow situations. At low Reynolds numbers, flows tend to be dominated by laminar flow, while at high Reynolds numbers turbulence results from differences in the fluid's speed and direction, which may sometimes intersect or even move counter to the overall direction of the flow (eddy currents). These eddy currents begin to churn the flow, using up energy in the process, which for liquids increases the chances of cavitation.

Vortex shedding behind a cylinder significantly depends on the Reynolds number. Figure 1.2 shows the vortex formations at different Reynolds number.

When the Re>40, oscillations are so strong that one of the two vortices break away from the cylinder and these formations called Strouhal instability. At this critical Re, unsteadiness arises spontaneously even though all the imposed conditions are being held steady and vortex shedding appears behind the circular cylinder.

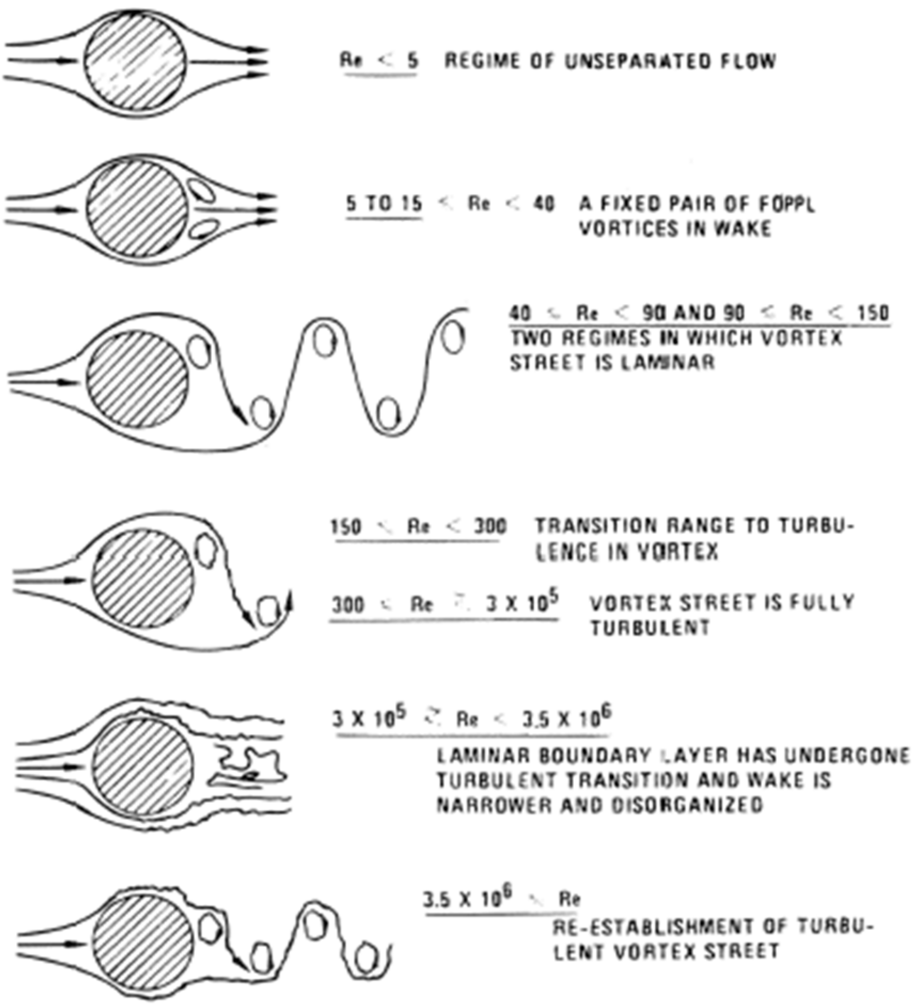

Figure 1.2. Flow across a cylinder due to Reynolds number. (Lienhard, 1966)

The second vortex is shed while the first one is shaped again. The vortices appear and are shed alternatively at a constant frequency (Tritton, 1987). When the Reynolds number reaches 150, the structure of Von Karman Vortex Street (Figure 1.3) becomes accompanying a periodically oscillating lift force.

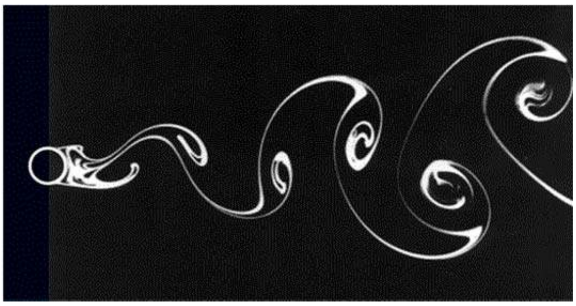

Figure 1.3. Von Karman vortex street (Van Dyke, 1982)

The frequency at which vortex shedding takes place for a cylinder is related to the Strouhal number by the following equation:

$$S_t = \frac{fD}{V}$$

Where S_t is Strouhal number, f is vortex shedding frequency, D is cylinder diameter and V is the flow velocity. Strouhal number depends on Reynolds number and surface quality. Zahari gives the change of the Strouhal number by the Reynolds number as seen in Figure 1.4.

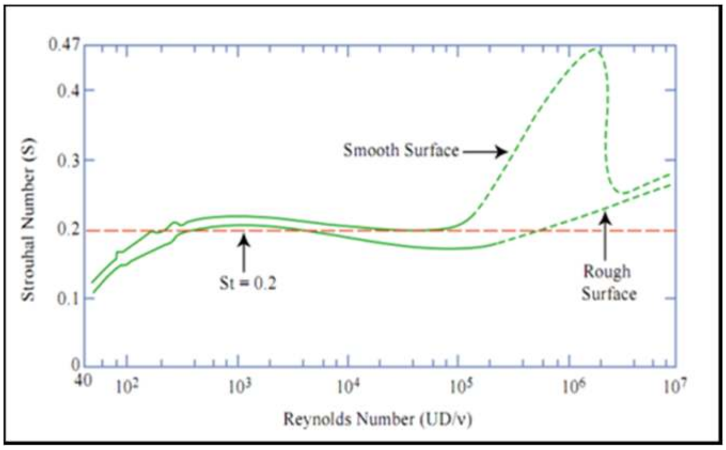

Figure 1.4. Strouhal number vs. Reynolds number (Zahari, 2015)

1.2. Flow Control

Flow control involves passive or active devices to effect a beneficial change in wall-bounded or free-shear flows, whether the task is to delay or advance transition, to suppress or enhance turbulence, or to prevent or provoke separation, useful end results include drag reduction, lift enhancement, mixing augmentation and flow-induced noise suppression. (Figure 1.5) (Gad-el-Hak, 2000)

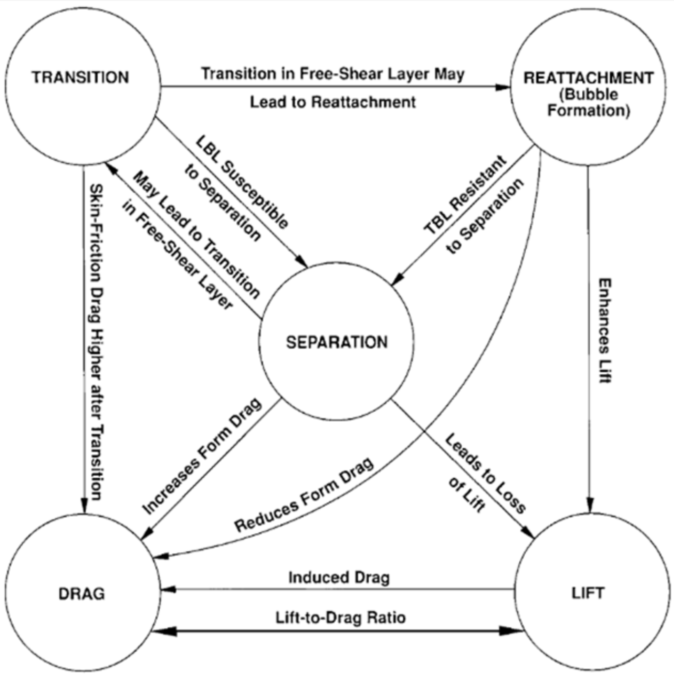

Figure 1.5. The interrelation between flow control goals (Gad-el-Hak, 2000)

1.2.1. Passive Vortex Control Methods

Passive vortex control methods modify the shape of the bluff body or attach additional geometries in the flow stream like surface protrusion (Favier, Dauptain, Basso, & Bottaro, 2009), control cylinder applications (Ozdil, 2013) and splitter plates (Roshko, 1954b).

1.2.2. Active Vortex Control Methods

Active vortex control method deploys an external energy in to the flow field like flow suction and blowing (Chen et al., 2013), feedback control (Fujisawa, 2001), electro-magnetic control (T. Weier, G. Gerbeth, G. Mutschke, E. Platacis, 1998), rotary oscillation of cylinder (E. Guilmineau, 2002), heating (Lecordier, J. C., L. Hamma, 1991), acoustics excitations (Blevins, 1985), plasma actuator (Tabatabaeian S., M. Mirzaei, A. Sadighzadeh, V. Damideh, Shadaram, 2015). The main principle is, by disturbing the flow by any means to achieve a wake flow profile and drag control. There are two main advantages over passive control methods. First, active flow control technology leverages and controls the natural stability of the flow to attain a large effect using small localized energy input. Control is most effective when the control input is introduced locally at a high receptivity region. Secondly, active control can be used to control complex, dynamical processes like turbulence production in turbulent boundary layers to reduce skin friction and hence viscous drag where the reduction is proportional to the surface area covered by the actuators. On the other hand, to put energy from outside is the disadvantage of the active control techniques. (AKAR, 2008).

1.3. Research Objective

The aim of this thesis is to investigate passive control of unsteady flow structure behind a cylinder using splitter plates with different porosity by using two-dimensional Particle Image Velocimetry (PIV) techniques. Experiments were undertaken in a water channel in Fluid Mechanics Laboratory, Mechanical Engineering Department of Cukurova University.

2. PREVIOUS STUDIES

2.1. Vortex Shedding Control Using Splitter Plates

A splitter plate is a plate attached after a structure in the wake flow area. Splitter plates may be attached to structure or not. The main idea is, isolating flow on either side of the structure. Because splitter plates are very efficient suppressing vortex shedding, scientists study on using splitter plates as a control device for vortex shedding behind a cylinder for a few decades.

Roshko (Roshko, 1954a, 1954b) made a series of experiment to illustrate the dependence of the periodic shedding on communication among the free vortex layers (Re=14500). He mounted a thin flat plate behind the cylinder in the center plane of the wake and found that it is completely effective. When splitter plate length reaches 5d (d is the diameter of the cylinder), vortex shedding is completely disappeared and pressure drag is significantly reduced. He also found that when the length of the splitter plate is 1d and attached to cylinder, it does not change the shedding frequency slightly, but as there release a gap between cylinder and plate, shedding frequency decreases and base pressure is increased. When the gap is reached 3,85d, then shedding frequency is minimized and base pressure is maximized. Here, Roshko gives the gap as distance between the cylinder surface and trailing side of splitter plate.(Figure 2.1) (Roshko, 1954a, 1954b).

Cardell (Cardell, 1993) studied on measurements in the near wake region of a circular cylinder in a uniform flow in the Reynolds number range $2.5\ 10^3 \leq Re \leq 1.8\ 10^4$ with permeable splitter plates spanning the wake center plane. He defined permeability by the pressure drop across the plates, and the relationship between permeability and plate solidity is determined for a set of plates constructed from woven wire mesh, permitting unambiguous characterization of the splitter plates by the solidity.

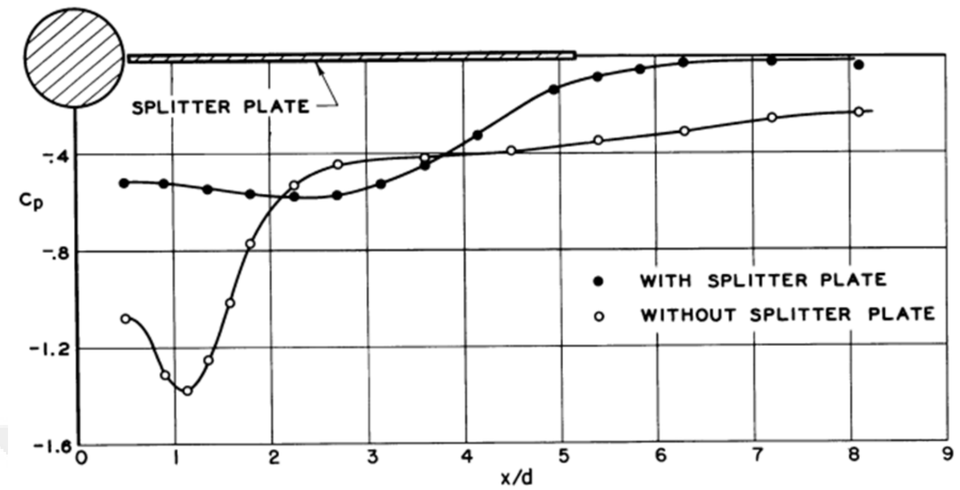

Figure 2.1. Pressure on wake centerline with and without splitter plate. Re:14500 (Roshko, 1954b)

The effects of different solidities on the flow in the near wake are investigated using smoke wire flow visualization, hot-wire anemometry, and measurements of the mean pressure at the cylinder surface, and the results are related to cylinder flow without a splitter plate. Cardell stated that the introduction of low solidity splitter plates does not change the basic near wake structure and that sufficiently high solidity uncouples the large-scale wake instability from the body, with the primary vortex formation occurring downstream of the separation bubble due to the instability of the wake profile. When the permeability is high, the basic structure of the near wake is preserved, and the primary wake instability leading to the formation of the large-scale vortices very similar to that when no splitter plate is present. When the permeability is low, the near wake becomes largely independent of the large-scale vortex formation, and the large-scale vortices develop downstream of the end of the separation bubble from an instability of the wake profile. Cardell also stated that the permeable splitter pates reduce the drag and modify the primary wake frequency. When the solidity is high enough that the wake is convectively unstable, the base pressure is independent of the Reynolds number and solidity. For a wide range of solidities, the same asymptotic value of the Strouhal number is reached at high Reynolds numbers. The different Reynolds number dependencies of the base suction coefficient, the Strouhal number, and the length of the separation bubble indicate that although the Reynolds number dependency of the changes in the base suction and the formation length is directly related to the occurrence of large-scale vortex formation at the end of the separation bubble, changes in the large-scale vortex formation do not appear to depend strongly upon the base suction. The large-scale vortex formation is not well-characterized by the Strouhal number alone, as shown by the different trends in St(Re) observed for different permeabilities.

Kwon and Choi (Kwon & Choi, 1996) simulated laminar vortex shedding behind a circular cylinder and its control using splitter plates. They found that when the length of the splitter plate is larger than a critical length, which is proportional to the Reynolds number, vortex shedding behind a cylinder completely disappears. As the plate length (*l*) converges to cylinder diameter (*d*), vortex shedding Strouhal number is decreased. They found that there exists an optimum length for minimizing drag between $1<l/d<2$ for a given Reynolds number.

Istiarto (Istiarto, 2001) studied on the flow pattern around a cylinder protruding vertically on a scoured channel bed experimentally and numerically. Detailed measurements were obtained with a non-intrusive instrument, the Acoustic Doppler Velocity Profiler (ADVP), which measures the profiles of the 3D instantaneous velocity vectors. The numerical simulation model uses the k-ε turbulence closure model to compute the turbulence stresses and the Semi-Implicit Method for Pressure-Linked Equation (SIMPLE) method to link the velocity to the pressure. The measured velocity data shows that a three-dimensional flow establishes itself, which is characterized by a rotating flow inside the scour hole upstream of the cylinder formed by a strong downward flow along the cylinder face and a reversed flow along the scour bed. This structure, which is known as horseshoe vortex, disappears behind the cylinder where a flow reversal towards the water surface is observed immediately behind the cylinder. These observations are supported by numerical simulation.

Hwang et al. (Hwang, Yang, & Sun, 2003) studied control of flow-induced forces on a circular cylinder using a detached splitter plate numerically. They placed a splitter plate with the same length as the cylinder diameter horizontally in the wake region. They found that when G/d=2.6 (distance between splitter plate/diameter of the cylinder), splitter plates drag force and lift fluctuation reduction is maximized.

Akilli et al. (Akilli, Sahin, & Filiz Tumen, 2005) controlled the flow behavior around a vertical circular cylinder placed in shallow by a splitter plate inserted at various locations downstream of the cylinder. The splitter plate has a fixed length which is equal to the diameter of the cylinder, D = 50 mm. The effect of plate thickness, T, was examined using three plates with different thicknesses, T/D = 0.016, 0.04 and 0.08. The gap between the base of the cylinder and the leading edge of the splitter plate was increased successively from 0 to 100 mm with 12.5 mm increments. Particle Image Velocimetry (PIV) was used to measure the instantaneous velocity vector field in the wake region at Reynolds number Re = 5000. They found that splitter plate thickness has no effect on the flow characteristics. And, they found that the splitter plate has a substantial effect on suppression of the vortex shedding for the gap ratio between 0 and 1.75D, and flow control is achieved for gap/diameter ratio of 1,75.

Matsumoto et al. (Matsumoto, Hashimoto, Yagi, Nakase, & Maeta, 2008) studied Karman vortex shedding control by use of perforated splitter plate by wind tunnel tests. They found that using a splitter plate with a perforation ratio of 60% or 70%, Karman vortex shedding can be mitigated by almost around 10% in comparison with no splitter plate. (Figure 2.2)

Xiao et al. (Xiao, Sun, Liu, & Hu, 2011) made a series of numerical studies on the hydrodynamic performance of undulation NACA0012 foil in the near wake of the D-section cylinder. Their investigations are focused on the gap between cylinder and foil tip in laminar flow.

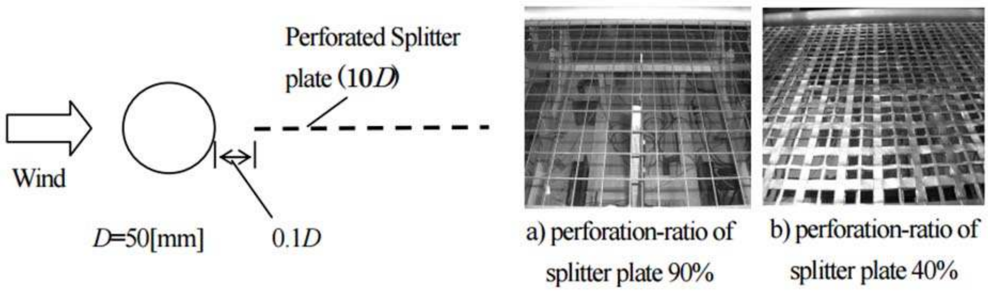

Figure 2.2. Experimental arrangement. (Matsumoto, Hashimoto, Yagi, Nakase, & Maeta, 2008)

Xiao et al found that the effects of undulating foil on the cylinder drag and lift amplitude considerably relied on the gap ratio as well as undulation ratio. They stated that for low frequency which is closer to the inherent cylinder vortex shedding frequency (St=0.25), the effect of the foil on the drag and lift amplitude reduction is significant when the foil is closer to the cylinder (L/D <= 1.0). By increasing gap ratio, the cylinder drag force and lift amplitude increase. They also noted for high frequencies, except for very close situation (L/D=0.5), the cylinder drag coefficient considerably decreases with the insertion of foil. However, lift amplitude is always larger than its counterpart in a single-cylinder case. The distinctive difference is caused by the change in cylinder wake including the vortex shedding formation, size, and strength with the insertion of undulation foil.

Kunze and Brucker (Kunze & Brücker, 2012)made a series of experiment on separation control using flexible self-adaptive hairy-flaps in a range of Reynolds number 5000 <Re< 31000. They found that the hairy-flaps alter the natural vortex separation cycle in such a way that the vortices do not shed in a zig-zag like arrangement as in the classical von Karman vortex street but in line in a row with the cylinder wake axis. Thus, the wake-deficit is largely reduced. Furthermore, flow fluctuations by 42% in streamwise and 35% in transversal direction are considerably reduced compared to the reference case without hairy-flaps.

One can refer to Chakrabarty and. Wankhede's (Chakrabarty & Wankhede, 2012) study for an extended review on vortex shedding behind cylinders.

Chan (Chan, 2012) investigated vortex suppression techniques by numerical simulations using SIMPLE as incompressible flow solver and SD as compressible flow solver. (SD: a high order solver developed in Stanford. A series of complementary experiment is also performed. Chan stated that, at low Reynolds numbers, in an unbounded flow, a short and thin splitter plate can alter the shedding characteristics but does not eliminate the wake oscillation. However, the mean drag on the body is generally reduced. In a bounded flow, a splitter plate placed at a proper separation distance can eliminate the vortex instability and consequent force oscillations on a two-dimensional circular cylinder.

Ghadimi et al. (Ghadimi, Kermani, Razughi, & Zamanian, 2013) investigated effects of splitters with different length and location on sound pressure level of a circular cylinder by COMOSL software where Reynolds number is 200. They found that splitters do not have any effect on the frequency of lift force oscillation. When splitters are used in double form and positioned at a location half a radius of cylinder away from the centerline, lift force oscillation reduces by about 99.6 percent and the sound pressure level (SPL) increases by about 15.4 percent (case8). Finally, when one splitter is situated at the same designated location, the SPL is reduced by 6.4 percent and lift force oscillation also exhibits a 90.5 percent reduction (Case7). Casework explanations are given in Figure 2.3.

Chakrabarty et al. (Chakrabarty, Yadav, & Wagh, 2013) investigated the heat transfer and pressure drop behavior of circular cylinder with different attachments as splitter plate (L=D, L=1.5D, and L=2D) and V-shaped profile. They stated that V-Shaped profile plate attached downstream of the circular cylinder provides maximum reduction in pressure drop but has low heat transfer rate. Addition of splitter plate in the downstream side of the circular cylinder shows the enhancement in the heat transfer with decrease in pressure drop.

Case	Length of splitter (m)	Vertical position of splitter from the center of cylinder (m)	Shape
1	-	-	
2	0.1	0	
3	0.075	0	
4	0.05	0	
5	0.025	0	
6	0.1	0.025	
7	0.1	0.05	
8	0.1	0.025	

Figure 2.3. Cylinder conditions (Ghadimi et al., 2013)

Gozmen et al. (Gozmen, Fırat, Akilli, & Sahin, 2013) investigated experimentally the effects of surrounding outer porous cylinder on vortex structure downstream of a circular inner cylinder in deep water flow where Reynolds number is equal to 5000. They defined porosity as the ratio of the gap area on the body to the whole-body surface area. The ratio of outer cylinder diameter to inner cylinder diameter, Do/Di was selected as 2.0. It has been observed that the outer porous cylinders have influence on the attenuation of vortex shedding in the wake region for all porosities. The turbulent intensity of the flow is reduced at least 45% by the presence of outer porous cylinder compared to the bare cylinder case. The porosities $\beta = 0.4$ and 0.5 are most suitable cases to control the flow downstream of the circular cylinder and for these porosities; the occurrence of Von-Karman vortex street is prevented. The wake region behind the cylinders extends along the streamwise direction.

Bao and Tao (Bao & Tao, 2013) investigated the wake control of a circular cylinder by dual plates symmetrically attached at the rear surface is numerically within the laminar flow regime (Re=20-160). They performed extensive parametric studies by varying the fitted position (attachment angle, θ_f) of the control plates with a short length of 0.3D. It is shown that the properly positioned dual plate device yields a greater advantage than the traditional splitter plate in wake control. They found that, for ($40^0 \leq \theta_f \leq 50^0$), the main recirculation structure in the near wake is split into two bubbles, owing to the presence of the control plates. For this angle range, the drag reduction and wake stabilization effects of the dual control plates are maximized. The maximum drag reduction of up to 13.1% is obtained at Re=160, which is nearly double that of the single splitter plate at the same plate length. The maximum suppression of lift is obtained at the same Re with a reducing rate of 60.1%, which also is nearly two times that of the single splitter plate. The optimum attachment angle is insensitive to variations in Re.

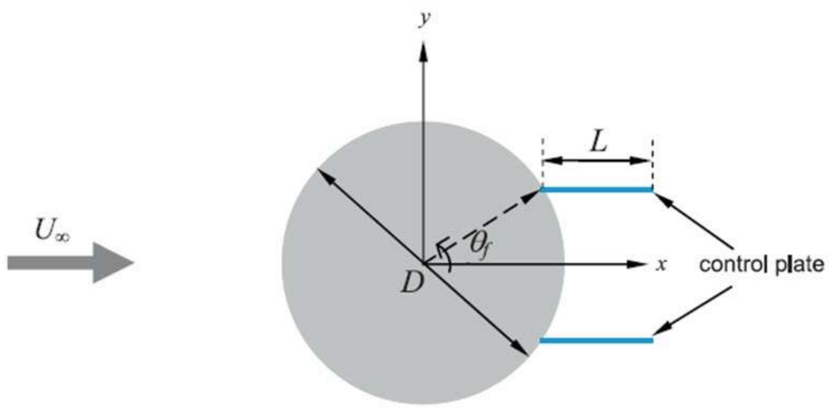

Figure 2.4. Dual plate parameters (Bao & Tao, 2013)

Reza-zadeh (S. Reza-zadeh, 2013) applied wire-plate electrodes and a splitter plate simultaneously to control fluid flow around a cylinder. The angle of the splitter plate changes between 0^0 to 45^0 with 5^0 degrees increment. They observed how corona wind effect changes due to this arrangement.

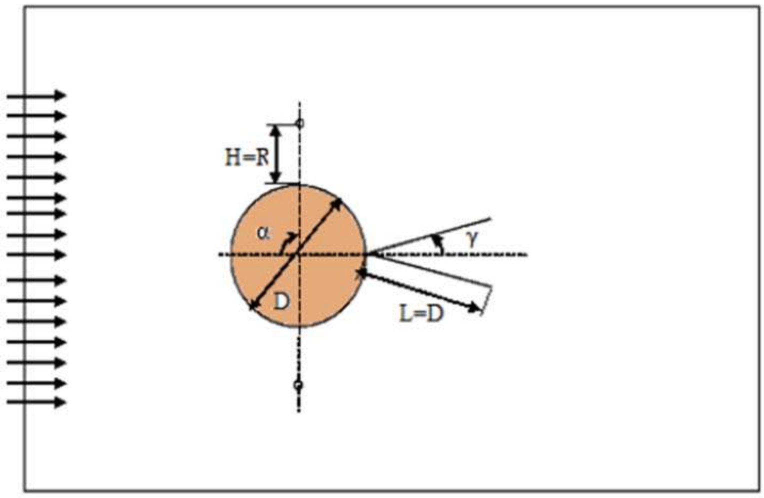

Figure 2.5. Schematic diagram of geometry. (S. Reza-zadeh, 2013)

Lee and You (Lee & You, 2013) studied on computational analysis to understand effects of the length and flexibility of a splitter plate on the drag and lift of a cylinder and vibration of the attached plate. They performed a series of simulations of flow over a circular cylinder with a flexible splitter plate by varying the length and the bending stiffness of the splitter plate. They found that the flexibility of a splitter plate adversely modulates the drag and lift forces acting on the cylinder surface while it promotes the oscillation of the plate.

Oruç et al (Oruc, Akar, Akilli, & Sahin, 2013) investigated the flow behavior downstream of two side by side cylinders. They located a splitter plate with a length of L ($1 \leq L/D \leq 5$) between two cylinders. They found that the deflection of the wake and thereby the bistability of the wake was considerably prevented with the presence of the splitter plate for $L/D \geq 3$ which resulted in two well symmetric, stable wakes having approximately the same order of magnitudes of vortex shedding frequencies around the cylinders.

Gozmen et al (Gozmen, Akilli, & Sahin, 2013) studied the control of vortex shedding of a circular cylinder in shallow water using a splitter plate located in the downstream of the circular cylinder. The plate was submerged into the water at different height ratios (h_p/h_w) such as 0.25, 0.5, 0.75 and 1.0 here h_p is plate height, h_w is water height. As the ratio of h_p/h_w increases, the effect of the splitter plate on the suppression of the vortex shedding increases. They demonstrate that the mean flow and turbulent quantities change considerably with height and length ratios of the splitter plates in shallow flow because of the prevention of interaction of shear layers located on both sides of the cylinder.

Teksin and Yayla (Teksin & Yayla, 2016) investigated the problem of flexible splitter plate in the wake of a circular cylinder using Particle Image Velocimetry (PIV) experimentally. They selected the diameter of cylinder, D as 60 mm while the Reynolds number based on the cylinder diameter kept constant as 2500, the characteristics length of the control element, L was tested for four different cases that the values of L/D were 0, 1.25, 2.25, 2.5 in the investigation. The splitter plate which has a certain amount of modulus of elasticity freely deforms along its length because of the fluid forces on plate. They found that the variable parameter of L/D affects the flow structures and noted that it decreased maximum level of all characteristic values.

Soumya and Prakash (Soumya & Prakash, 2017) studied numerical examination of the effect of splitter plate length on fluid flow characteristics past an equilateral triangular cylinder. They studied the effect of splitter plate on parameters like lift and drag where the Reynolds number is between 50 to 200. They observed that drag decreases with the attachment of the splitter plate. And they also observed vortex shedding suppression in the range of Re=50-150, but they also found that for Re=200, vortex shedding suppression is not observed.

Gao et al. (Gao, Wang, Zong, Zou, & Peng, 2017) studied splitter plate length on characteristics of flow past a circular cylinder at high Reynolds numbers is investigated using large eddy simulation (LES). They compared Lift coefficients, drag coefficients, Strouhal numbers and vortex shedding patterns of different splitter plate lengths. They divided the splitter plate lengths into three different regimes due to lift and drag coefficients: stable regime I (when the splitter plate length L=0D, D is the diameter of the circular cylinder), the unstable regime II (L=0.5D-1.0D), and the stable again regime III (L=1.5D-8.0D). they found that When splitter plate length changes from regime I to regime II, there is a sudden drop of Strouhal number and when splitter plate length changes from regime II to regime III, there is a sudden increase of Strouhal number. They also found that with the increase of splitter plate length, the vortex shedding pattern of flow field changes from 2S to 2P.

3. MATERIAL AND METHOD

3.1. Experimental Arrangement

In this study, the wake flow behavior of a circular cylinder, positioned in vertical is investigated both experimentally and numerically. A permeable splitter plate, located at various downstream locations, have been used to control the wake flow. Here, porosity has been defined as ratio of total hole areas to splitter side area.

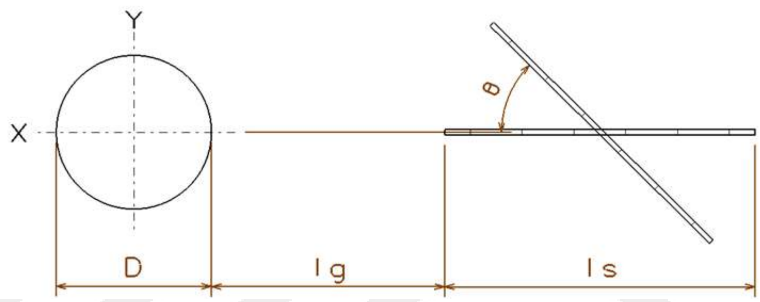

Figure 3.1. Experimental parameters

In Figure 3.2 and Figure 3.3 main geometrical dimensional representation is given and in Table 3.1 list of parameters is given. For parameterization, some geometric dimensions have been normalized with cylinder diameter d and have been indicated with superscript "*":

$$l_g^* = \frac{l_g}{D}\, ;\, l_s^* = \frac{l_s}{D};\, \beta = \frac{A_{hole_{total}}}{A_{Splitterplatearea}} \tag{3.1}$$

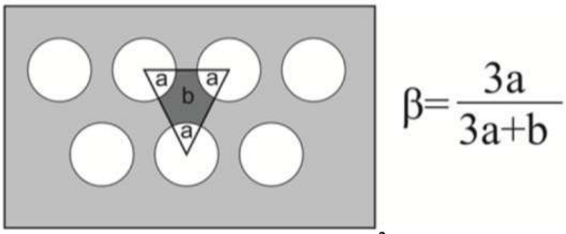

Figure 3.2. Porosity definition (a and b are in mm^2)

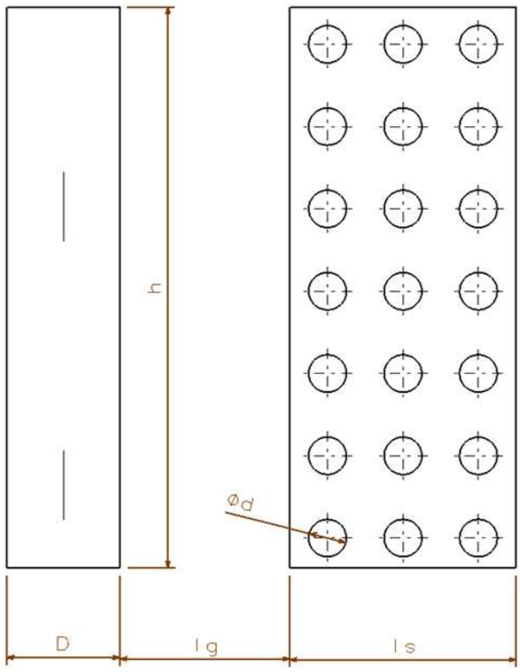

Figure 3.3. Experimental parameters

Table 3.1. Parameter definition table

D	Diameter of cylinder
l_g^*	Distance between splitter plate and cylinder
l_s^*	Length of splitter plate
θ	Angle of splitter plate
β	Porosity of splitter plate

For parameterization, cylinder diameter (D) is fixed to 60 mm. Height of the cylinder (h) fixed to 7D. The gap (l_g) between the base of the cylinder and the leading edge of the splitter plate have been ranged between D/2 to 2D with D/2 increment (30/60/90/120mm). The length of the splitter plate (l_s) have been ranged between D to 3D with D increment (60/120/180mm). The angle of the splitter plate has been ranged between 0^0-90^0 with 15^0 increments (0^0 /15^0 /30^0 /45^0 /60^0 /75^0 /90^0). Splitter plate thickness is chosen constant as 0.8 mm.

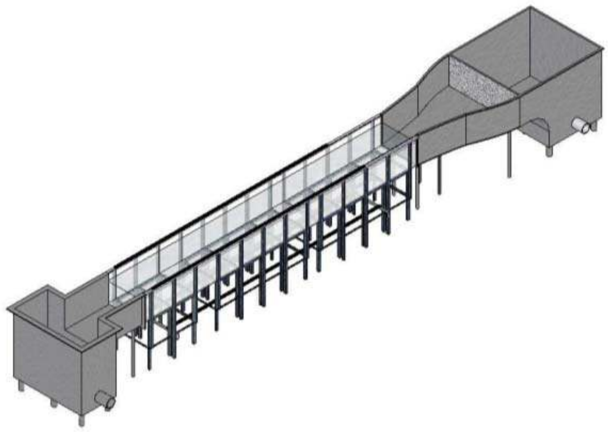

Figure 3.4. The water channel in CU

All experiments have been carried out in a large-scale closed-loop water channel in the Fluid Mechanics Laboratory at Cukurova University. The overall dimensions of the water channel are 8000 mm in length, 1000 mm in width and 750 mm in depth and constructed from transparent Plexiglas (Figure 3.4, Figure 3.5). Recirculation is maintained by an axial flow pump controlled by ABB controller unit. All experiments have been carried out in water having 420 mm water height using Dantec PIV system. PIV has been used to measure instantaneous velocity vector field in the wake region at Reynolds number based on cylinder diameter Re=5000. Reynolds number formulation is given below.

$$Re = \frac{\rho U D_h}{\mu} = \frac{U D_h}{\vartheta} \qquad D_h = 2.\frac{wet\ area}{wet\ area\ perimeter} \qquad (3.2)$$

Where ρ is density, U is mean velocity, D_h is hydraulic diameter and ϑ is kinematic viscosity. From the given formulation, calculated velocity for Re=5000 is 0,016972m/s. The flow structures in the downstream region of the cylinder base are highly unstable. As a result, this type of flow requires spatial and transient information throughout the entire flow area to allow for the identification of spatial structures that are not able to record with the point-rate measurement system. The PIV technique is a suitable technique for measuring velocity areas at the specified flow distance. The PIV technique does not only result in the quantitative data of 2D flow fields but also allows verification by numerical studies. The aim of the present study was to perform quantitative measurements on the side-laser planes along the circular cylinder mounted on a flat plate to reveal the structure of the vortical flow details using instantaneous and time-averaged flow.

Dantec PIV System uses two Nd: YAG pulsed laser sources of a wavelength of 532 nm, each with a maximum energy output of 120 mJ for flow field illumination. The water was seeded with the neutrally buoyant spherical particles of 12μm in diameter. All experiments have been done as two sets, both sets include 1000 instantaneous images. The image capturing was performed by an 8-bit cross-correlation charge-coupled device (CCD) camera having a resolution of 1,600 pixels x 1,200 pixels, equipped with a Nikon AF Micro 60 f/2.8D lens. In the image processing, 32 x 32 pixels rectangular effective interrogation window was used. The total 7326 (99 x 74) velocity vectors were obtained for an instantaneous velocity field at a rate of 15 frames/s.

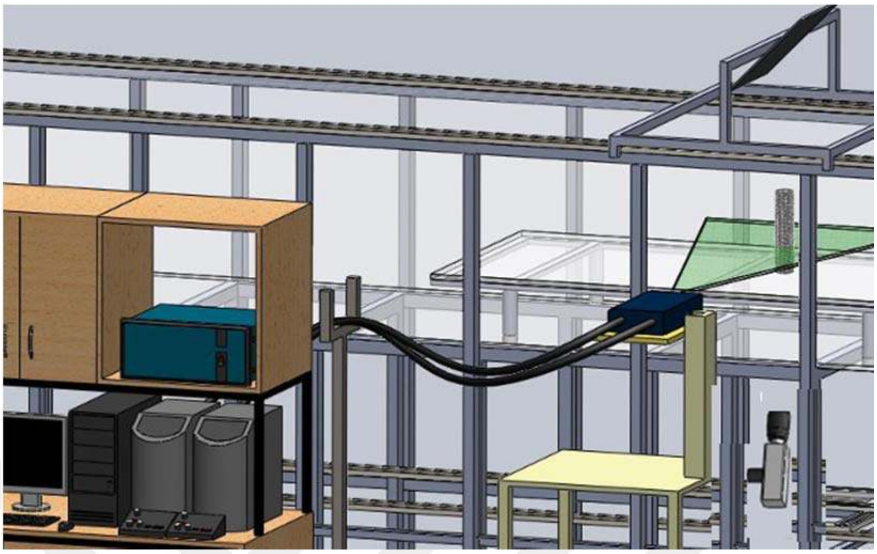

Figure 3.5. Overview of the experimental setup

The time interval between pulses was 1750 microsecond, and the thickness of the laser sheet illuminating the measuring plane was nearly 1 mm throughout the experiments. Erroneous vectors have been removed (less than 2%) and replaced by using interpolation between surrounding vectors in the post-processing step. Velocity vectors of the flow have been calculated from this displacement vector field. The vorticity patterns of the wake flow have been calculated from the velocity field using a finite difference scheme. Streamlines and circulation have been obtained by post-processing of the velocity data. The overall field of view was 230,7 x 170,8 mm^2. The raw velocity vector fields were calculated from the displacement vectors using the frame-to-frame cross-correlation technique available in the Dantec PIV Software. Spurious vectors were detected and removed by applying the local median filter technique (Westerweel, 1994) and replaced by using a bilinear least-square-fit technique between neighboring vectors. Then, the resulting vector fields were improved and smoothed by a neighborhood averaging technique. The instantaneous velocity vectors were finally averaged to obtain time-averaged velocity vectors and other flow statistics.

3.2. Particle Image Velocimetry (PIV)

Particle image velocimetry (PIV) is an optical method of flow visualization used in research. It is used to obtain instantaneous velocity measurements and related properties in fluids. The fluid is seeded with tracer particles which, for sufficiently small particles, are assumed to faithfully follow the flow dynamics (the degree to which the particles faithfully follow the flow is represented by the Stokes number). The fluid with entrained particles is illuminated so that particles are visible. The motion of the seeding particles is used to calculate speed and direction (the velocity field) of the flow being studied.

PIV produces two-dimensional or even three-dimensional vector fields. During PIV, the particle concentration is such that it is possible to identify individual particles in an image, but not with certainty to track it between images.

Typical PIV apparatus consists of a camera (normally a digital camera with a CCD chip in modern systems), a strobe or laser with an optical arrangement to limit the physical region illuminated (normally a cylindrical lens to convert a light beam to a line), a synchronizer to act as an external trigger for control of the camera and laser, the seeding particles and the fluid under investigation. A fiber optic cable or liquid light guide may connect the laser to the lens setup. PIV software is used to post-process the optical images. (Figure 3.6)

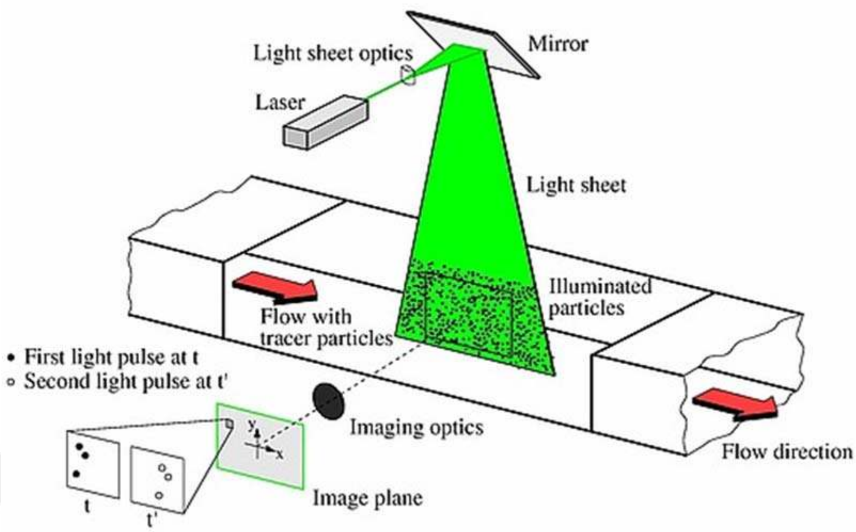

Figure 3.6. Typical PIV setup (Particle Image Velocimetry (PIV), 2019)

3.3. Turbulence Kinetic Energy (TKE)

In fluid dynamics, turbulence kinetic energy (TKE) is the mean kinetic energy per unit mass associated with eddies in a turbulent flow. Physically, the turbulence kinetic energy is characterized by measured root-mean-square (RMS) velocity fluctuations. TKE can be produced by fluid shear, friction or buoyancy, or through external forcing at low-frequency eddy scales. Turbulence kinetic energy is then transferred down the turbulence energy cascade and is dissipated by viscous forces at the Kolmogorov scale. The value of TKE directly represents the strength of the turbulence in the flow. Dimensionless Turbulence kinetic energy (TKE) is a measure of the intensity of the turbulence and can be calculated with the following equations:

$$TKE = \frac{1}{2}(u'^2 + v'^2 + w'^2) \tag{3.3}$$

Assuming isotropic flow, the third fluctuating velocity component (w'^2) can be estimated by a 2D approximation (FENG & WANG, 2000), namely, the third component has been supposed to be equal to

$$w'^2 = \frac{u'^2 + v'^2}{2} \tag{3.4}$$

then TKE can be calculated with the following expression

$$TKE = \frac{3}{4}(u'^2 + v'^2) = \frac{3}{4}(< u'u' > + < v'v' >) \tag{3.5}$$

.

4. RESULTS AND DISCUSSION

Turbulent flow is a type of fluid flow in which the fluid undergoes irregular fluctuations, or mixing, in contrast to laminar flow, in which the fluid moves in smooth paths or layers. The speed and the flow direction of the fluid continuously change in a turbulent flow.

To define the effect of splitter plates with different porosities to flow structure in the wake region of a bare cylinder were investigated. For this purpose, peak value of turbulent kinetic energy and formation point of peak value of turbulent kinetic energy were compared due to bare cylinder case. 251 different cases are inspected by PIV system. Most valuable ones are evaluated in three different cases due to TKE formation: 1) Flow control of a circular cylinder by permeable splitter plate with different porosities and gap values. 2) Flow control of a circular cylinder by permeable splitter plate with different porosities and length values. 3) Flow control of a circular cylinder by permeable splitter plate with different porosities and angle values. All experiment results are notated due to following example: Naming notation example: LG30.B03Ls60T00-1-1. Here LG30 means, distance between splitter plate and cylinder is 30 mm. B03 means, porosity of splitter plate is 0.3. Ls60 means, length of splitter plate is 60 mm. T00 means, angle of splitter plate is 00 degrees due to wake centerline.

Figure 4.1 shows the vorticity contours, time-averaged velocity vector map, and, the streamline patterns in the downstream base of the cylinder cross-sectional plane for Reynolds number of 5000. For the bare cylinder flow contours extended symmetrically due to cylinder axis in flow direction. The peak value of turbulence kinetic energy (TKE) is 0,135. Downstream of the cylinder, a counter-clockwise rotating focus F1, a clockwise rotating focus F2 and a saddle point S1 are detected for Reynolds number of 5000 as expected.

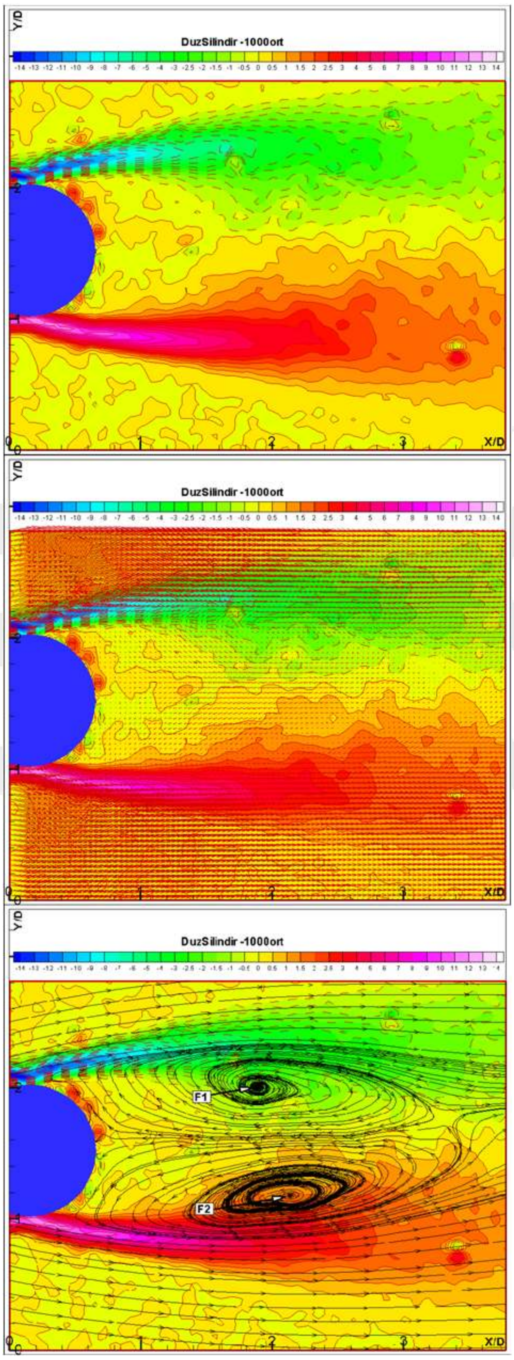

Figure 4.1. Vortex formations for bare cylinder, cylinder diameter=60 mm, Re=5000 (without splitter plate). All values are normalized due to cylinder diameter.

The locations of the saddle points and the position and the strength of the foci vary depending on the Reynolds number. The average value of dimensionless distances on X-axis ($(X/D)_{F1}$) and Y-axis ($(Y/D)_{F1}$)for focus point of the F1 are equal to 1.90274 and 2.00354. The average value of dimensionless distances on X-axis ($(X/D)_{F2}$) and Y-axis ($(Y/D)_{F2}$)for focus point of the F2 are equal to 2.13887 and 1.18182. After the peak value reached, the turbulent kinetic energy contours dissipate gradually in the flow direction. Negative values for vorticity contours represented with dashed lines. All values are normalized due to cylinder diameter.

4.1. Flow Control of a Circular Cylinder by Permeable Splitter Plate with Different Porosities and Gap Values.

In this case, cylinder diameter (D) is fixed to 60 mm. Height of the cylinder (h) fixed to 7D. The gap (l_{g*}) between the base of the cylinder and the leading edge of the splitter plate have been ranged between 0.5 to 2 with 0.5 increments. The length of splitter plate (l_{s*}) is fixed to 1. The angle of splitter (θ) plate is fixed to 0^0. Splitter plate thickness is chosen constant as 0.8 mm. Splitter plate porosity (β) is taken as 0.3/0.5/0.7 in order. For each combination two different experiments were performed. The maximum value of Turbulent Kinetic Energy formation and the coordinate where the maximum value reached is evaluated.

Figure 4.2 shows the vorticity contours, time-averaged velocity vector map, and, the streamline patterns in the downstream base of the cylinder cross-sectional plane for Reynolds number of 5000. All values are normalized due to cylinder diameter. For the cylinder with the splitter plate, for porosity value of β: 0.3 and gap value between cylinder and leading edge of splitter plate (lg*) is 0.5, flow contours extended in flow direction. Length of splitter plate (ls) is equal to cylinder diameter. The peak value of turbulence kinetic energy (TKE) is 0,11467. Downstream of the cylinder, a counterclockwise rotating focus F1, a clockwise rotating focus F2 is detected for Reynolds number of 5000 as expected.

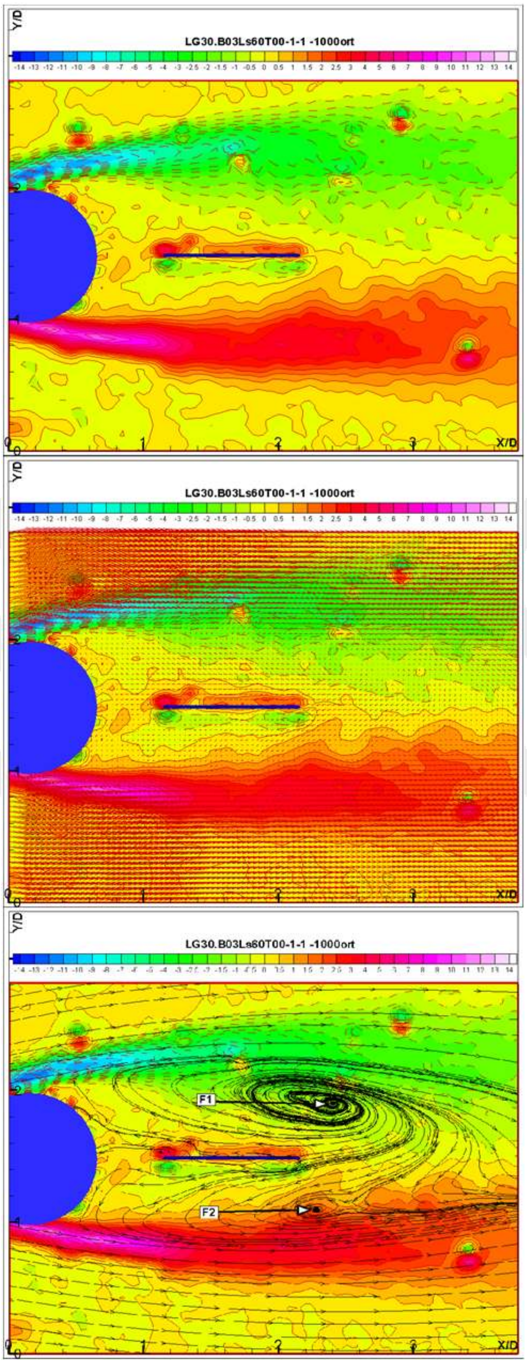

Figure 4.2. Vortex formations for porosity β: 0.3. The gap between cylinder and leading edge of splitter plate (lg*) is 0.5. Splitter plate length (ls*) is 1.

The position and the strength of the foci vary depending on splitter plate porosity.

The average value of dimensionless distances on X-axis ($(X/D)_{F1}$) and Y-axis ($(Y/D)_{F1}$) for focus point of the F1 are equal to 2.37016 and 1.90769. The average value of dimensionless distances on X-axis ($(X/D)_{F2}$) and Y-axis ($(Y/D)_{F2}$) for focus point of the F2 are equal to 2.25455 and 1.09837. After the peak value reached, the turbulent kinetic energy contours dissipate gradually in the flow direction. Negative values for vorticity contours represented with dashed lines. It is also observed that in the turbulent flow regime, the size of the foci F becomes wider with the splitter plate, and their central points shift downwards along the flow axis. F2 foci lose strength due to momentum loss as a result of the splitter plate.

Figure 4.3 shows the vorticity contours, time-averaged velocity vector map, and, the streamline patterns in the downstream base of the cylinder cross-sectional plane for Reynolds number of 5000. All values are normalized due to cylinder diameter. For the cylinder with the splitter plate, for porosity value of β: 0.5 and gap value between cylinder and leading edge of splitter plate (lg*) is 0.5, flow contours extended in flow direction. Length of splitter plate (ls) is equal to cylinder diameter. value of turbulence kinetic energy (TKE) is 0,132. Downstream of the cylinder, a counter-clockwise rotating focus F1 and a clockwise rotating focus F2 are detected for Reynolds number of 5000 as expected. The position and the strength of the foci vary depending on splitter plate porosity. The average value of dimensionless distances on X-axis ($(X/D)_{F1}$) and Y-axis ($(Y/D)_{F1}$) for focus point of the F1 are equal to 2.41197 and 1.89711. The average value of dimensionless distances on X-axis ($(X/D)_{F2}$) and Y-axis ($(Y/D)_{F2}$) for focus point of the F2 are equal to 2.56874 and 1.15648. After the peak value reached, the turbulent kinetic energy contours dissipate gradually in the flow direction. Negative values for vorticity contours represented with dashed lines. It is also observed that in the turbulent flow regime, the size of the foci F becomes wider with the splitter plate, and their central points shift downwards along the flow axis

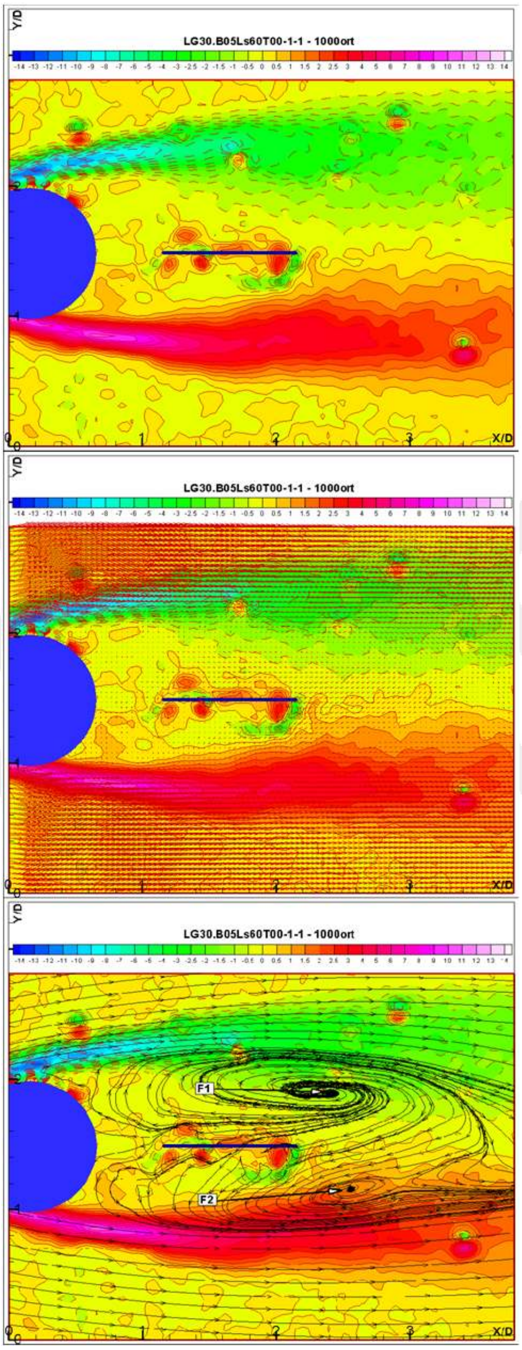

Figure 4.3. Vortex formations for porosity β: 0.5. The gap between cylinder and leading edge of splitter plate (lg*) is 0.5. Splitter plate length (ls*) is 1.

Figure 4.4 shows the vorticity contours, time-averaged velocity vector map, and, the streamline patterns in the downstream base of the cylinder cross-sectional plane for Reynolds number of 5000. All values are normalized due to cylinder diameter. For the cylinder with the splitter plate, for porosity value of β: 0.7 and gap value between cylinder and leading edge of splitter plate (lg*) is 0.5, flow contours extended in flow direction. Length of splitter plate (ls) is equal to cylinder diameter. The peak value of turbulence kinetic energy (TKE) is 0,114. Downstream of the cylinder, a counterclockwise rotating focus F1 and a clockwise rotating focus F2 is detected for Reynolds number of 5000 as expected. The position and the strength of the foci vary depending on splitter plate porosity. The average value of dimensionless distances on X-axis ($(X/D)_{F1}$) and Y-axis ($(Y/D)_{F1}$) for focus point of the F1 are equal to 2.10922 and 1.85387. The average value of dimensionless distances on X-axis ($(X/D)_{F2}$) and Y-axis ($(Y/D)_{F2}$) for focus point of the F2 are equal to 2.33628 and 1.13485. After the peak value reached, the turbulent kinetic energy contours dissipate gradually in the flow direction. Negative values for vorticity contours represented with dashed lines. It is also observed that in the turbulent flow regime, the size of the foci F becomes wider with the splitter plate, and their central points shift downwards along the flow axis. F2 foci lose strength due to momentum loss as a result of the splitter plate.

Figure 4.5 shows the vorticity contours, time-averaged velocity vector map, and, the streamline patterns in the downstream base of the cylinder cross-sectional plane for Reynolds number of 5000. All values are normalized due to cylinder diameter. For the cylinder with the splitter plate, for porosity value of β: 0.3 and gap value between cylinder and leading edge of splitter plate (lg*) is 1, flow contours extended in flow direction. Length of splitter plate (ls) is equal to cylinder diameter. The peak value of turbulence kinetic energy (TKE) is 0,113. Downstream of the cylinder, a counterclockwise rotating focus F1, a clockwise rotating focus F2 is detected for Reynolds number of 5000 as expected. The position and the strength of the foci vary depending on splitter plate porosity.

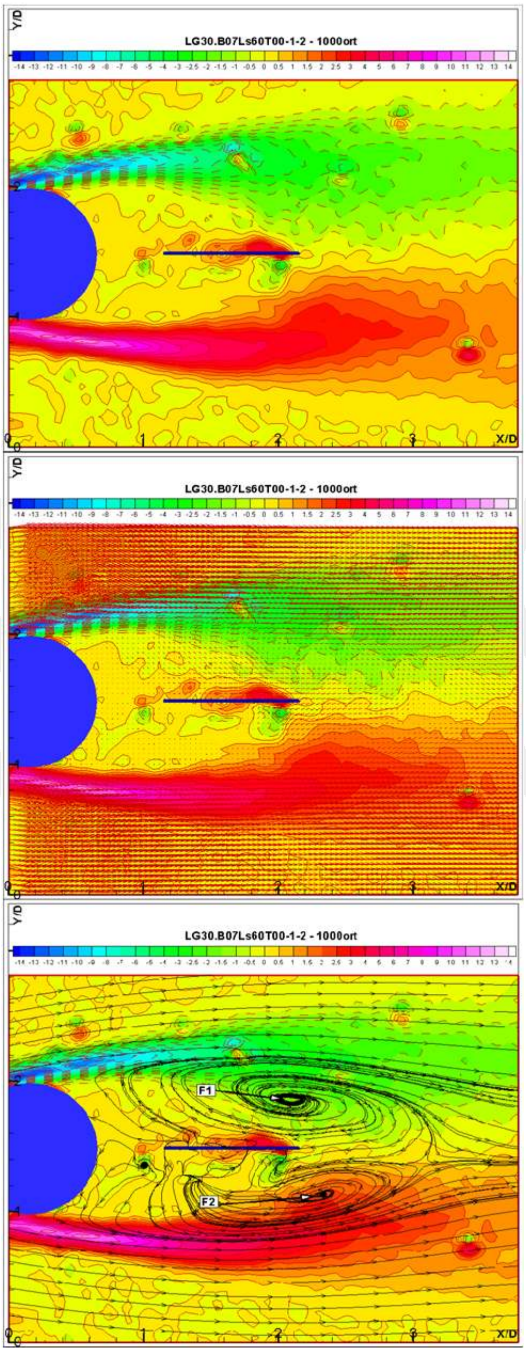

Figure 4.4. Vortex formations for porosity β: 0.7. The gap between cylinder and leading edge of splitter plate (lg*) is 0.5. Splitter plate length (ls*) is 1.

The average value of dimensionless distances on X-axis ($(X/D)_{F1}$) and Y-axis ($(Y/D)_{F1}$) for focus point of the F1 are equal to 2.51468 and 2.00524. The average value of dimensionless distances on X-axis ($(X/D)_{F2}$) and Y-axis ($(Y/D)_{F2}$) for focus point of the F2 are equal to 2.45521 and 1.15107. After the peak value reached, the turbulent kinetic energy contours dissipate gradually in the flow direction. Negative values for vorticity contours represented with dashed lines. It is also observed that in the turbulent flow regime, the size of the foci F1 becomes wider with the splitter plate, and their central points shift downwards along the flow axis. F2 foci lose strength due to momentum loss as a result of the splitter plate.

Figure 4.6 shows the vorticity contours, time-averaged velocity vector map, and, the streamline patterns in the downstream base of the cylinder cross-sectional plane for Reynolds number of 5000. All values are normalized due to cylinder diameter. For the cylinder with the splitter plate, for porosity value of β: 0.5 and gap value between cylinder and leading edge of splitter plate (lg*) is 1, flow contours extended in flow direction. Length of splitter plate (ls) is equal to cylinder diameter. The peak value of turbulence kinetic energy (TKE) is 0,128. Downstream of the cylinder, a counterclockwise rotating focus F1 and a clockwise rotating focus F2 is detected for Reynolds number of 5000 as expected. The position and the strength of the foci vary depending on splitter plate porosity. The average value of dimensionless distances on X-axis ($(X/D)_{F1}$) and Y-axis ($(Y/D)_{F1}$) for focus point of the F1 are equal to 2.21735 and 1.96739. The average value of dimensionless distances on X-axis ($(X/D)_{F2}$) and Y-axis ($(Y/D)_{F2}$) for focus point of the F2 are equal to 3.15819 and 1.27541. After the peak value reached, the turbulent kinetic energy contours dissipate gradually in the flow direction. Negative values for vorticity contours represented with dashed lines. It is also observed that in the turbulent flow regime, the size of the foci F1 becomes wider with the splitter plate, and their central points shift downwards along the flow axis. F2 foci lose strength due to momentum loss as a result of splitter plate.

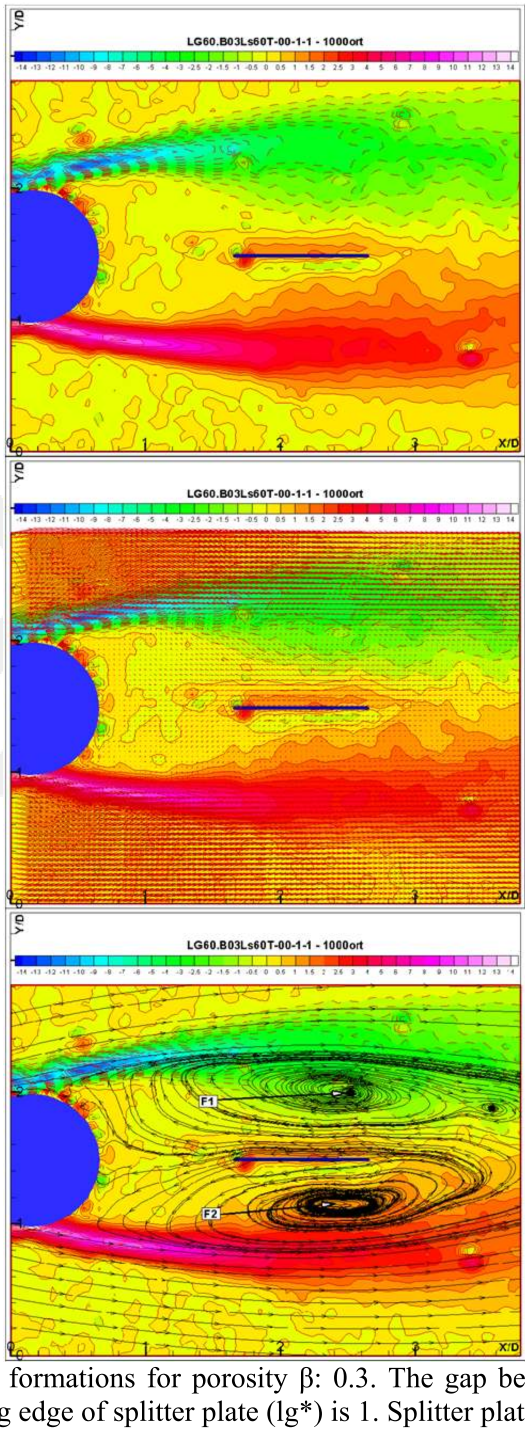

Figure 4.5. Vortex formations for porosity β: 0.3. The gap between cylinder and leading edge of splitter plate (lg*) is 1. Splitter plate length (ls*) is 1.

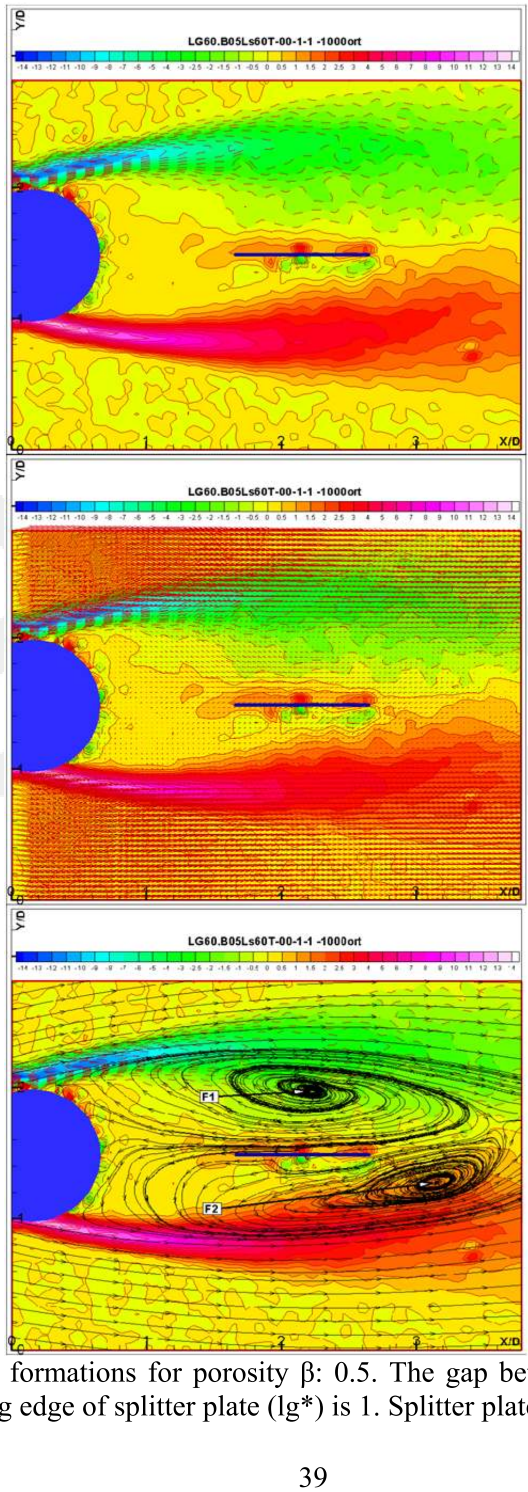

Figure 4.6. Vortex formations for porosity β: 0.5. The gap between cylinder and leading edge of splitter plate (lg*) is 1. Splitter plate length (ls*) is 1.

Figure 4.7 shows the vorticity contours, time-averaged velocity vector map, and, the streamline patterns in the downstream base of the cylinder cross-sectional plane for Reynolds number of 5000. All values are normalized due to cylinder diameter. For the cylinder with the splitter plate, for porosity value of β: 0.7 and gap value between cylinder and leading edge of splitter plate (lg*) is 1, flow contours extended in flow direction. Length of splitter plate (ls) is equal to cylinder diameter. The peak value of turbulence kinetic energy (TKE) is 0,128. Downstream of the cylinder, a counterclockwise rotating focus F1 a clockwise rotating focus F2 is detected for Reynolds number of 5000 as expected. The position and the strength of the foci vary depending on splitter plate porosity. The average value of dimensionless distances on X-axis ($(X/D)_{F1}$) and Y-axis ($(Y/D)_{F1}$) for focus point of the F2 are equal to 3.33101 and 1.76737. The average value of dimensionless distances on X-axis ($(X/D)_{F2}$) and Y-axis ($(Y/D)_{F2}$) for focus point of the F1 are equal to 2.1466 and 1.07538. After the peak value reached, the turbulent kinetic energy contours dissipate gradually in the flow direction. Negative values for vorticity contours represented with dashed lines. It is also observed that in the turbulent flow regime, the size of the foci F1 becomes wider with the splitter plate, and their central points shift downwards along the flow axis. F2 foci lose strength due to momentum loss as a result of the splitter plate.

Figure 4.8 shows the vorticity contours, time-averaged velocity vector map, and, the streamline patterns in the downstream base of the cylinder cross-sectional plane for Reynolds number of 5000. All values are normalized due to cylinder diameter. For the cylinder with the splitter plate, for porosity value of β: 0.3 and gap value between cylinder and leading edge of splitter plate (lg*) is 1.5, flow contours extended in flow direction. Length of splitter plate (ls) is equal to cylinder diameter. The peak value of turbulence kinetic energy (TKE) is 0,107. Downstream of the cylinder, a counterclockwise rotating focus F1 and a clockwise rotating focus F2 is detected for Reynolds number of 5000 as expected. The position and the strength of the foci vary depending on splitter plate porosity.

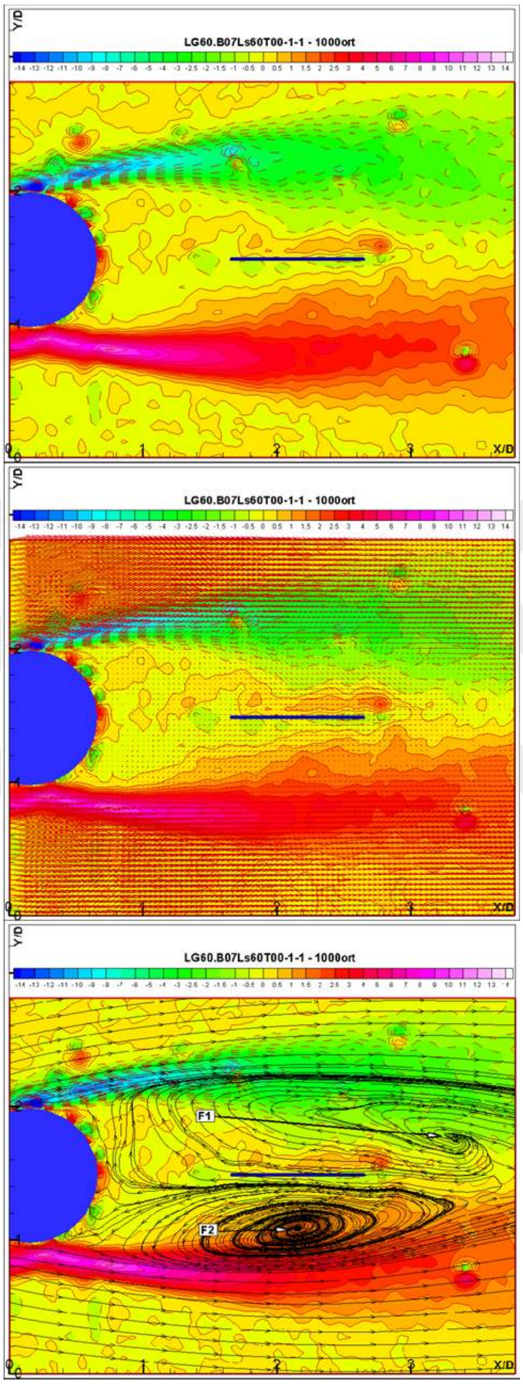

Figure 4.7. Vortex formations for porosity β: 0.7. The gap between cylinder and leading edge of splitter plate (lg*) is 1. Splitter plate length (ls*) is 1.

The average value of dimensionless distances on X-axis ($(X/D)_{F1}$) and Y-axis ($(Y/D)_{F1}$)for focus point of the F2 are equal to 2.15518 and 2.04849. The average value of dimensionless distances on X-axis ($(X/D)_{F2}$) and Y-axis ($(Y/D)_{F2}$) for focus point of the F1 are equal to 2.04165 and 1.14026. After the peak value reached, the turbulent kinetic energy contours dissipate gradually in the flow direction. Negative values for vorticity contours represented with dashed lines. It is also observed that in the turbulent flow regime, the size of the foci F2 becomes wider with the splitter plate, and their central points shift downwards along the flow axis. F1 foci lose strength due to momentum loss as a result of the splitter plate. Minor vortices foci have appeared behind F1.

Figure 4.9 shows the vorticity contours, time-averaged velocity vector map, and, the streamline patterns in the downstream base of the cylinder cross-sectional plane for Reynolds number of 5000. All values are normalized due to cylinder diameter. For the cylinder with the splitter plate, for porosity value of β: 0.5 and gap value between cylinder and leading edge of splitter plate (lg*) is 1.5, flow contours extended in flow direction. Length of splitter plate (ls) is equal to cylinder diameter. The peak value of TKE is 0,106. Downstream of the cylinder, a counterclockwise rotating focus F1 and a clockwise rotating focus F2 is detected for Reynolds number of 5000 as expected. The position and the strength of the foci vary depending on splitter plate porosity. The average value of dimensionless distances on X-axis ($(X/D)_{F1}$) and Y-axis ($(Y/D)_{F1}$) for focus point of the F1 are equal to 2.25249 and 2.02686. The average value of dimensionless distances on X-axis ($(X/D)_{F2}$) and Y-axis ($(Y/D)_{F2}$) for focus point of the F2 are equal to 2.30114 and 1.12404. After the peak value reached, the turbulent kinetic energy contours dissipate gradually in the flow direction. Negative values for vorticity contours represented with dashed lines. It is also observed that in the turbulent flow regime, the size of the foci F2 becomes wider with the splitter plate, and their central points shift downwards along the flow axis. F1 foci lose strength due to momentum loss as a result of the splitter plate. Minor vortices foci have appeared behind F1.

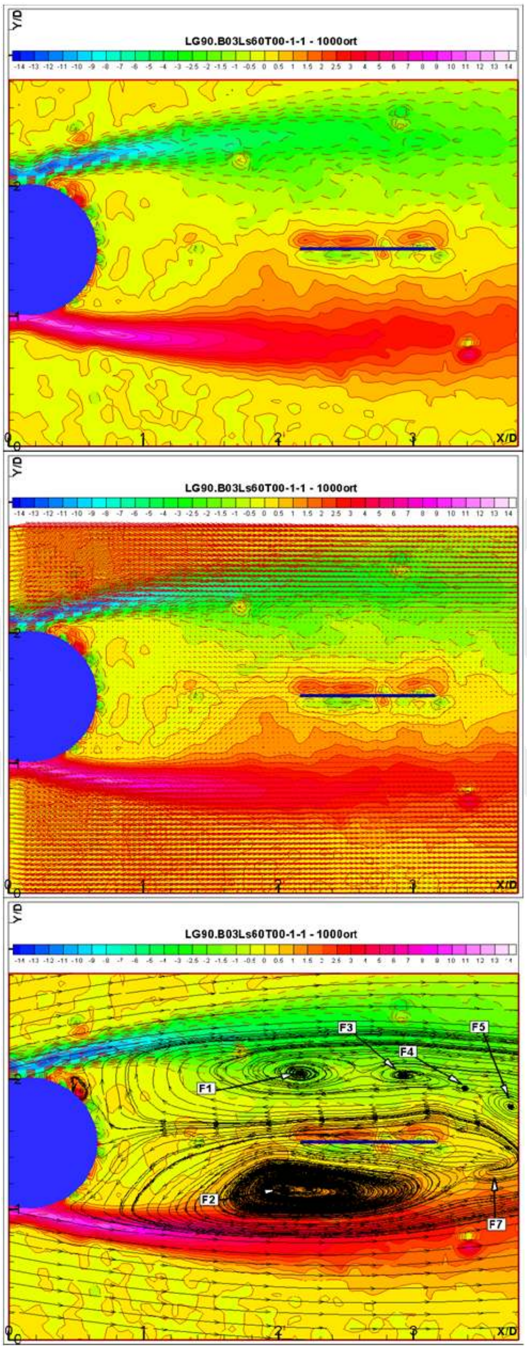

Figure 4.8. Vortex formations for porosity β: 0.3. The gap between cylinder and leading edge of splitter plate (lg*) is 1.5. Splitter plate length (ls*) is 1.

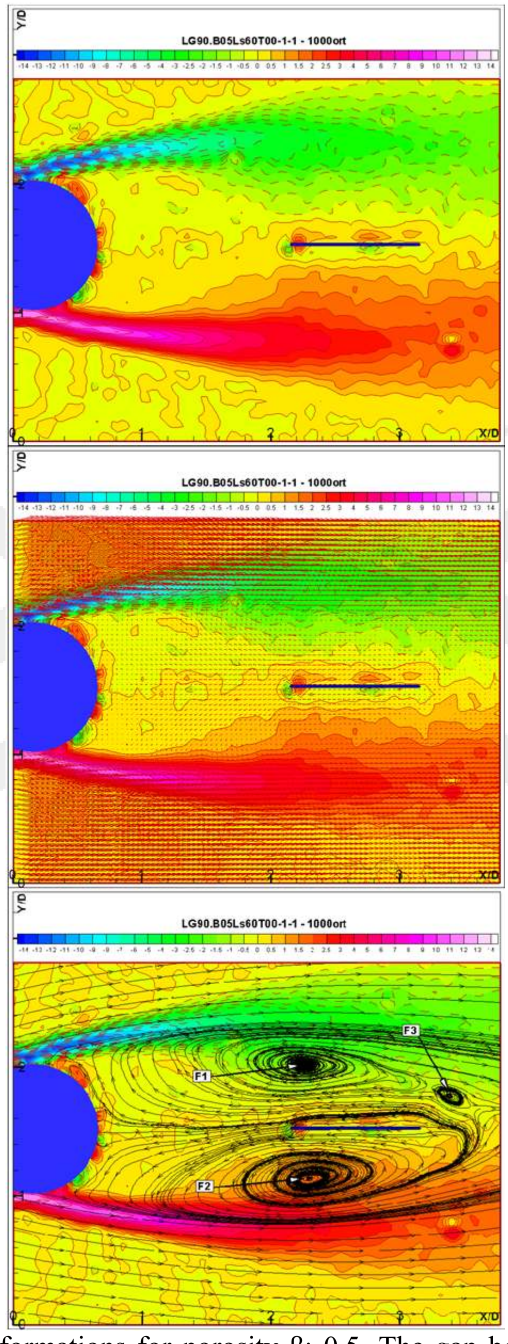

Figure 4.9. Vortex formations for porosity β: 0.5. The gap between cylinder and leading edge of splitter plate (lg*) is 1.5. Splitter plate length (ls*) is 1.

Figure 4.10 shows the vorticity contours, time-averaged velocity vector map, and, the streamline patterns in the downstream base of the cylinder cross-sectional plane for Reynolds number of 5000. All values are normalized due to cylinder diameter. For the cylinder with the splitter plate, for porosity value of β: 0.7 and gap value between cylinder and leading edge of splitter plate (lg*) is 1.5, flow contours extended in flow direction. Length of splitter plate (ls) is equal to cylinder diameter. The peak value of turbulence kinetic energy (TKE) is 0,106. Downstream of the cylinder, a counterclockwise rotating focus F1 and a clockwise rotating focus F2 is detected for Reynolds number of 5000 as expected. The position and the strength of the foci vary depending on splitter plate porosity. The average value of dimensionless distances on X-axis ($(X/D)_{F1}$) and Y-axis ($(Y/D)_{F1}$) for focus point of the F1 are equal to 2.15518 and 2.02146. The average value of dimensionless distances on X-axis ($(X/D)_{F2}$) and Y-axis ($(Y/D)_{F2}$) for focus point of the F2 are equal to 2.24167 and 1.13485. After the peak value reached, the turbulent kinetic energy contours dissipate gradually in the flow direction. Negative values for vorticity contours represented with dashed lines. It is also observed that in the turbulent flow regime, the size of the foci F2 becomes wider with the splitter plate, and their central points shift downwards along the flow axis. F1 foci lose strength due to momentum loss as a result of the splitter plate. Minor vortices foci have appeared behind F1.

Figure 4.11 shows the vorticity contours, time-averaged velocity vector map, and, the streamline patterns in the downstream base of the cylinder cross-sectional plane for Reynolds number of 5000. All values are normalized due to cylinder diameter. For the cylinder with the splitter plate, for porosity value of β: 0.3 and gap value between cylinder and leading edge of splitter plate (lg*) is 2, flow contours extended in flow direction. Length of splitter plate (ls) is equal to cylinder diameter. The peak value of turbulence kinetic energy (TKE) is 0,108. Downstream of the cylinder, a counterclockwise rotating focus F1 and a clockwise rotating focus F2 is detected for Reynolds number of 5000 as expected.

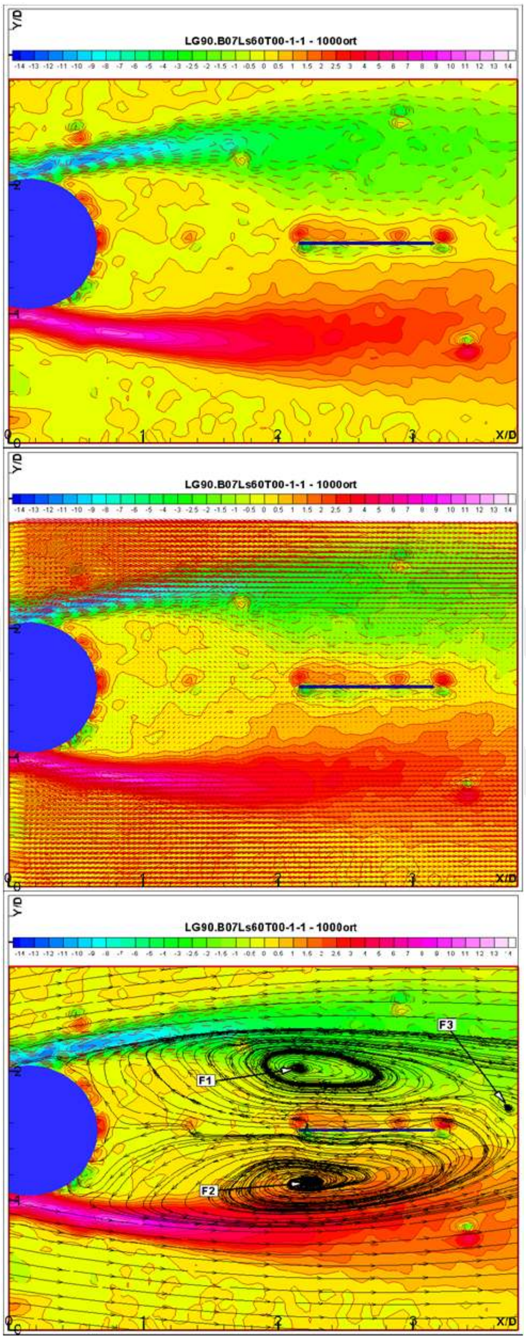

Figure 4.10. Vortex formations for porosity β: 0.7. The gap between cylinder and leading edge of splitter plate (lg*) is 1.5. Splitter plate length (ls*) is 1.

The position and the strength of the foci vary depending on splitter plate porosity. The average value of dimensionless distances on X-axis ($(X/D)_{F1}$) and Y-axis ($(Y/D)_{F1}$)for focus point of the F1 are equal to 2.93366 and 1.91874 The average value of dimensionless distances on X-axis ($(X/D)_{F2}$) and Y-axis ($(Y/D)_{F2}$) for focus point of the F2 are equal to 2.39845 and 1.14566. After the peak value reached, the turbulent kinetic energy contours dissipate gradually in the flow direction. Negative values for vorticity contours represented with dashed lines. It is also observed that in the turbulent flow regime, the size of the foci F2 becomes wider with the splitter plate, and their central points shift downwards along the flow axis. F1 foci lose strength due to momentum loss as a result of the splitter plate.

Figure 4.12 shows the vorticity contours, time-averaged velocity vector map, and, the streamline patterns in the downstream base of the cylinder cross-sectional plane for Reynolds number of 5000. All values are normalized due to cylinder diameter. For the cylinder with the splitter plate, for porosity value of β: 0.5 and gap value between cylinder and leading edge of splitter plate (lg*) is 2, flow contours extended in flow direction. The peak value of turbulence kinetic energy (TKE) is 0,104. Downstream of the cylinder, a counterclockwise rotating focus F1 and a clockwise rotating focus F2 is detected for Reynolds number of 5000 as expected. The position and the strength of the foci vary depending on splitter plate porosity. The average value of dimensionless distances on X-axis ($(X/D)_{F1}$) and Y-axis ($(Y/D)_{F1}$) for focus point of the F1 are equal to 2.31457 and 1.9227. The average value of dimensionless distances on X-axis ($(X/D)_{F2}$) and Y-axis ($(Y/D)_{F2}$) for focus point of the F2 are equal to 2.05805 and 1.10351. After the peak value reached, the turbulent kinetic energy contours dissipate gradually in the flow direction. Negative values for vorticity contours represented with dashed lines. It is also observed that in the turbulent flow regime, the size of the foci F2 becomes wider with the splitter plate, and their central points shift downwards along the flow axis. F1 foci lose strength due to momentum loss as a result of splitter plate.

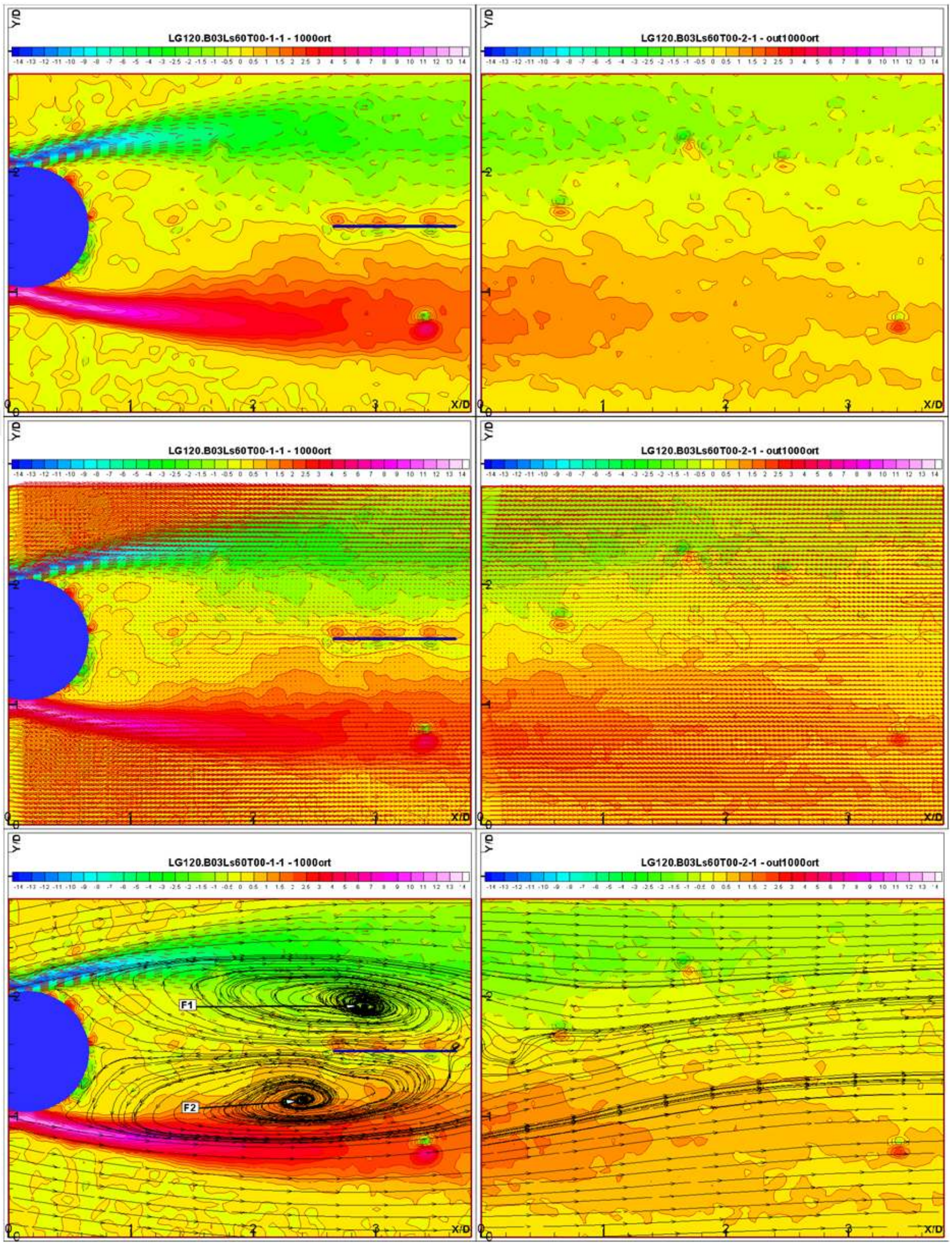

Figure 4.11 Vortex formations for porosity β: 0.3. The gap between cylinder and leading edge of splitter plate (lg*) is 2. Splitter plate length (ls*) is 1.

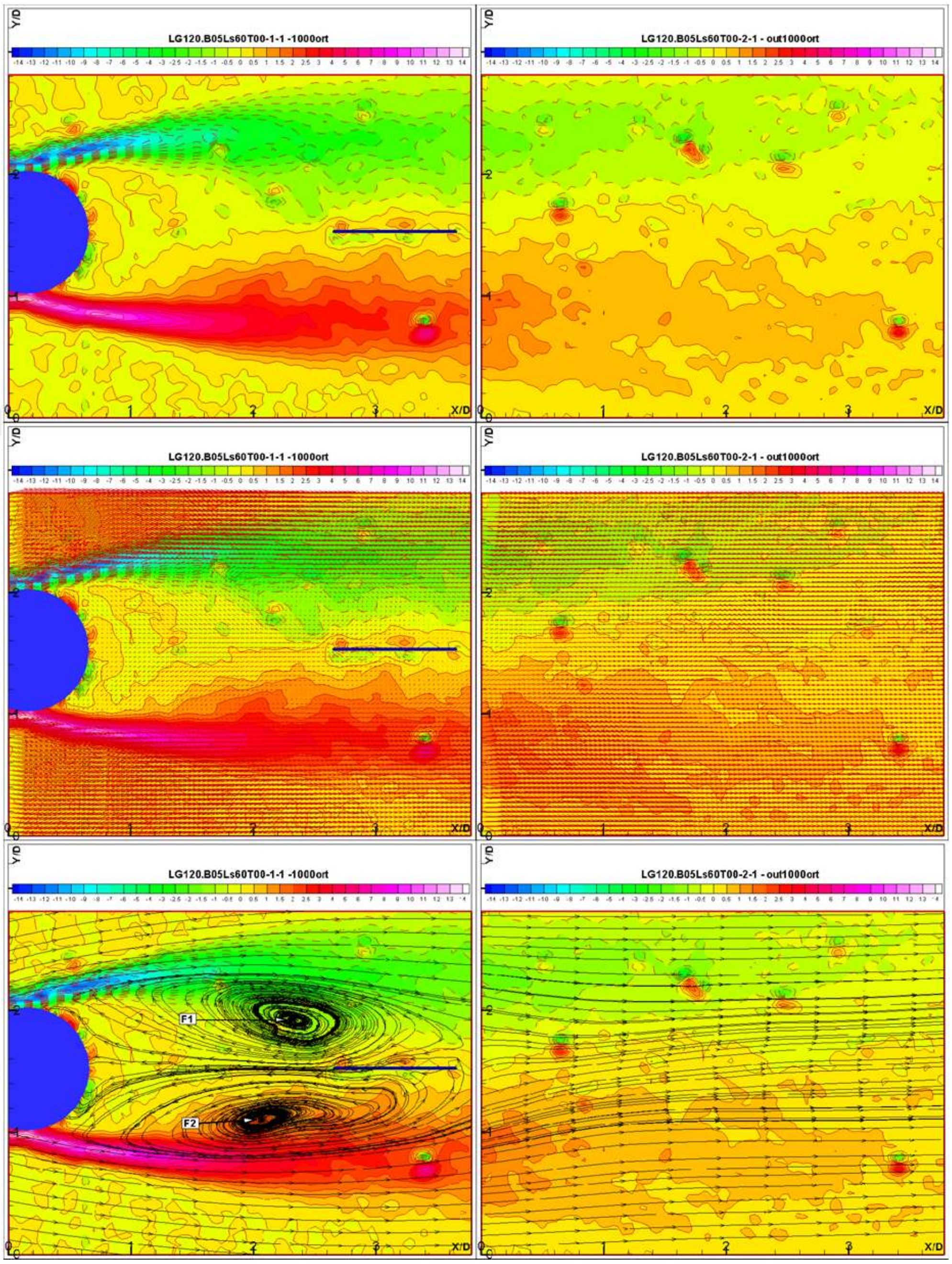

Figure 4.12. Vortex formations for porosity β: 0.5. The gap between cylinder and leading edge of splitter plate (lg*) is 2. Splitter plate length (ls*) is 1.

Figure 4.13 shows the vorticity contours, time-averaged velocity vector map, and, the streamline patterns in the downstream base of the cylinder cross-sectional plane for Reynolds number of 5000. All values are normalized due to cylinder diameter. For the cylinder with the splitter plate, for porosity value of β: 0.7 and gap value between cylinder and leading edge of splitter plate (lg*) is 2, flow contours extended in flow direction. Length of splitter plate (ls) is equal to cylinder diameter. The peak value of turbulence kinetic energy (TKE) is 0,088. Downstream of the cylinder, a counterclockwise rotating focus F1 and a clockwise rotating focus F2 is detected for Reynolds number of 5000 as expected. The position and the strength of the foci vary depending on splitter plate porosity. The average value of dimensionless distances on X-axis ($(X/D)_{F1}$) and Y-axis ($(Y/D)_{F1}$)for focus point of the F1 are equal to 2.44283 and 1.91029. The average value of dimensionless distances on X-axis ($(X/D)_{F2}$) and Y-axis ($(Y/D)_{F2}$) for focus point of the F2 are equal to 2.38904 and 1.20694. After the peak value reached, the turbulent kinetic energy contours dissipate gradually in the flow direction. Negative values for vorticity contours represented with dashed lines. It is also observed that in the turbulent flow regime, the size of the foci F2 becomes wider with the splitter plate, and their central points shift downwards along the flow axis. F1 foci lose strength due to momentum loss as a result of the splitter plate.

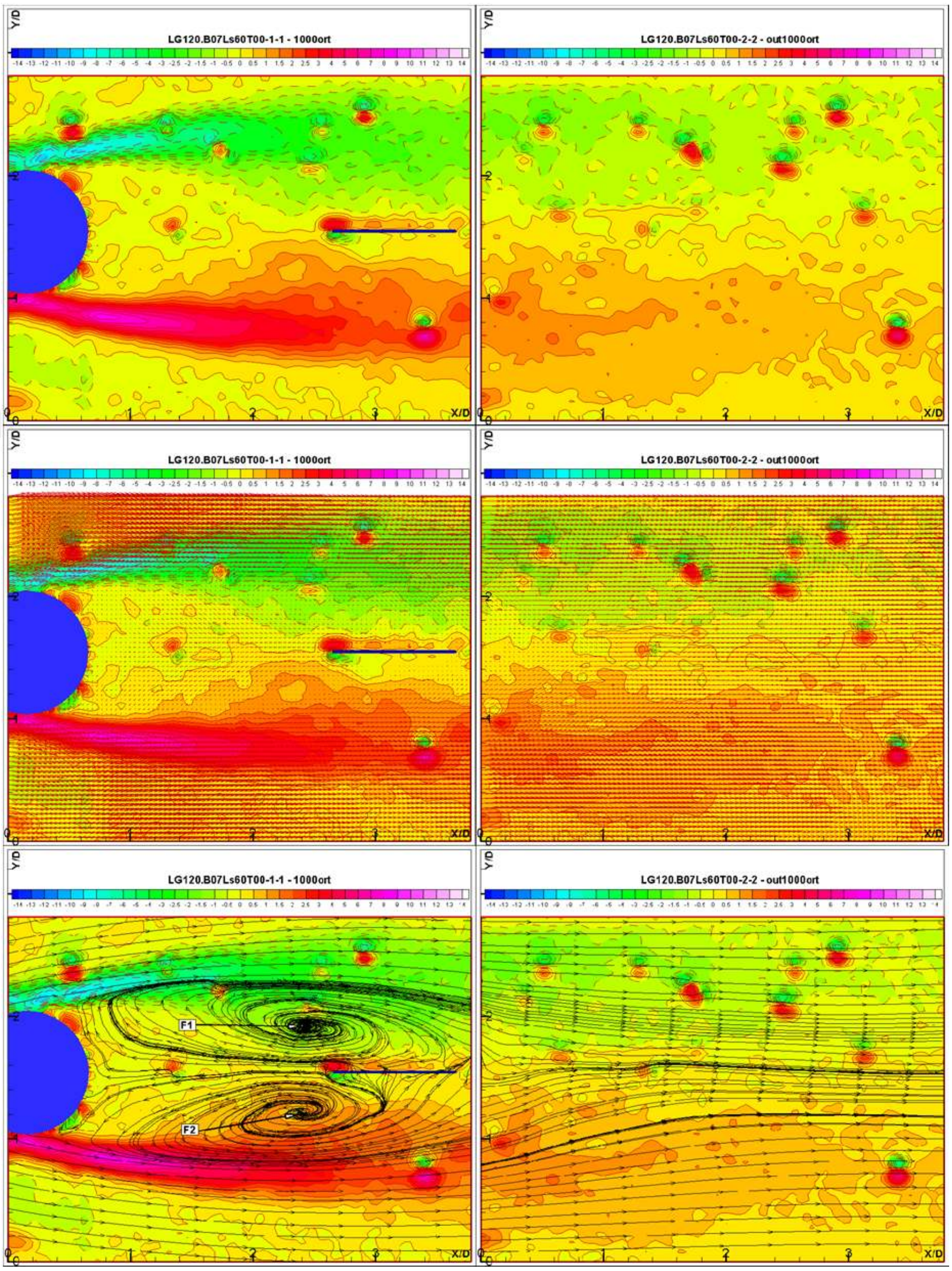

Figure 4.13. Vortex formations for porosity β: 0.7. The gap between cylinder and leading edge of splitter plate (lg*) is 2. Splitter plate length (ls*) is 1.

Results show that a decrease in turbulent kinetic energy is obtained by the lg^* increase. The peak values of turbulent kinetic energy for splitter plate-cylinder gap values lg^* =0.5, 1, 1.5 and 2 are reduced by %15, 16%, 20%, and %28 in order, for the porosity value β=0.3 (Figure 4.14),.

The peak values of turbulent kinetic energy for splitter plate-cylinder gap values lg^* =0.5, 1, 1.5 and 2 are reduced by 2%, 5%, 22% and 20% in order for the porosity value β=0.5 (Figure 4.16). The peak values of turbulent kinetic energy for splitter plate-cylinder gap values lg^* =0.5, 1, 1.5 and 2 are reduced by 16%, 12%, 20% and 35% in order (Figure 4.18), for the porosity value β=0.7.

Formation point of the peak value of turbulent kinetic energy in the flow direction for splitter plate-cylinder gap values lg^* =1, 1.5 and 2 are increased by 0%, 1% and 27% in order, for the porosity value β=0.3. Only for lg^*=0,5, formation point of peak value of turbulent kinetic energy in the flow direction is reduced by 10% (Figure 4.15).

Formation point of the peak value of turbulent kinetic energy in the flow direction for splitter plate-cylinder gap values lg^* =0.5 and 2 are increased by 1%, 3% in order, for the porosity value β=0.5. For lg^* =1 and 1.5, formation point of peak value of turbulent kinetic energy in the flow direction is reduced by 9% and 2% (Figure 4.17).

Formation point of the peak value of turbulent kinetic energy in the flow direction for splitter plate-cylinder gap values lg^* =2 are increased by 21% for the porosity value β=0.7. For lg^* =0,5 and 1, formation point of peak value of turbulent kinetic energy in the flow direction is reduced by 14% and 2%. For lg^* =1,5 formation point of peak value of turbulent kinetic energy in the flow direction is not changed. (Figure 4.19).

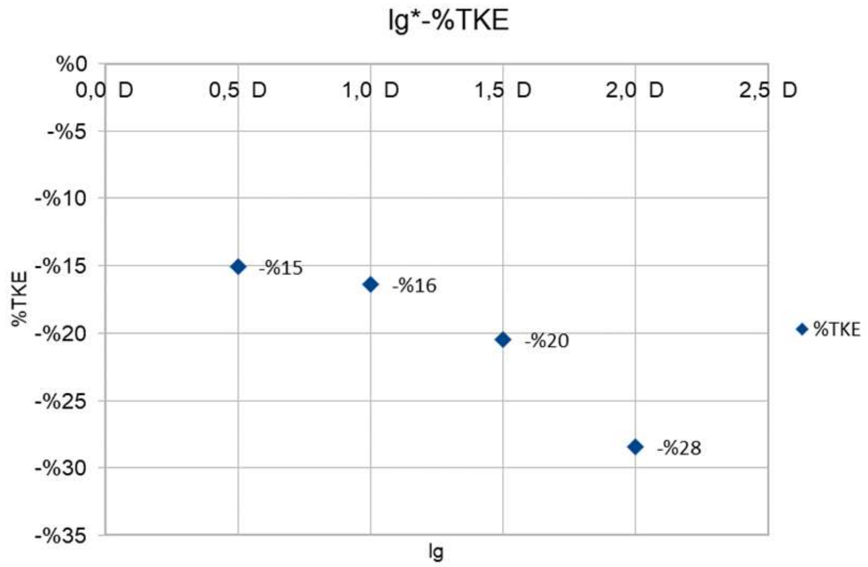

Figure 4.14 TKE var. due to diff. gaps between the cylinder and leading edge of splitter plate (lg*) for porosity β=0.30. Splitter plate length (ls*) is 1.

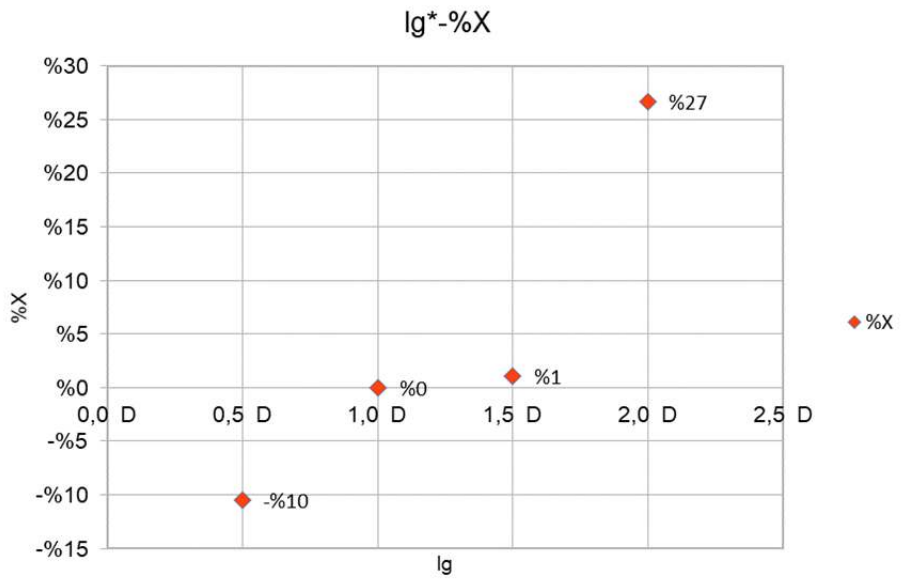

Figure 4.15. Position of max. TKE formation due to different gaps between the cylinder and leading edge of splitter plate (lg*) for porosity β=0.30. Splitter plate length (ls*) is 1.

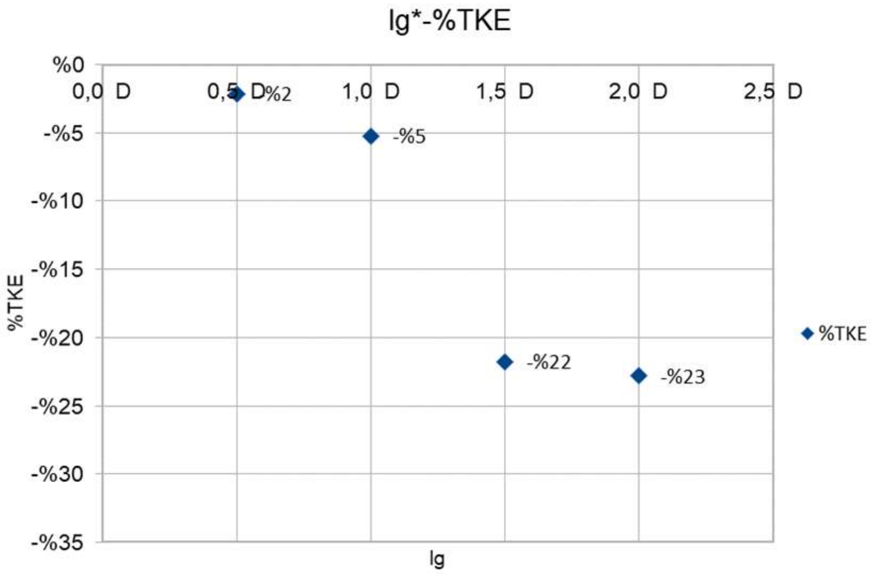

Figure 4.16. TKE var. due to different gaps between the cylinder and leading edge of splitter plate (lg*) for porosity β=0.50. Splitter plate length (ls*) is 1.

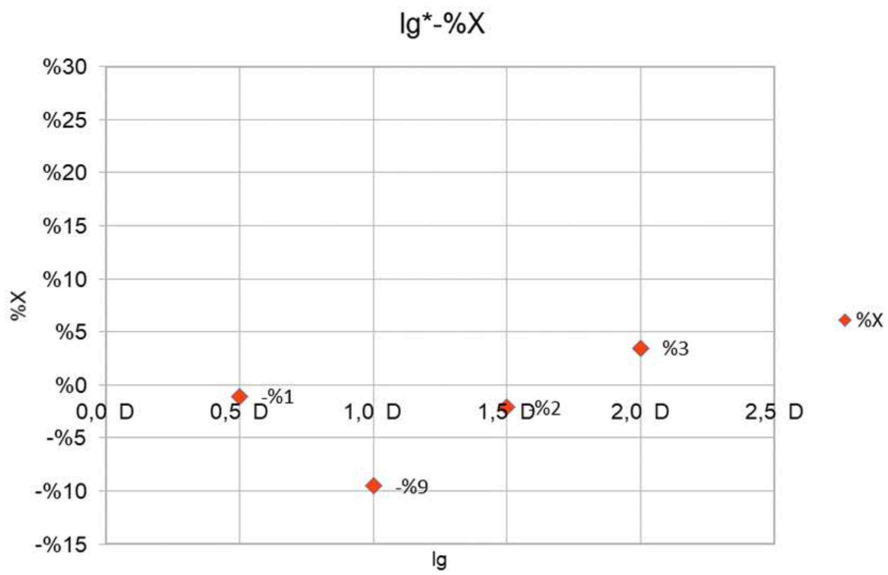

Figure 4.17. Position of max. TKE formation due to different gaps between the cylinder and leading edge of splitter plate (lg*) for porosity β=0.50. Splitter plate length (ls*) is 1.

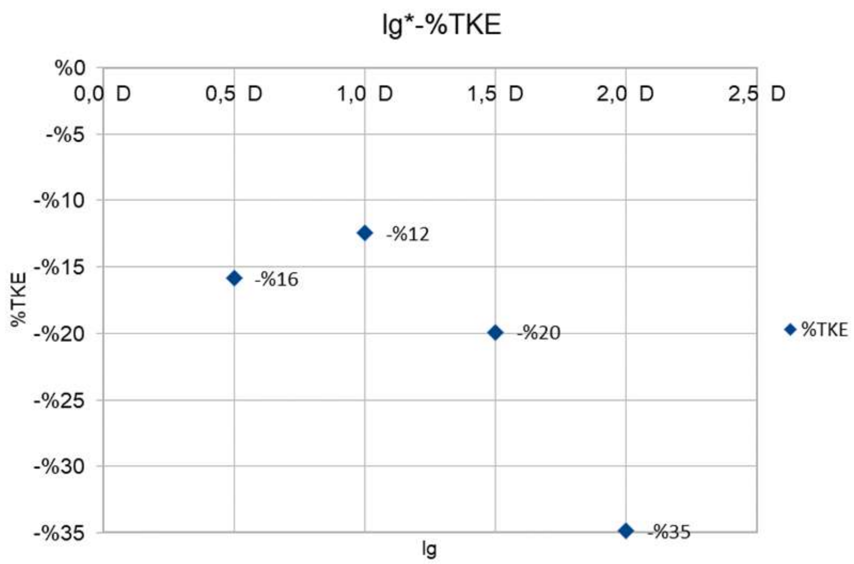

Figure 4.18. TKE var. due to different gaps between the cylinder and leading edge of splitter plate (lg*) for porosity β=0.70. Splitter plate length (ls*) is 1.

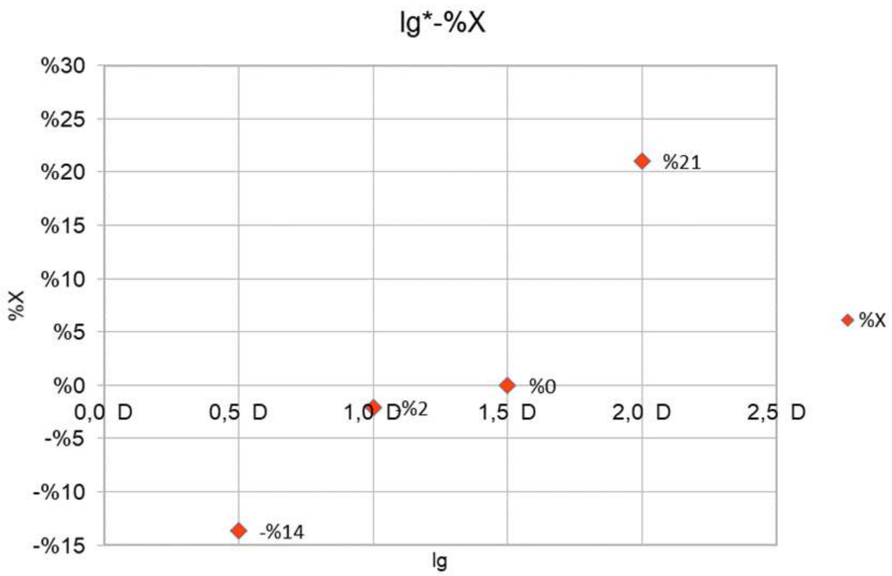

Figure 4.19. Position of max. TKE formation due to different gaps between the cylinder and leading edge of splitter plate (lg*) for porosity β=0.70. Splitter plate length (ls*) is 1.

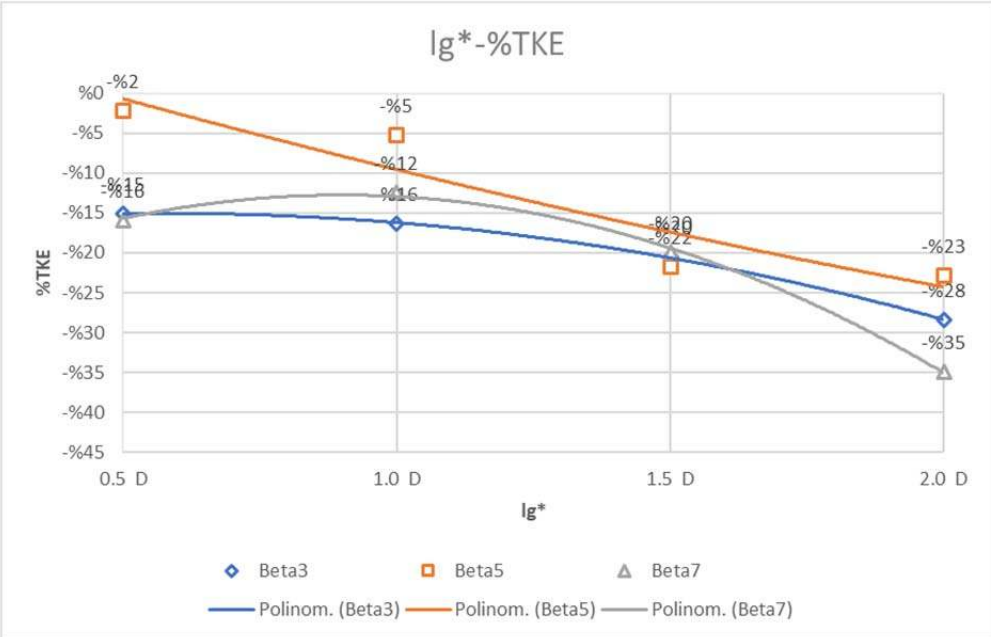

Figure 4.20. TKE var. due to different gaps between the cylinder and leading edge of splitter plate (lg*) for porosity β=0.30, 0.50, 0.70. Splitter plate length (ls*) is 1.

The porosities of the splitter plate were taken as β=0.3, 0.5 and 0.7. Four different gaps where between the cylinder and the splitter plate (lg*=0.5, 1, 1.5 and 2) were investigated (Figure 4.20) and the splitter plate angle and length were kept to constant during the experiments as ls*=1. It is observed that vortex formation delayed with increasing the gap between the splitter plate and the cylinder. Flow control is achieved for the gap lg*=2 and β=0.7. The peak magnitude of TKE is reduced up to 35%, although the location of the peak magnitude of TKE is decreased compared to the bare cylinder for the gap lg*=2 and β=0.7.

It is obviously seen that as the gap between splitter plate and the cylinder increases, turbulent kinetic energy reduced and as the gap between splitter plate and the cylinder increase, formation point of the peak value of turbulent kinetic energy in the flow direction reduced. Any correlation between porosity and maximum TKE formation is not observed.

4.2. Flow Control of a Circular Cylinder by Permeable Splitter Plate with Different Porosities and Length Values

In this case, cylinder diameter (D) is fixed to 60 mm. Height of the cylinder (h) fixed to 7D. The gap (l_g*) between the base of the cylinder and the leading edge of the splitter plate have been chosen constant as lg*=1. The length of the splitter plate (l_s*) have been taken as 1, 2 and 3 in order. The angle of splitter (θ) plate is fixed to 0^0. Splitter plate thickness is chosen constant as 0.8 mm. Splitter plate porosity (β) have been taken as 0.3/0.5/0.7 in order. For each combination two different experiments were performed. The max. value of TKE formation and the coordinate where the maximum value reached is evaluated.

Figure 4.21 shows the vorticity contours, time-averaged velocity vector map, and the streamline patterns in the downstream base of the cylinder cross-sectional plane for Reynolds number of 5000. All values are normalized due to cylinder diameter. For the cylinder with the splitter plate, for porosity value β equals to 0.3 and splitter plate length value equals to 1. Gap value between cylinder and leading edge of splitter plate (lg*) is 1, flow contours extended in flow direction. The peak value of TKE is 0,113. Downstream of the cylinder, a counterclockwise rotating focus F1 and a clockwise rotating focus F2 is detected for Reynolds number of 5000 as expected. The position and the strength of the foci vary depending on splitter plate porosity. The average value of dimensionless distances on X-axis ($(X/D)_{F1}$) and Y-axis ($(Y/D)_{F1}$) for focus point of the F1 are equal to 2.51468 and 2.00524 The average value of dimensionless distances on X-axis ($(X/D)_{F2}$) and Y-axis ($(Y/D)_{F2}$) for focus point of the F2 are equal to 2.45521 and 1.15107. After the peak value reached, the turbulent kinetic energy contours dissipate gradually in the flow direction. Negative values for vorticity contours represented with dashed lines.

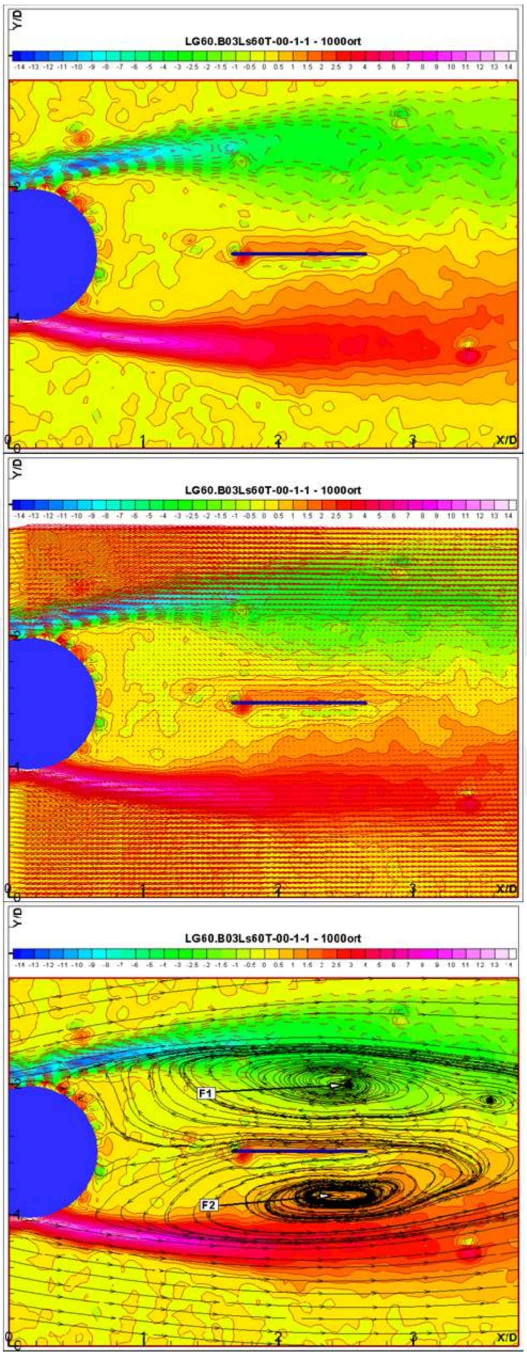

Figure 4.21. Vortex formations for porosity β: 0.3. Splitter plate length (ls*) is 1. The gap between cylinder and leading edge of splitter plate (lg*) is 1.

It is also observed that in the turbulent flow regime, the size of the foci F2 becomes wider with the splitter plate, and their central points shift downwards along the flow axis. F1 foci lose strength due to momentum loss as a result of the splitter plate.

Figure 4.22 shows the vorticity contours, time-averaged velocity vector map, and, the streamline patterns in the downstream base of the cylinder cross-sectional plane for Reynolds number of 5000. All values are normalized due to cylinder diameter. For the cylinder with the splitter plate, for porosity value β equals to 0.3 and splitter plate length value equals to 2. Gap value between cylinder and leading edge of splitter plate (lg*) is 1, flow contours extended in flow direction. The peak value of turbulence kinetic energy (TKE) is 0,093. Downstream of the cylinder, a counterclockwise rotating focus F1 and a clockwise rotating focus F2 is detected for Reynolds number of 5000 as expected. The position and the strength of the foci vary depending on splitter plate porosity. The average value of dimensionless distances on X-axis ($(X/D)_{F1}$) and Y-axis ($(Y/D)_{F1}$) for focus point of the F1 are equal to 2.88138 and 1.95994 The average value of dimensionless distances on X-axis ($(X/D)_{F2}$) and Y-axis ($(Y/D)_{F2}$) for focus point of the F2 are equal to 2.20286 and 1.06627. After the peak value reached, the turbulent kinetic energy contours dissipate gradually in the flow direction. Negative values for vorticity contours represented with dashed lines. It is also observed that in the turbulent flow regime, the size of the foci F2 becomes wider with the splitter plate, and their central points shift downwards along the flow axis. F1 foci lose strength due to momentum loss as a result of the splitter plate.

Figure 4.23 shows the vorticity contours, time-averaged velocity vector map, and, the streamline patterns in the downstream base of the cylinder cross-sectional plane for Reynolds number of 5000. All values are normalized due to cylinder diameter. For the cylinder with the splitter plate, for porosity value β equals to 0.3 and splitter plate length value equals to 3. Gap value between cylinder and leading edge of splitter plate (lg*) is 1, flow contours extended in flow direction.

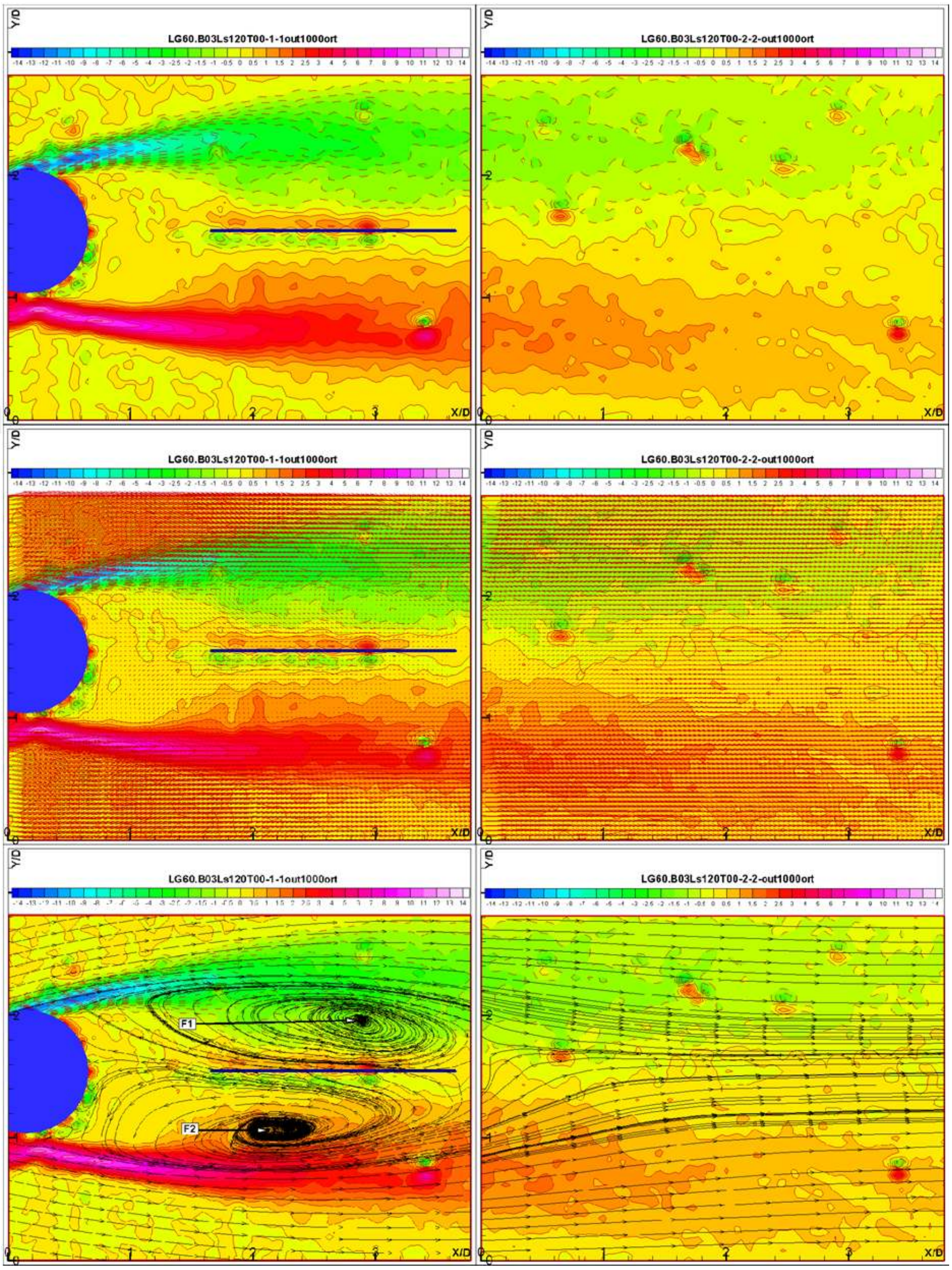

Figure 4.22. Vortex formations for porosity β: 0.3. Splitter plate length (ls*) is 2. The gap between cylinder and leading edge of splitter plate (lg*) is 1.

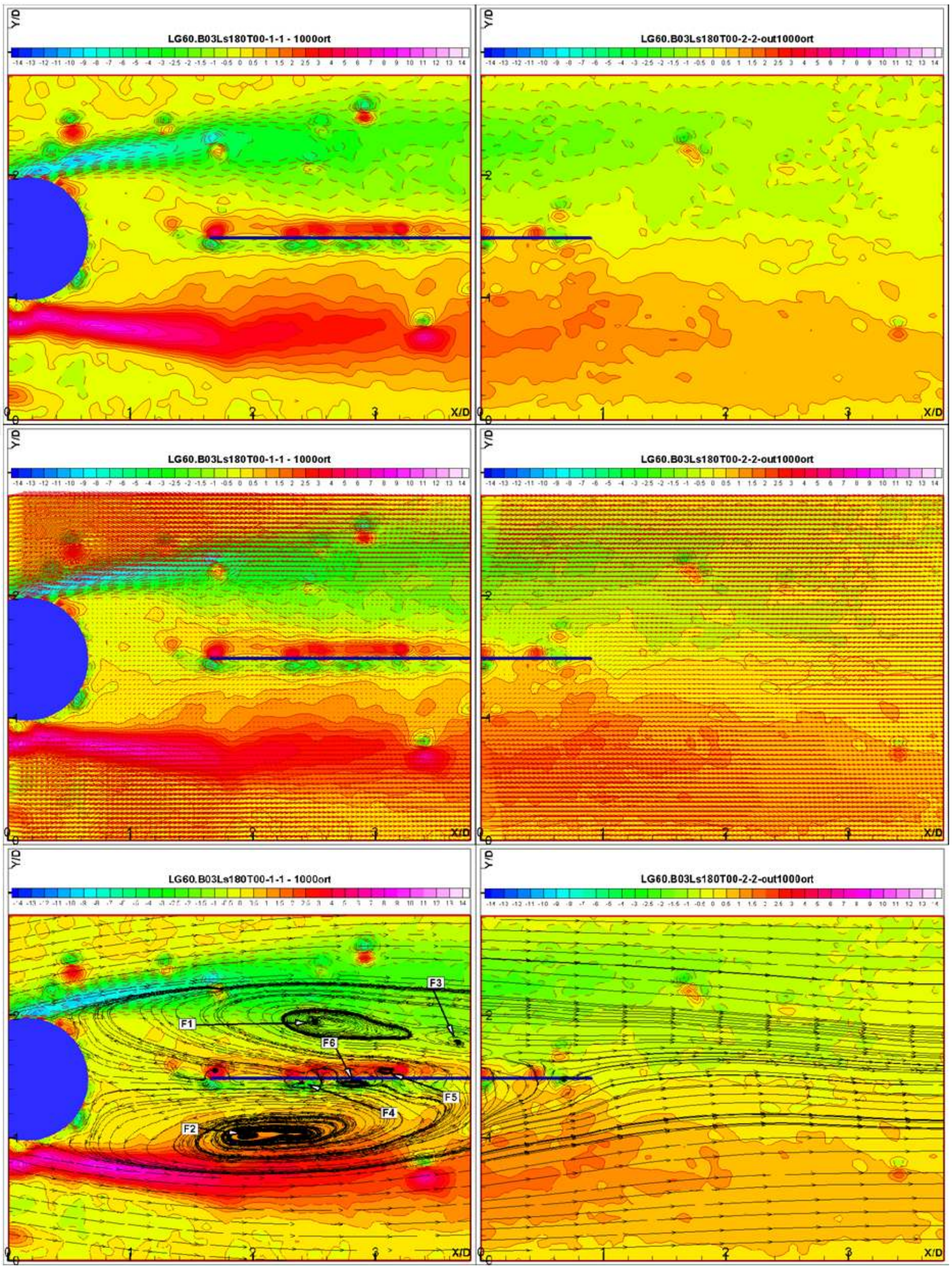

Figure 4.23. Vortex formations for porosity β: 0.3. Splitter plate length (ls*) is 3. The gap between cylinder and leading edge of splitter plate (lg*) is 1.

The peak value of turbulence kinetic energy (TKE) is 0.078. Downstream of the cylinder, a counterclockwise rotating focus F1 and a clockwise rotating focus F2 is detected for Reynolds number of 5000 as expected. The position and the strength of the foci vary depending on splitter plate porosity. The average value of dimensionless distances on X-axis ($(X/D)_{F1}$) and Y-axis ($(Y/D)_{F1}$) for focus point of the F1 are equal to 2.49925 and 1.95229 The average value of dimensionless distances on X-axis ($(X/D)_{F2}$) and Y-axis ($(Y/D)_{F2}$) for focus point of the F2 are equal to 1.95549 and 1.02427. After the peak value reached, the turbulent kinetic energy contours dissipate gradually in the flow direction. Negative values for vorticity contours represented with dashed lines. It is also observed that in the turbulent flow regime, the size of the foci F2 becomes wider with the splitter plate, and their central points shift downwards along the flow axis. F1 foci lose strength due to momentum loss as a result of the splitter plate. Minor vortices foci are appeared behind F1 and around splitter plate.

Figure 4.0-24 shows the vorticity contours, time-averaged velocity vector map, and, the streamline patterns in the downstream base of the cylinder cross-sectional plane for Reynolds number of 5000. All values are normalized due to cylinder diameter. For the cylinder with the splitter plate, for porosity value β equals to 0.5 and splitter plate length value equals to 1. Gap value between cylinder and leading edge of splitter plate (lg*) is 1, flow contours extended in flow direction. The peak value of turbulence kinetic energy (TKE) is 0.128. Downstream of the cylinder, a counterclockwise rotating focus F1 and a clockwise rotating focus F2 is detected for Reynolds number of 5000 as expected. The position and the strength of the foci vary depending on splitter plate porosity. The average value of dimensionless distances on X-axis ($(X/D)_{F1}$) and Y-axis ($(Y/D)_{F1}$) for focus point of the F1 are equal to 2.21735 and 1.96739 The average value of dimensionless distances on X-axis ($(X/D)_{F2}$) and Y-axis ($(Y/D)_{F2}$) for focus point of the F2 are equal to 3.15801 and 1.27541. After the peak value reached, the turbulent kinetic energy contours dissipate gradually in the flow direction.

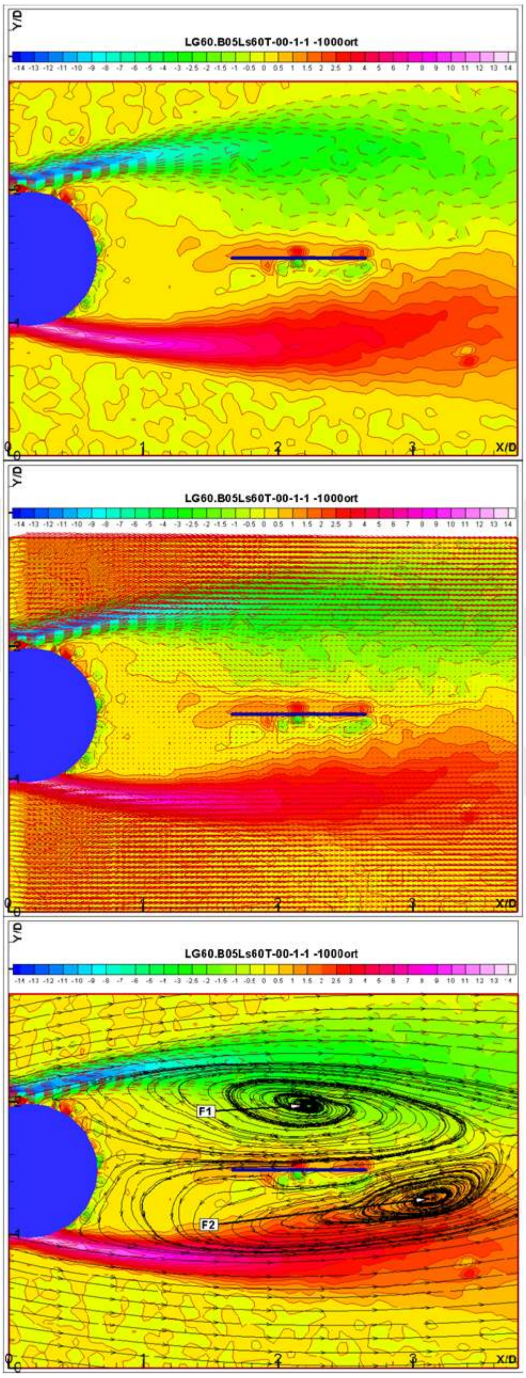

Figure 4.0-24. Vortex formations for porosity β: 0.5. Splitter plate length (ls*) is 1. The gap between cylinder and leading edge of splitter plate (lg*) is 1.

Negative values for vorticity contours represented with dashed lines. It is also observed that in the turbulent flow regime, the size of the foci F2 becomes wider with the splitter plate, and their central points shift downwards along the flow axis. F1 foci lose strength due to momentum loss as a result of the splitter plate.

Figure 4.25 shows the vorticity contours, time-averaged velocity vector map, and, the streamline patterns in the downstream base of the cylinder cross-sectional plane for Reynolds number of 5000. All values are normalized due to cylinder diameter. For the cylinder with the splitter plate, for porosity value β equals to 0.5 and splitter plate length value equals to 2. Gap value between the cylinder and leading edge of splitter plate (lg*) is 1, flow contours extended in flow direction. The peak value of turbulence kinetic energy (TKE) is 0.104. Downstream of the cylinder, a counterclockwise rotating focus F1 and a clockwise rotating focus F2 is detected for Reynolds number of 5000 as expected. The position and the strength of the foci vary depending on splitter plate porosity. The average value of dimensionless distances on X-axis ($(X/D)_{F1}$) and Y-axis ($(Y/D)_{F1}$)for focus point of the F1 are equal to 2.66624 and 1.9227 The average value of dimensionless distances on X-axis ($(X/D)_{F2}$) and Y-axis ($(Y/D)_{F2}$) for focus point of the F2 are equal to 2.63728 and 1.058. After the peak value reached, the turbulent kinetic energy contours dissipate gradually in the flow direction. Negative values for vorticity contours represented with dashed lines. It is also observed that in the turbulent flow regime, the size of the foci F2 becomes wider with the splitter plate, and their central points shift downwards along the flow axis. F1 foci lose strength due to momentum loss as a result of splitter plate. Minor vortices foci have appeared before F2.

Figure 4.26 shows the vorticity contours, time-averaged velocity vector map, and, the streamline patterns in the downstream base of the cylinder cross-sectional plane for Reynolds number of 5000. All values are normalized due to cylinder diameter. For the cylinder with the splitter plate, for porosity value β equals to 0.5 and splitter plate length value equals to 3. Gap value between cylinder and leading edge of splitter plate (lg*) is 1, flow contours extended in flow direction.

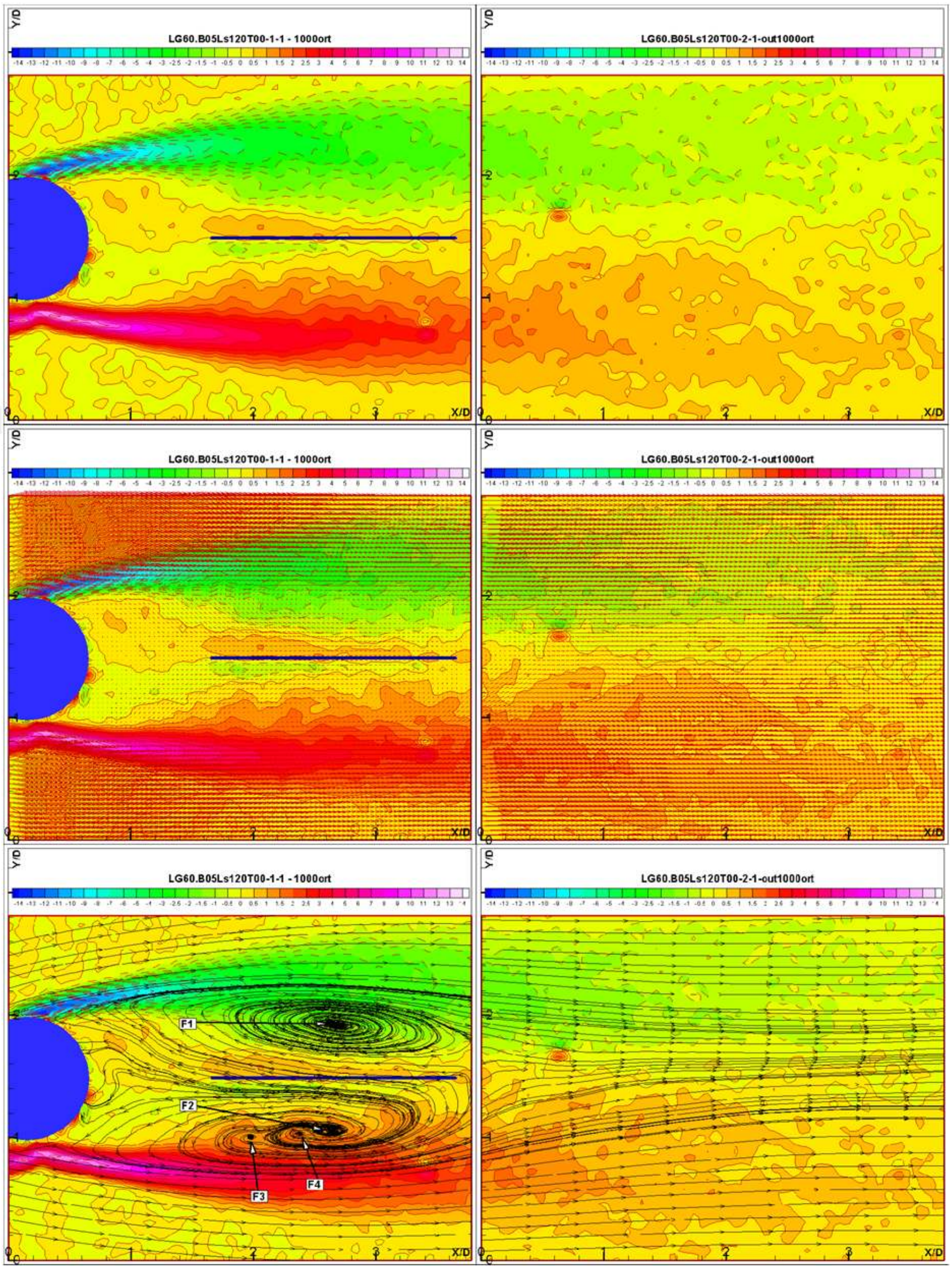

Figure 4.25. Vortex formations for porosity β: 0.5. Splitter plate length (ls*) is 2. Gap between the cylinder and leading edge of splitter plate (lg*) is 1.

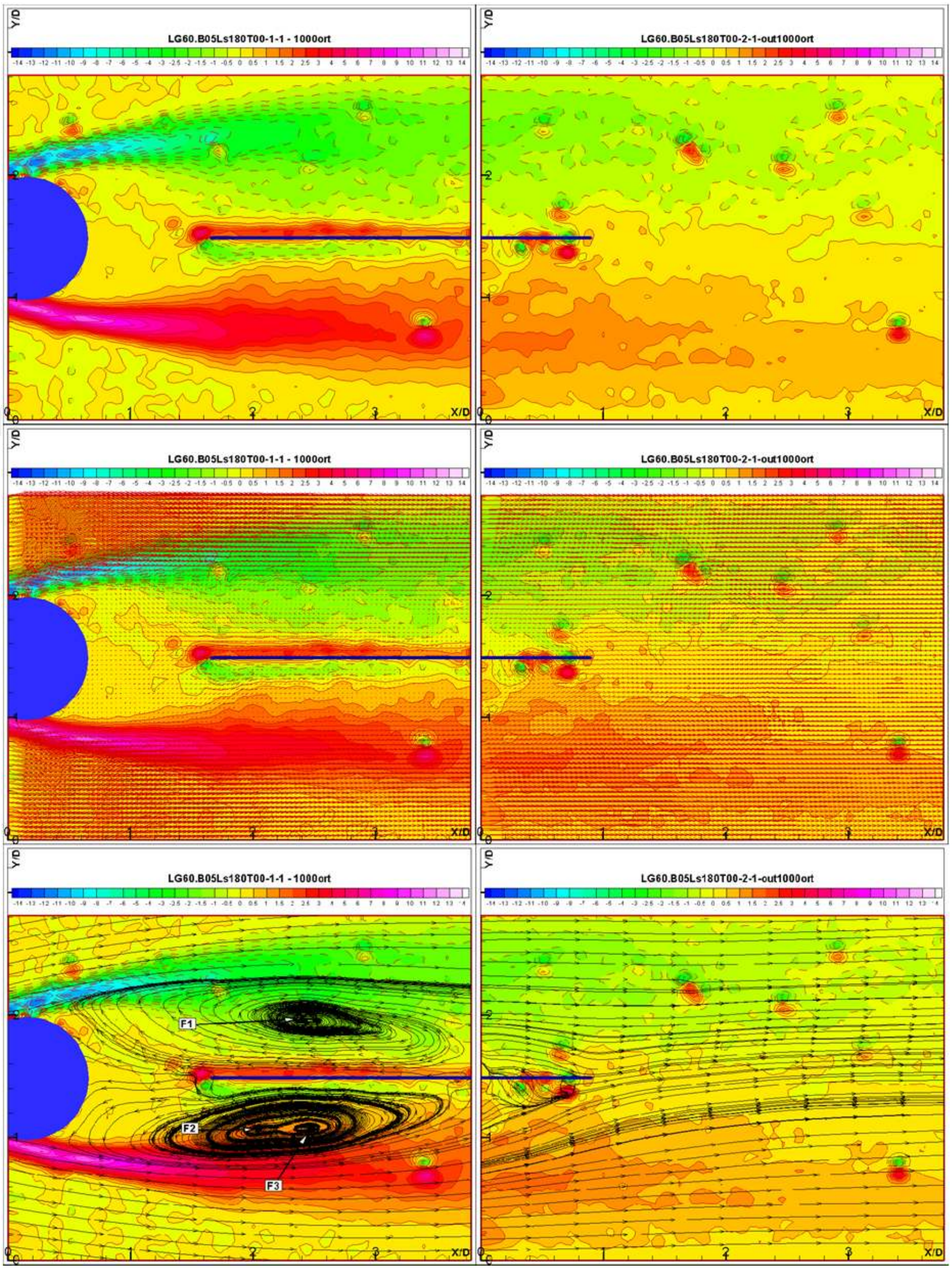

Figure 4.26. Vortex formations for porosity β: 0.5. Splitter plate length (ls*) is 3. Gap between the cylinder and leading edge of splitter plate (lg*) is 1.

The peak value of turbulence kinetic energy (TKE) is 0.083. Downstream of the cylinder, a counterclockwise rotating focus F1 and a clockwise rotating focus F2 is detected for Reynolds number of 5000 as expected. The position and the strength of the foci vary depending on splitter plate porosity. The average value of dimensionless distances on X-axis ($(X/D)_{F1}$) and Y-axis ($(Y/D)_{F1}$) for focus point of the F1 are equal to 2.47593 and 1.95994 The average value of dimensionless distances on X-axis ($(X/D)_{F2}$) and Y-axis ($(Y/D)_{F2}$) for focus point of the F2 are equal to 2.04564 and 1.06214. After the peak value reached, the turbulent kinetic energy contours dissipate gradually in the flow direction. Negative values for vorticity contours represented with dashed lines. It is also observed that in the turbulent flow regime, the size of the foci F2 becomes wider with the splitter plate, and their central points shift downwards along the flow axis. F1 foci lose strength due to momentum loss as a result of the splitter plate. Minor vortices foci have appeared before F2.

Figure 4.27 shows the vorticity contours, time-averaged velocity vector map, and, the streamline patterns in the downstream base of the cylinder cross-sectional plane for Reynolds number of 5000. All values are normalized due to cylinder diameter. For the cylinder with the splitter plate, for porosity value β equals to 0.3 and splitter plate length value equals to 1. Gap value between cylinder and leading edge of splitter plate (lg*) is 1, flow contours extended in flow direction. The peak value of turbulence kinetic energy (TKE) is 0.118. Downstream of the cylinder, a counterclockwise rotating focus F1 and a clockwise rotating focus F2 is detected for Reynolds number of 5000 as expected. The position and the strength of the foci vary depending on splitter plate porosity. The average value of dimensionless distances on X-axis ($(X/D)_{F1}$) and Y-axis ($(Y/D)_{F1}$) for focus point of the F1 are equal to 3.33101 and 1.76737 The average value of dimensionless distances on X-axis ($(X/D)_{F2}$) and Y-axis ($(Y/D)_{F2}$) for focus point of the F2 are equal to 2.14166 and 1.07538. After the peak value reached, the turbulent kinetic energy contours dissipate gradually in the flow direction.

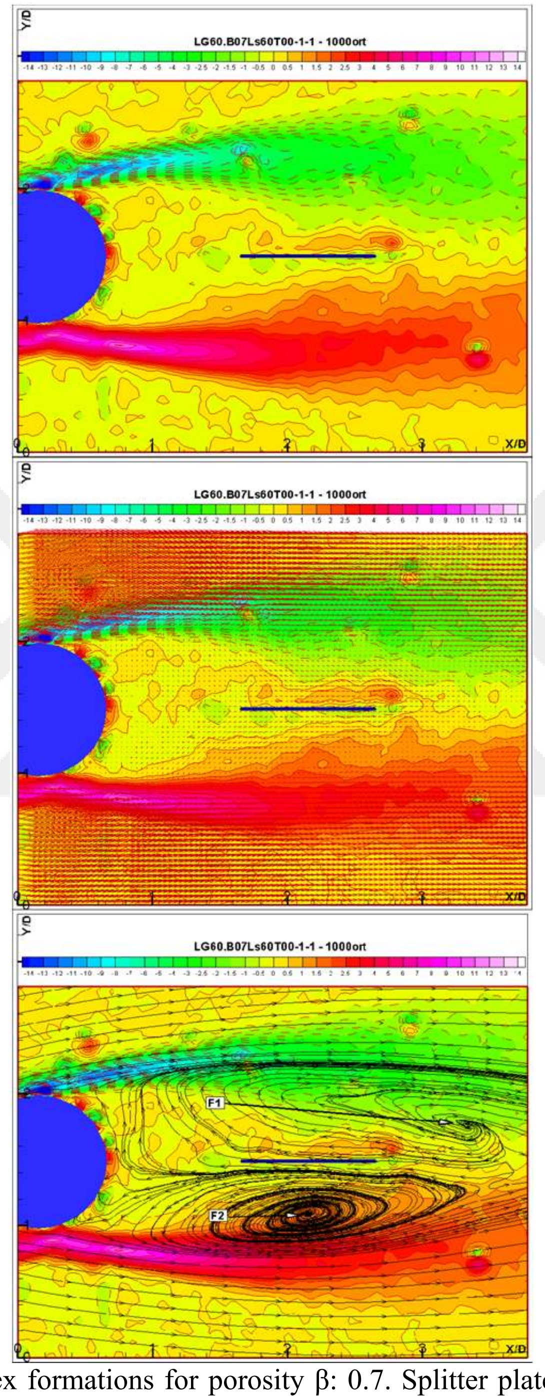

Figure 4.27. Vortex formations for porosity β: 0.7. Splitter plate length (ls*) is 1. The gap between cylinder and leading edge of splitter plate (lg*) is 1.

Negative values for vorticity contours represented with dashed lines. It is also observed that in the turbulent flow regime, the size of the foci F2 becomes wider with the splitter plate, and their central points shift downwards along the flow axis. F1 foci lose strength due to momentum loss as a result of the splitter plate.

Figure 4.28 shows the vorticity contours, time-averaged velocity vector map, and, the streamline patterns in the downstream base of the cylinder cross-sectional plane for Reynolds number of 5000. All values are normalized due to cylinder diameter. For the cylinder with the splitter plate, for porosity value β equals to 0.3 and splitter plate length value equals to 2. Gap value between cylinder and leading edge of splitter plate (lg*) is 1, flow contours extended in flow direction. The peak value of turbulence kinetic energy (TKE) is 0.099. Downstream of the cylinder, a counterclockwise rotating focus F1 and a clockwise rotating focus F2 is detected for Reynolds number of 5000 as expected. The position and the strength of the foci vary depending on splitter plate porosity. The average value of dimensionless distances on X-axis ($(X/D)_{F1}$) and Y-axis ($(Y/D)_{F1}$) for focus point of the F1 are equal to 2.43869 and 1.91443. The average value of dimensionless distances on X-axis ($(X/D)_{F2}$) and Y-axis ($(Y/D)_{F2}$) for focus point of the F2 are equal to 2.17804 and 1.07041. After the peak value reached, the turbulent kinetic energy contours dissipate gradually in the flow direction. Negative values for vorticity contours represented with dashed lines. It is also observed that in the turbulent flow regime, the size of the foci F2 becomes wider with the splitter plate, and their central points shift downwards along the flow axis. F1 foci lose strength due to momentum loss as a result of the splitter plate.

Figure 4.29 shows the vorticity contours, time-averaged velocity vector map, and, the streamline patterns in the downstream base of the cylinder cross-sectional plane for Reynolds number of 5000. All values are normalized due to cylinder diameter. For the cylinder with the splitter plate, for porosity value β equals to 0.3 and splitter plate length value equals to 2. Gap value between the cylinder and leading edge of splitter plate (lg*) is 1, flow contours extended in flow direction.

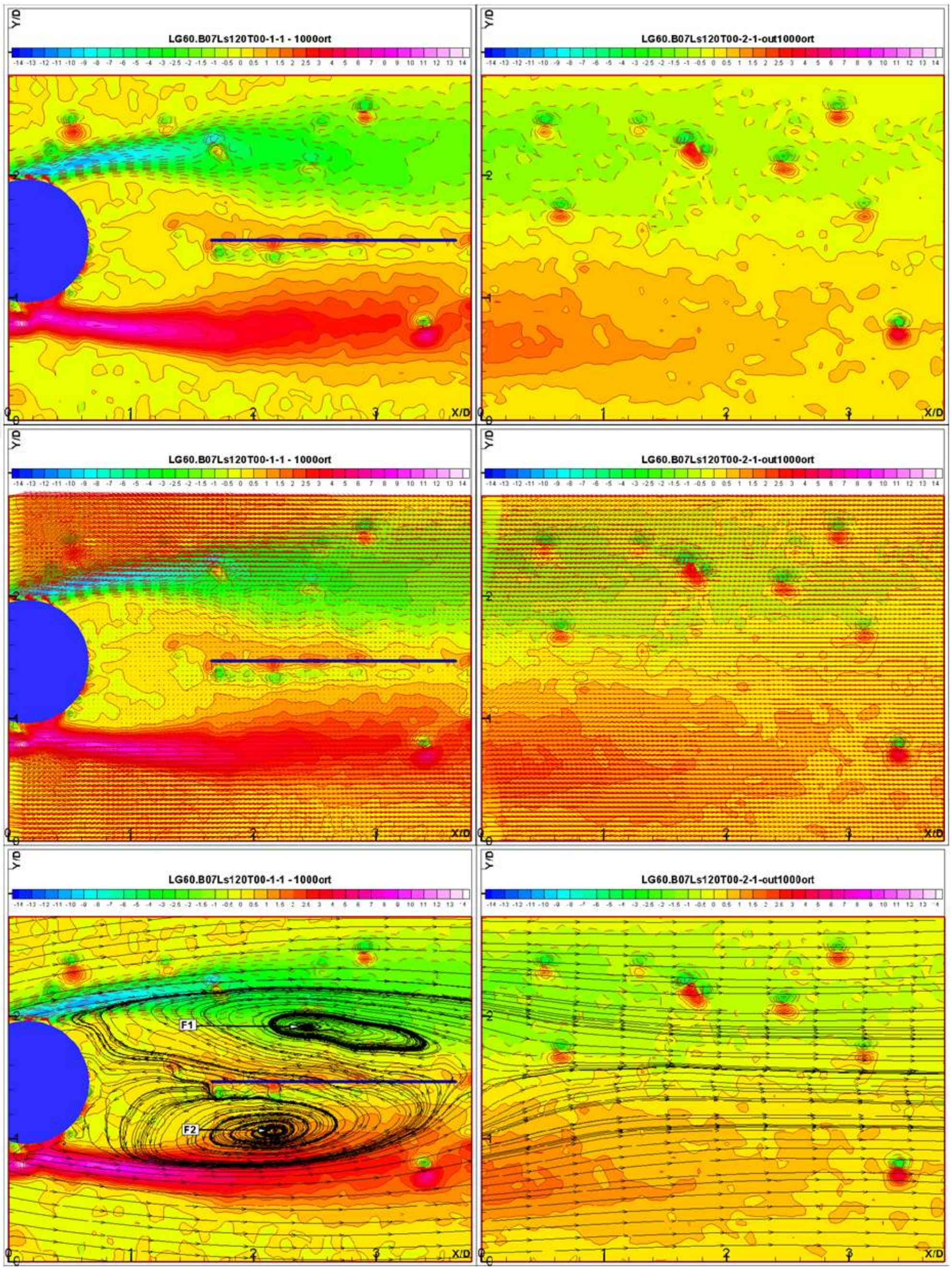

Figure 4.28. Vortex formations for the porosity of β: 0.7. Splitter plate length (ls*) is 2. The gap between cylinder and leading edge of splitter plate (lg*) is 1.

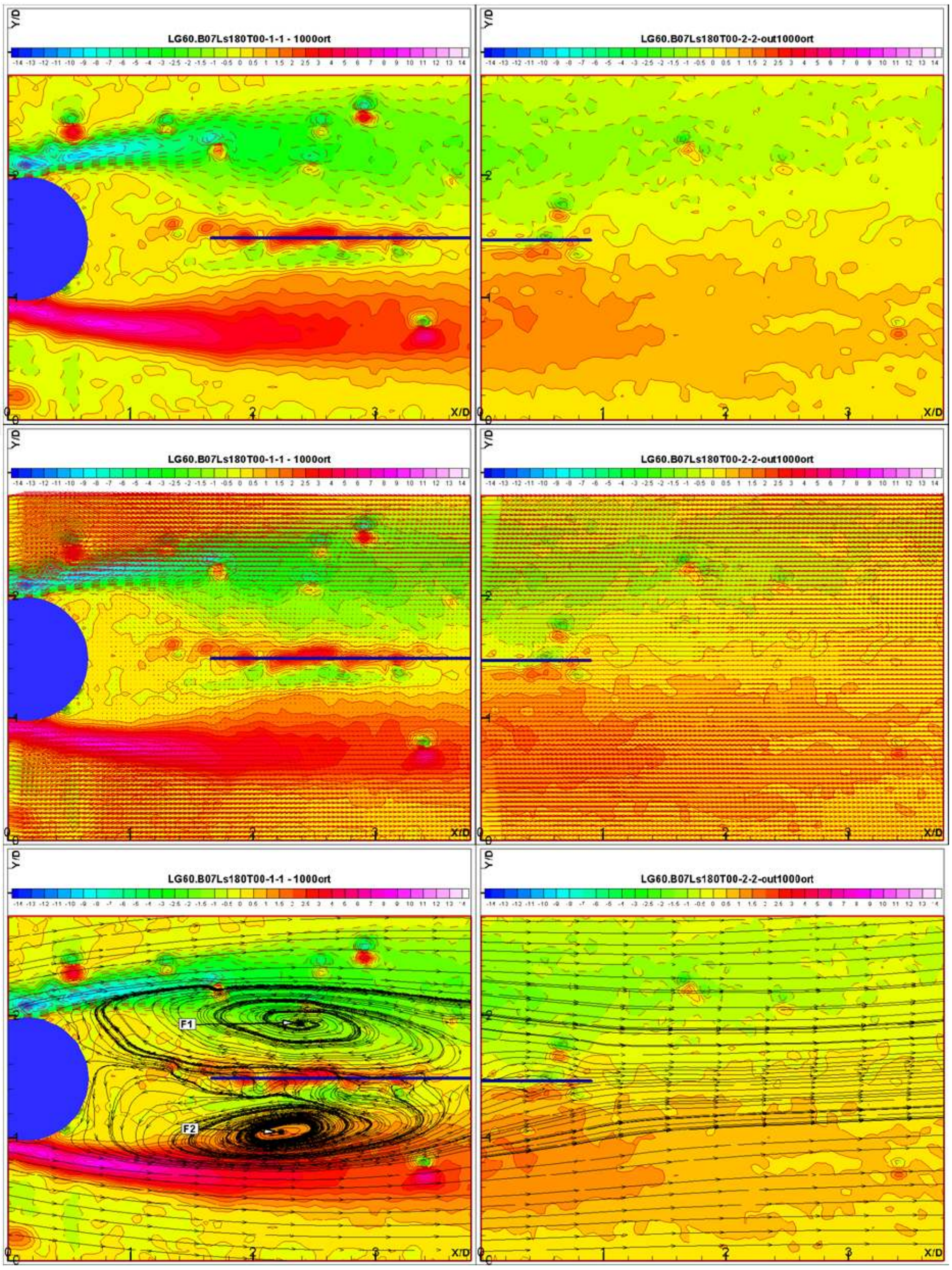

Figure 4.29. Vortex formations for porosity β: 0.7. Splitter plate length (ls*) is 3. The gap between cylinder and leading edge of splitter plate (lg*) is 1.

The peak value of turbulence kinetic energy (TKE) is 0.093. Downstream of the cylinder, a counter-clockwise rotating focus F1 and a clockwise rotating focus F2 is detected for Reynolds number of 5000 as expected. The position and the strength of the foci vary depending on splitter plate porosity. The average value of dimensionless distances on X-axis ($(X/D)_{F1}$) and Y-axis ($(Y/D)_{F1}$) for focus point of the F1 are equal to 2.39318 and 1.93925. The average value of dimensionless distances on X-axis ($(X/D)_{F2}$) and Y-axis ($(Y/D)_{F2}$) for focus point of the F2 are equal to 2.23182 and 1.04559. After the peak value reached, the turbulent kinetic energy contours dissipate gradually in the flow direction. Negative values for vorticity contours represented with dashed lines. It is also observed that in the turbulent flow regime, the size of the foci F2 becomes wider with the splitter plate, and their central points shift downwards along the flow axis. F1 foci lose strength due to momentum loss as a result of the splitter plate.

Figure 4.30 shows that a decrease in turbulent kinetic energy is obtained by the ls^* increase. The peak values of turbulent kinetic energy for splitter plate length values ls^* =1, 2 and 3 are reduced by 16%, %31 and 42% in order, for the porosity value β=0.3. Formation point of the peak value of turbulent kinetic energy in the flow direction for splitter plate length values ls^* =1, 2 and 3 are increased by 0%, 30% and 25% in order, for the porosity value β=0.3. (Figure 4.31)

The peak values of turbulent kinetic energy for splitter plate length values ls^* =1, 2 and 3 are reduced by 5%, 23% and 38% in order (Figure 4.16), for the porosity value β=0.5 (Figure 4.32). Formation point of the peak value of turbulent kinetic energy in the flow direction for splitter plate length values ls^* = 2 and 3 are increased by 33% and 21% in order, for the porosity value β=0.5. For ls^* = 1, formation point of peak value of turbulent kinetic energy in the flow direction is reduced by 9%.

The peak values of turbulent kinetic energy for splitter plate length values ls^* = 1, 2 and 3 are reduced by 12%, 27% and 31% in order (Figure 4.18), for the porosity value β=0.7 (Figure 4.34). Formation point of the peak value of turbulent kinetic energy in the flow direction for splitter plate length values ls^* =2 and 3 are increased by 20% and 3% in order, for the porosity value β=0.7. For ls^* = 1, formation point of peak value of turbulent kinetic energy in the flow direction is reduced by 2%.

It is obviously seen that as the splitter plate length increase, turbulent kinetic energy is reduced. Also, as the splitter plate length values increase, the formation point of the peak value of turbulent kinetic energy in the flow direction increased in most cases.

The peak values of turbulent kinetic energy for porosity values β=0.3, 0.5 and 0.7 are reduced by 16%, 5% and 12% in order (Figure 4.37), for the ls^* =1 and lg^*=1. Formation point of peak value of turbulent kinetic energy in the flow direction for porosity values β=0.3, 0.5 and 0.7 are reduced by 0%, 9% and 2% in order (Figure 4.38), for the ls^* = 1 and lg^* = 1.

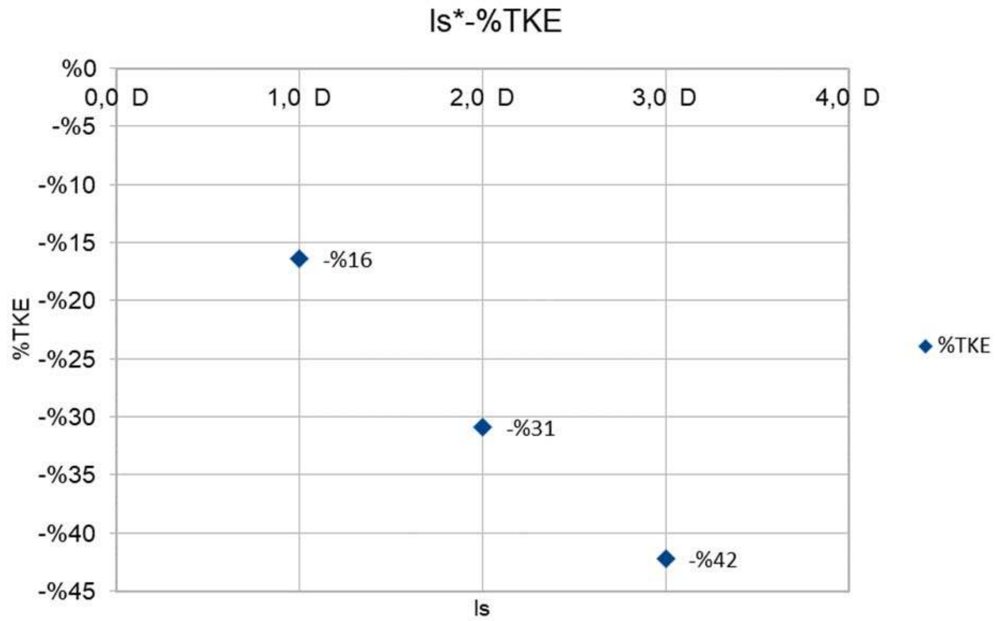

Figure 4.30. TKE var. due to different splitter plate lengths (ls*) for porosity β=0.30. The gap between cylinder and leading edge of splitter plate (lg*) is 1.

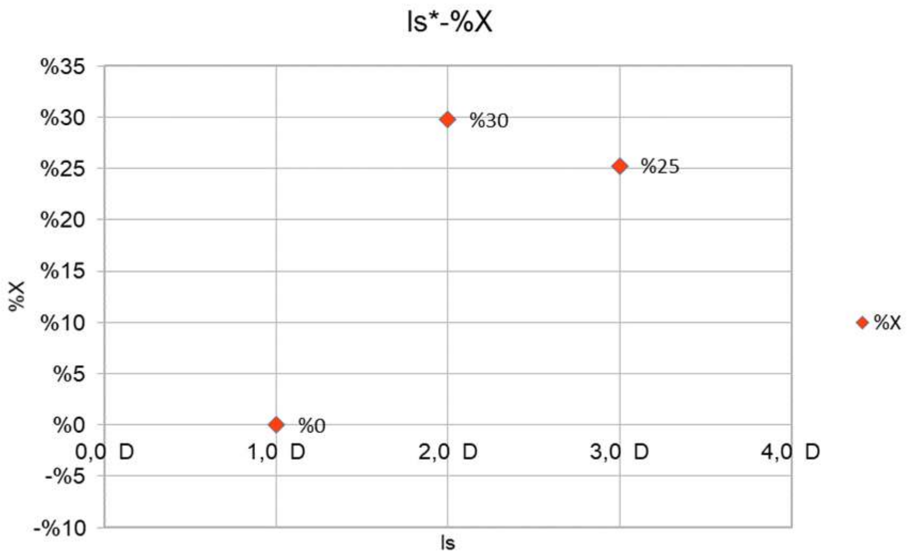

Figure 4.31. Position of max. TKE formation due to different splitter plate lengths (ls*) for porosity β=0.30. The gap between cylinder and leading edge of splitter plate (lg*) is 1.

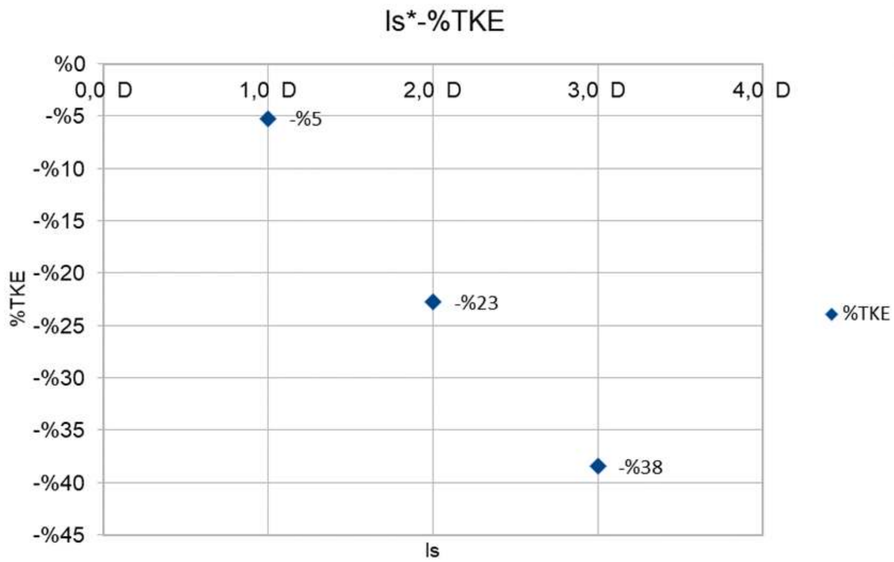

Figure 4.32. TKE var. due to different splitter plate lengths (ls*) for porosity β=0.50. The gap between cylinder and leading edge of splitter plate (lg*) is 1.

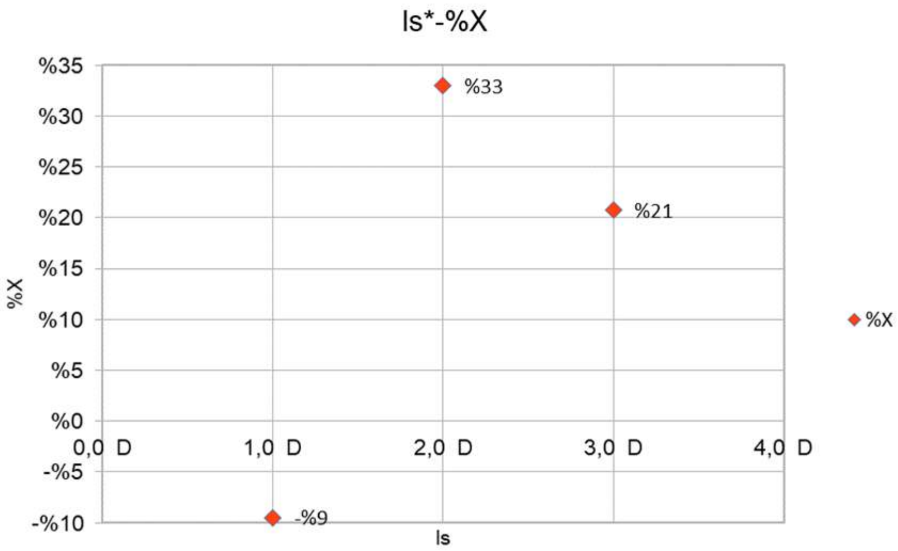

Figure 4.33. Position of max. TKE formation due to different splitter plate lengths (ls*) for porosity β=0.50. The gap between cylinder and leading edge of splitter plate (lg*) is 1.

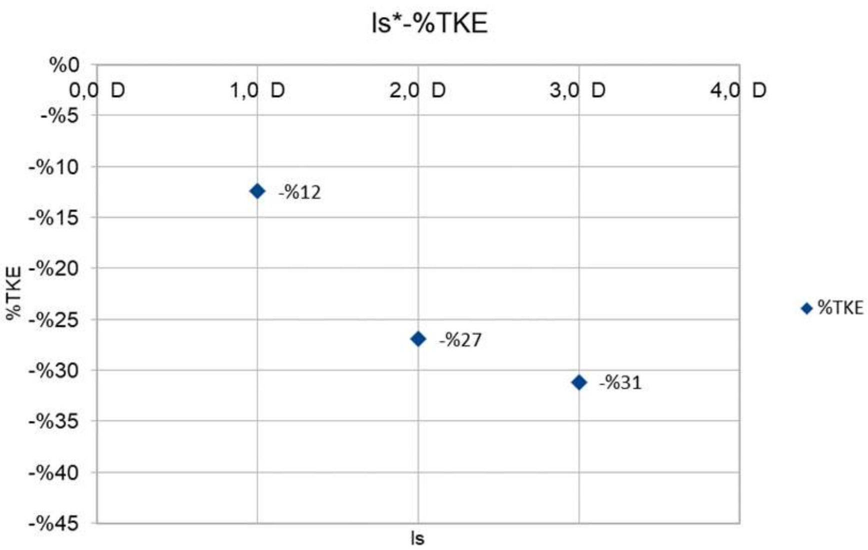

Figure 4.34. TKE var. due to different splitter plate lengths (ls*) for porosity β=0.70. The gap between cylinder and leading edge of splitter plate (lg*) is 1.

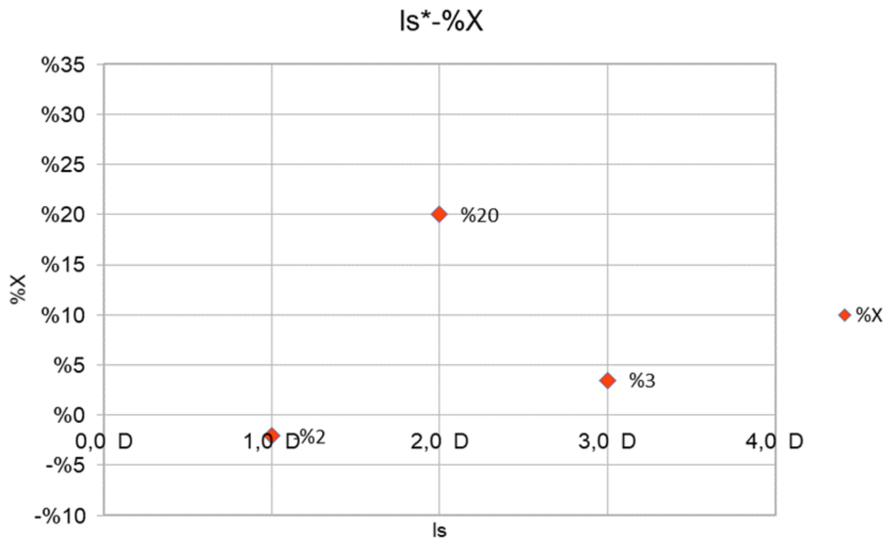

Figure 4.35. Position of max. TKE formation due to different splitter plate lengths (ls*) for porosity β=0.70. The gap between cylinder and leading edge of splitter plate (lg*) is 1.

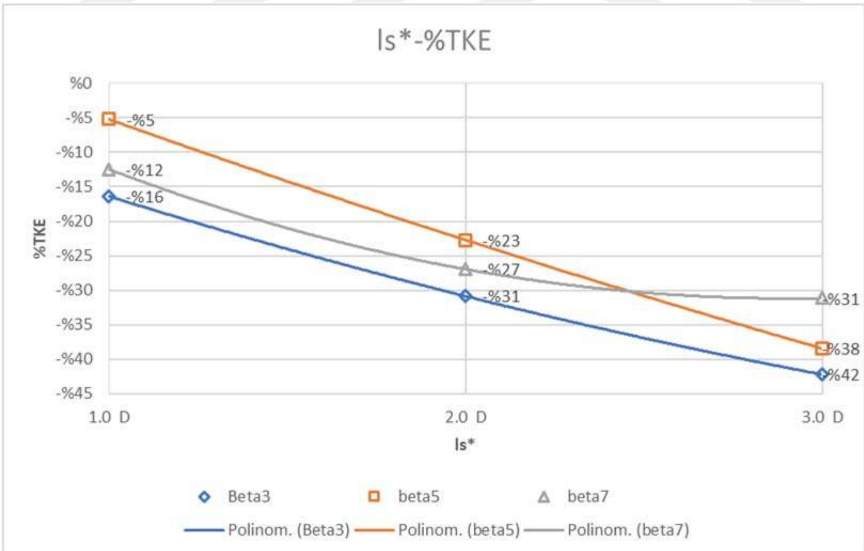

Figure 4.36. TKE variation due to different splitter plate lengths (ls*) for porosity β=0.30, 0.50, 0.70. The gap between cylinder and leading edge of splitter plate (lg*) is 1.

The peak values of turbulent kinetic energy for porosity values β=0.3, 0.5 and 0.7 are reduced by 31%, 23% and 27% in order (Figure 4.39), for the ls^* =2 and lg^* =1. Formation point of peak value of turbulent kinetic energy in the flow direction for porosity values β=0.3, 0.5 and 0.7 are increased by 30%, 33% and 20% in order (Figure 4,40), for the ls^* = 2 and lg^* = 1.

The peak values of turbulent kinetic energy for porosity values β=0.3, 0.5 and 0.7 are reduced by %42, %38 and %31 in order (Figure 4.41), for the ls^* =3 and lg^* =1. Formation point of peak value of turbulent kinetic energy in the flow direction for porosity values β=0.3, 0.5 and 0.7 are increased by 25%, 21% and 3% in order (Figure 4.42), for the ls^* = 3 and lg^* = 1.

Any correlation between porosity and TKE, and porosity and peak value coordinates of TKE is not observed.

Three different the splitter plate length values (ls*=1, 2 and 3) were investigated and the splitter plate angle and the gap between splitter plate and cylinder were kept to constant during the experiments as lg*=1. As splitter plate length increases, turbulent kinetic energy reduced in all situation. Also, the formation point of peak value of turbulent kinetic energy in the flow direction increased nearly in all situations except ls*=1, β=0.50, lg*=1 and ls*=1, β=0.70, lg*=1 situations.

To define the porosity effect, TKE variation due to porosity values 0.3/0.5/0.7, with constant values of ls and lg, is investigated. The effect of splitter plate length is obviously seen in these investigations, but the effect of the porosity is not observed.

Flow control is achieved for the gap ls*=3 and β=0.3. The peak magnitude of TKE is reduced up to 42%, although the location of the peak magnitude of TKE is increased by 25%.

The effect of splitter plate length is obviously seen in these investigations, but the effect of the porosity is not observed.

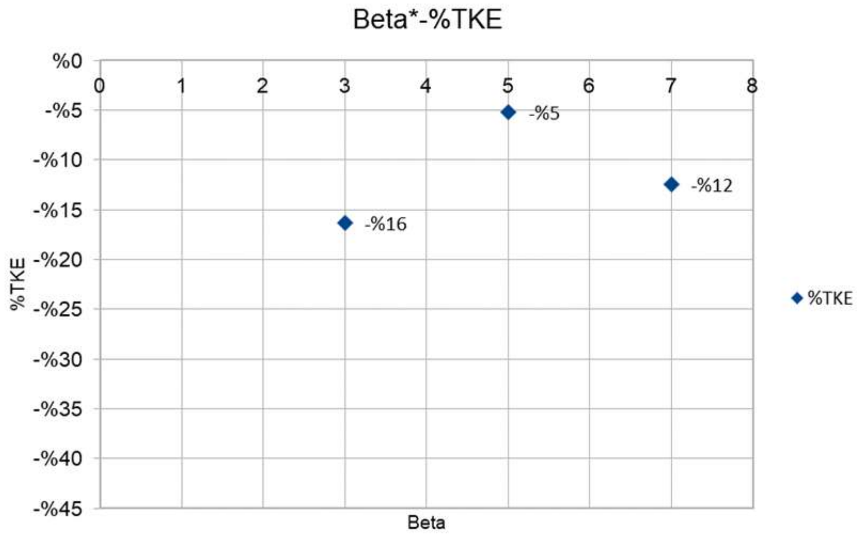

Figure 4.37. TKE variation due to different porosity values of β=0.30, 0.50, 0.70. The gap between cylinder and leading edge of splitter plate (lg*) is1. Splitter plate length (ls*) is 1.

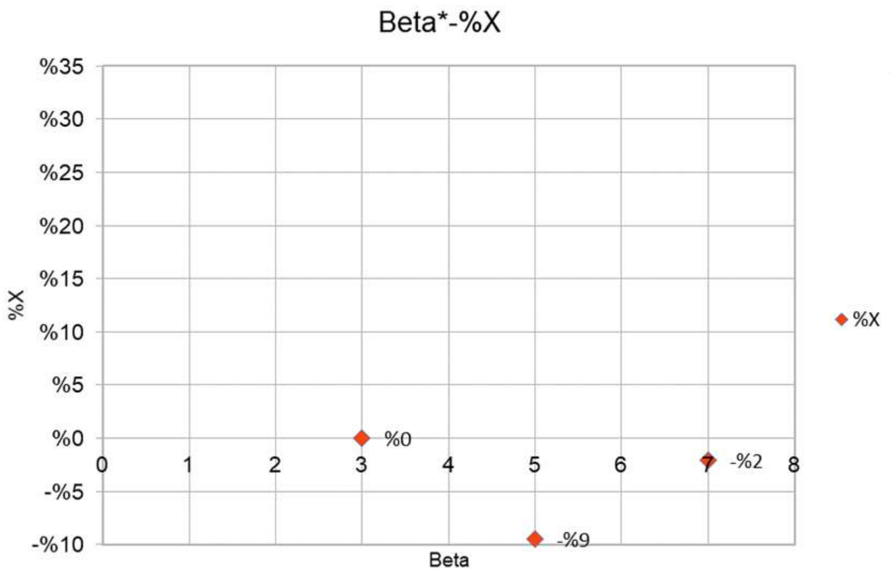

Figure 4.38. Position of max. TKE formation due to different porosity values of β=0.30, 0.50, 0.70. The gap between cylinder and leading edge of splitter plate (lg*) is 1. Splitter plate lengths (ls*) is 1.

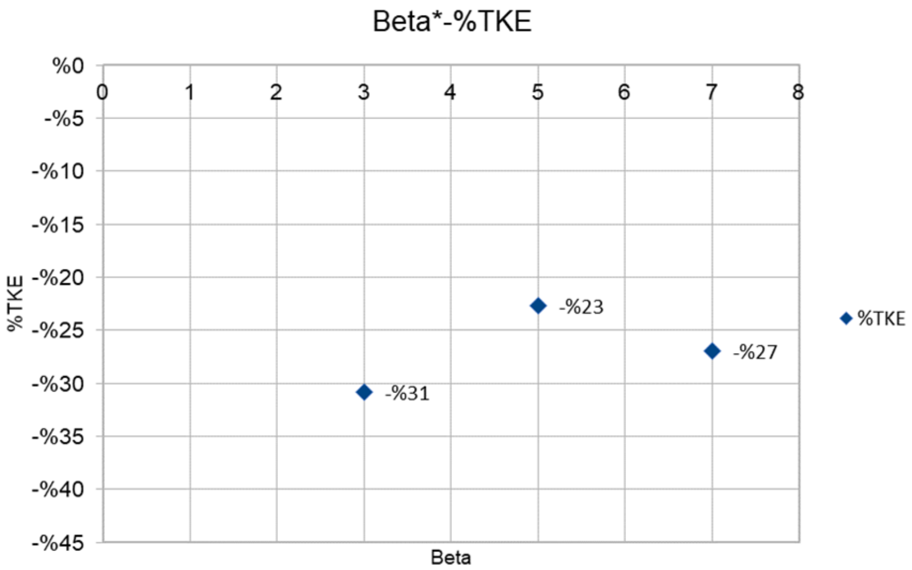

Figure 4.39. TKE variation due to different porosities β=0.30, 0.50, 0.70. The gap between cylinder and leading edge of splitter plate (lg*) is 1. Splitter plate length (ls*) is 2.

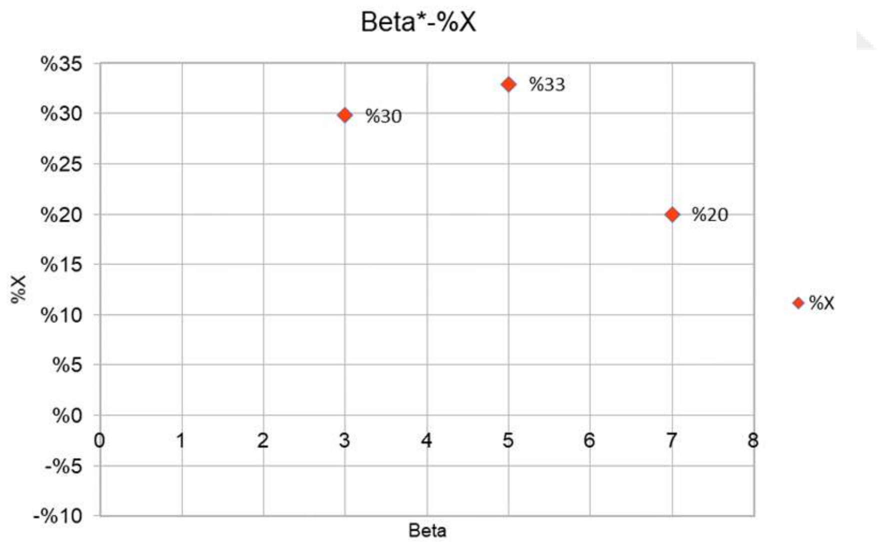

Figure 4,40. Position of max. TKE formation due to different porosity values of β=0.30, 0.50, 0.70. The gap between cylinder and leading edge of splitter plate (lg*) is 1. Splitter plate length (ls*) is 2.

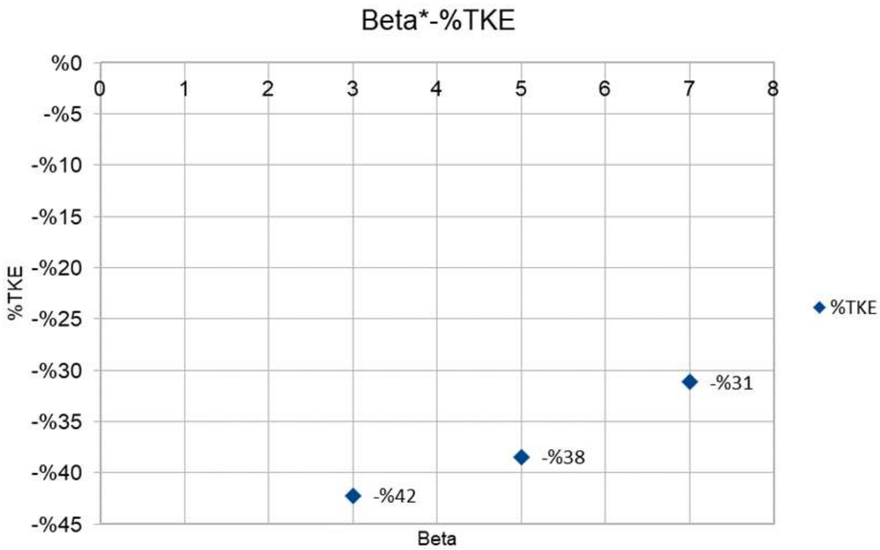

Figure 4.41. TKE var. due to different porosities β=0.30, 0.50, 0.70. The gap between cylinder and leading edge of splitter plate (lg*) is 1. Splitter plate length value (ls*) is 3.

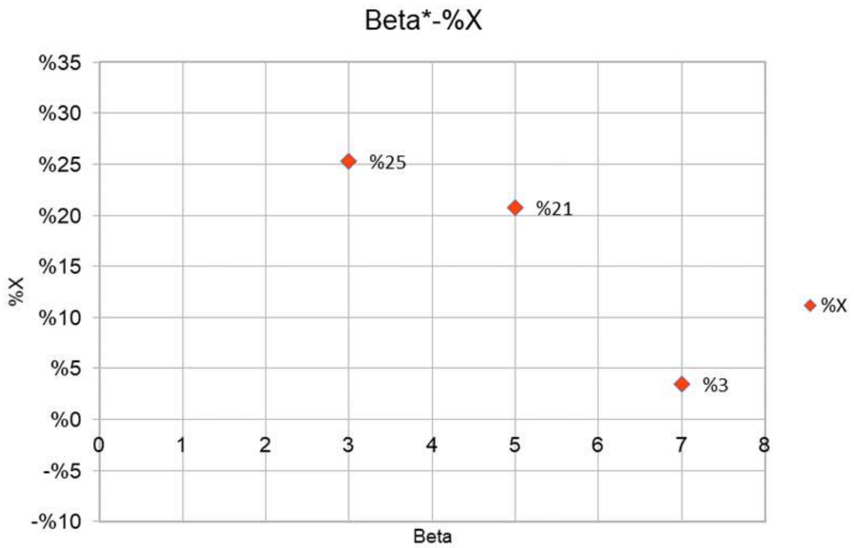

Figure 4.42. Position of max. TKE formation due to different porosity values of β=0.30, 0.50, 0.70. The gap between cylinder and leading edge of splitter plate (lg*) is 1. Splitter plate length value (ls*) is 3.

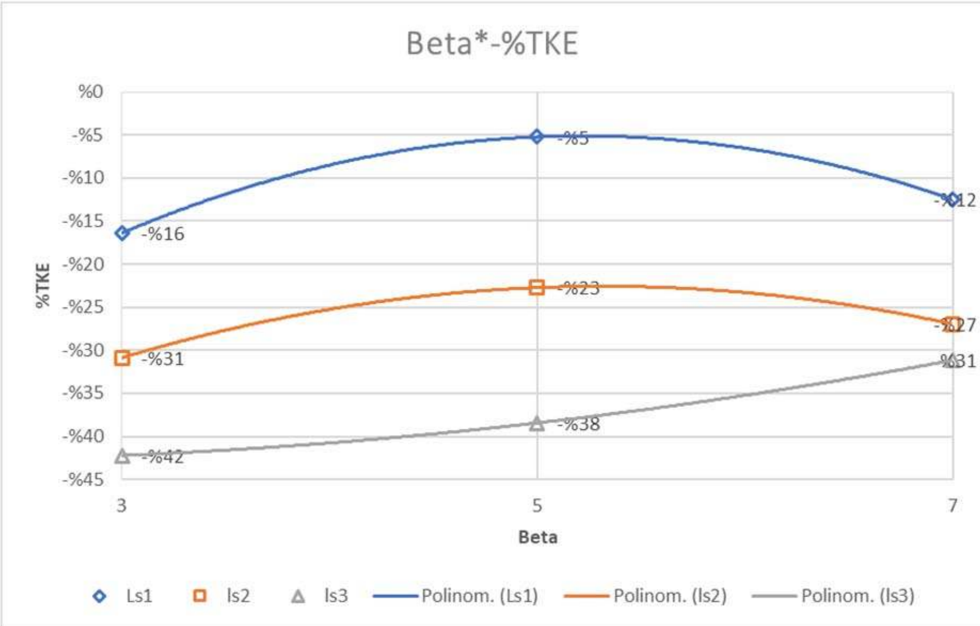

Figure 4.43. TKE variation due to different porosity values of β=0.30, 0.50, 0.70 due to splitter plate lengths (ls*) of 1, 2, 3. The gap between cylinder and leading edge of splitter plate (lg) is 1

4.3. Flow Control of a Circular Cylinder by Permeable Splitter Plate with Different Porosities and Angle Values

In this study, cylinder diameter (D) is fixed to 60 mm. Height of the cylinder (h) fixed to 7D. Seven different the splitter plate angle values (θ =0; 15; 30; 45; 60; 75; 90) and three different porosity values (β=0.30; 0.50; 0.70) were investigated and the splitter plate length (ls) and the gap between splitter plate midpoint and cylinder (lg^{**}) were kept to constant during the experiments as ls=D and lg^{**}=1,5D. Splitter plate thickness is chosen constant as 0.8 mm.

$$lg^{**} = \frac{lg}{D} + ls^{*}/2 \qquad (3.6)$$

For each combination, two different experiments were performed. The maximum value of Turbulent Kinetic Energy formation and the coordinate where the maximum value reached is evaluated.

The flow characteristics of a cylinder with splitter plates with different angle values of θ (0;15;30;45;60;75;90) and different porosity value of β 0.3 are given in Figure 4.44, Figure 4.45, Figure 4.46, Figure 4.47.

Figure 4.44 shows the vorticity contours, time-averaged velocity vector map, and, the streamline patterns in the downstream base of the cylinder cross-sectional plane for Reynolds number of 5000. All values are normalized due to cylinder diameter. For the cylinder with the splitter plate, for porosity value β equals to 0.3 and splitter plate length value equals to 1. the gap between splitter plate midpoint and cylinder (lg**) is equal to 1.5 times cylinder diameter. Flow contours extended in flow direction. Rotation angles of splitter plate due to its median are 0 and 15 degrees in order columns. The peak value of turbulence kinetic energy (TKE) is 0.107 for 0 degrees. Downstream of the cylinder, a counter-clockwise rotating focus F1 and a clockwise rotating focus F2 is detected for Reynolds number of 5000 as expected. The position and the strength of the foci vary depending on splitter plate porosity. The average value of dimensionless distances on X-axis ($(X/D)_{F1}$) and Y-axis ($(Y/D)_{F1}$)for focus point of the F1 are equal to 2.15518 and 2.04849 The average value of dimensionless distances on X-axis ($(X/D)_{F2}$) and Y-axis ($(Y/D)_{F2}$) for focus point of the F2 are equal to 2.04146 and 1.14026. After the peak value reached, the turbulent kinetic energy contours dissipate gradually in the flow direction. Negative values for vorticity contours represented with dashed lines. It is also observed that in the turbulent flow regime, the size of the foci F2 becomes wider with the splitter plate, and their central points shift downwards along the flow axis. F1 foci lose strength due to momentum loss as a result of the splitter plate. The peak value of turbulence kinetic energy (TKE) is 0.100 for 15 degrees. Downstream of the cylinder, a counter-clockwise rotating focus F1 and a clockwise rotating focus F2 is detected for Reynolds number of 5000 as expected.

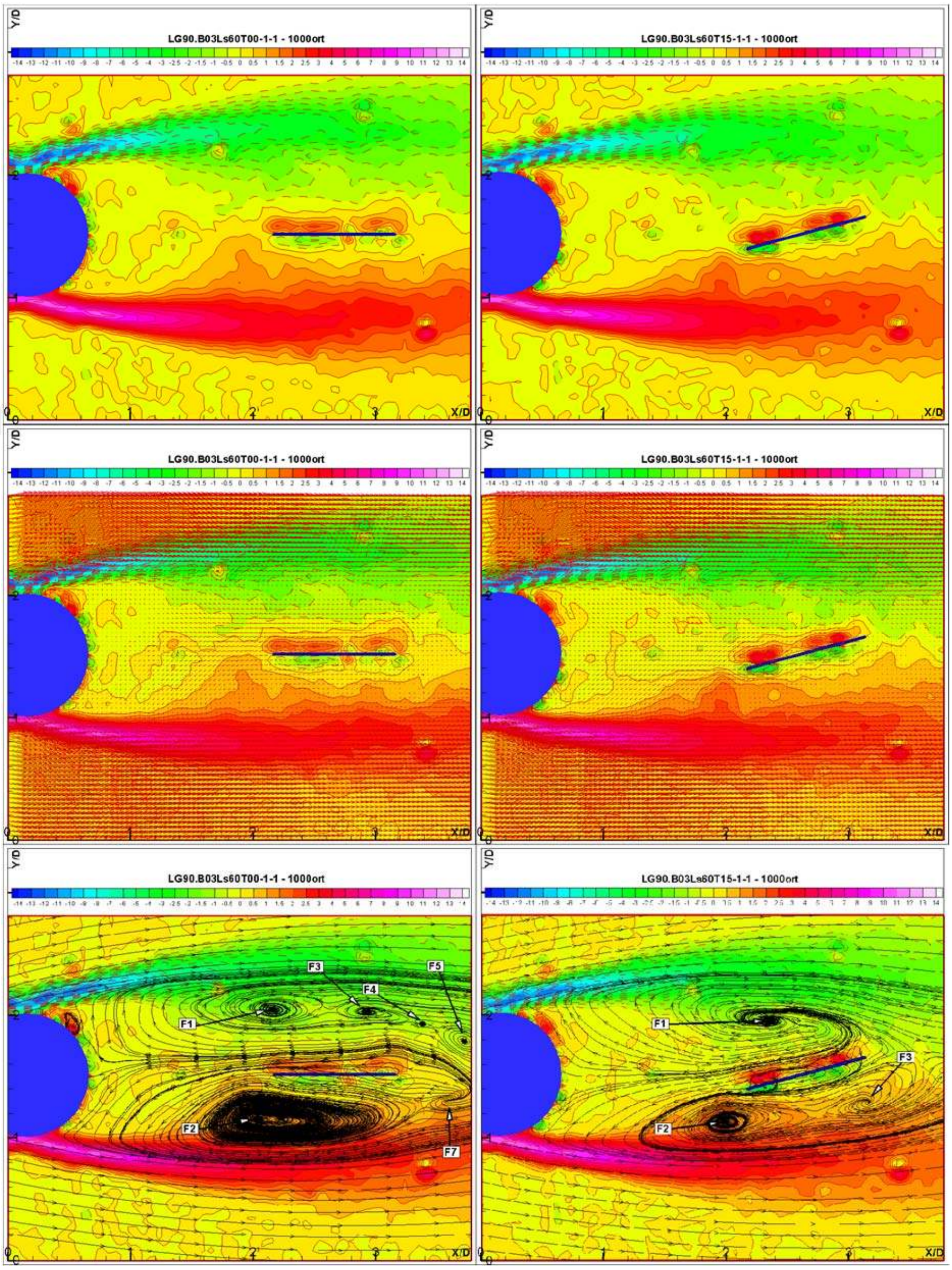

Figure 4.44. Vortex formations for porosity β: 0.3. Rotation angles of splitter plate due to its median are 0^0 and 15^0. Splitter plate length (ls*) is 1. The gap between splitter plate midpoint and cylinder (lg**) is 1.5.

The position and the strength of the foci vary depending on splitter plate porosity. The average value of dimensionless distances on X-axis ($(X/D)_{F1}$) and Y-axis ($(Y/D)_{F1}$) for focus point of the F1 are equal to 2.34337 and 1.96317 The average value of dimensionless distances on X-axis ($(X/D)_{F2}$) and Y-axis ($(Y/D)_{F2}$) for focus point of the F2 are equal to 1.99174 and 1.13302. After the peak value reached, the turbulent kinetic energy contours dissipate gradually in the flow direction. Negative values for vorticity contours represented with dashed lines. It is also observed that in the turbulent flow regime, the size of the foci F2 becomes wider with the splitter plate, and their central points shift downwards along the flow axis. F1 foci lose strength due to momentum loss as a result of the splitter plate.

Figure 4.45 shows the vorticity contours, time-averaged velocity vector map, and, the streamline patterns in the downstream base of the cylinder cross-sectional plane for Reynolds number of 5000. All values are normalized due to cylinder diameter. For the cylinder with the splitter plate, for porosity value β equals to 0.3 and splitter plate length value equals to 1, the gap between splitter plate midpoint and cylinder (lg**) is equal to 1.5 times cylinder diameter. Flow contours extended in flow direction. Rotation angles of splitter plate due to its median are 30 and 45 degrees in order columns. The peak value of turbulence kinetic energy (TKE) is 0.091 for 30 degrees. Downstream of the cylinder, a counter-clockwise rotating focus F1 and a clockwise rotating focus F2 is detected for Reynolds number of 5000 as expected. The position and the strength of the foci vary depending on splitter plate porosity. The average value of dimensionless distances on X-axis ($(X/D)_{F1}$) and Y-axis ($(Y/D)_{F1}$) for focus point of the F1 are equal to 2.44283 and 1.93511. The average value of dimensionless distances on X-axis ($(X/D)_{F2}$) and Y-axis ($(Y/D)_{F2}$) for focus point of the F2 are equal to 1.99186 and 1.12006. The average value of dimensionless distances on X-axis ($(X/D)_{F3}$) and Y-axis ($(Y/D)_{F3}$) for focus point of the F3 are equal to 2.69934 and 1.19453. After the peak value reached, the turbulent kinetic energy contours dissipate gradually in the flow direction. Negative values for vorticity contours represented with dashed lines.

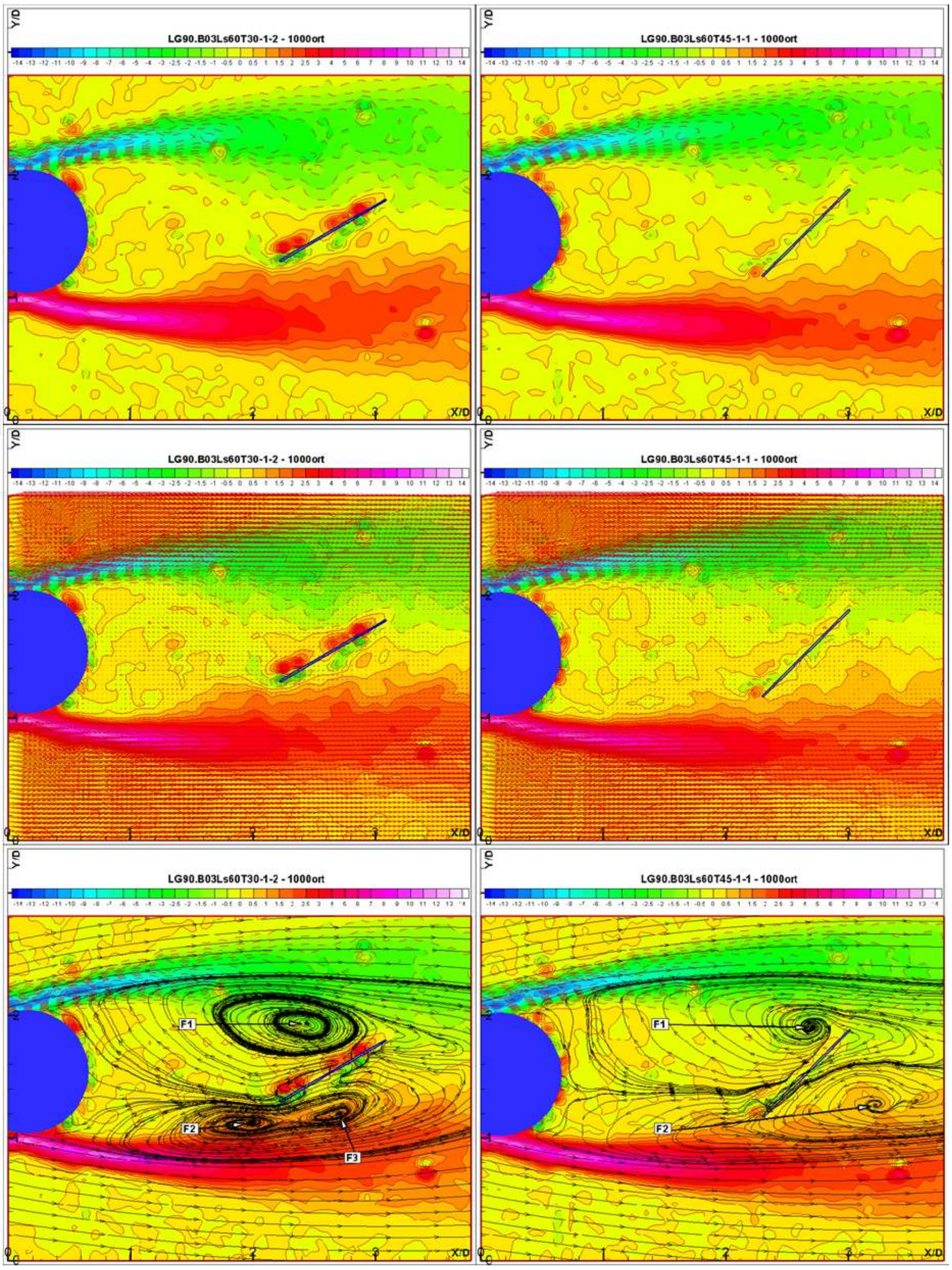

Figure 4.45. Vortex formations for porosity β: 0.3. Rotation angles of splitter plate due to its median are 30^0 and 45^0. Splitter plate length (ls*) is 1. The gap between splitter plate midpoint and cylinder (lg**) is 1.5.

It is also observed that in the turbulent flow regime, the size of the foci F2 divide into two foci named as F2 and F3 and their central points shift on both side of the splitter plate. F1 foci lose strength due to momentum loss as a result of splitter plate. The peak value of turbulence kinetic energy (TKE) is 0.098 for 45 degrees. Downstream of the cylinder, a counter-clockwise rotating focus F1, a clockwise rotating focus F2 is detected for Reynolds number of 5000 as expected. The position and the strength of the foci vary depending on splitter plate porosity. The average value of dimensionless distances on X-axis ($(X/D)_{F1}$) and Y-axis ($(Y/D)_{F1}$) for focus point of the F1 are equal to 2.71076 and 1.89555 The average value of dimensionless distances on X-axis ($(X/D)_{F2}$) and Y-axis ($(Y/D)_{F2}$) for focus point of the F2 are equal to 3.21904 and 1.2633. After the peak value reached, the turbulent kinetic energy contours dissipate gradually in the flow direction. Negative values for vorticity contours represented with dashed lines. It is also observed that in the turbulent flow regime, the size of the foci F2 becomes wider with the splitter plate, and their central points shift downwards along the flow axis. F1 foci lose strength due to momentum loss as a result of splitter plate.

Figure 4.46 shows the vorticity contours, time-averaged velocity vector map, and, the streamline patterns in the downstream base of the cylinder cross-sectional plane for Reynolds number of 5000. All values are normalized due to cylinder diameter. For the cylinder with the splitter plate, for porosity value β equals to 0.3 and splitter plate length value equals to 1. the gap between splitter plate midpoint and cylinder (lg**) is equal to 1.5 times cylinder diameter. Flow contours extended in flow direction. Rotation angles of splitter plate due to its median are 60 and 75 degrees in order columns. The peak value of turbulence kinetic energy (TKE) is 0.096 for 60 degrees. Downstream of the cylinder, a counter-clockwise rotating focus F1 and a clockwise rotating focus F2 is detected for Reynolds number of 5000 as expected. The position and the strength of the foci vary depending on splitter plate porosity. The average value of dimensionless distances on X-axis ($(X/D)_{F1}$) and Y-axis ($(Y/D)_{F1}$)for focus point of the F1 are equal to 2.57439 and 1.84596.

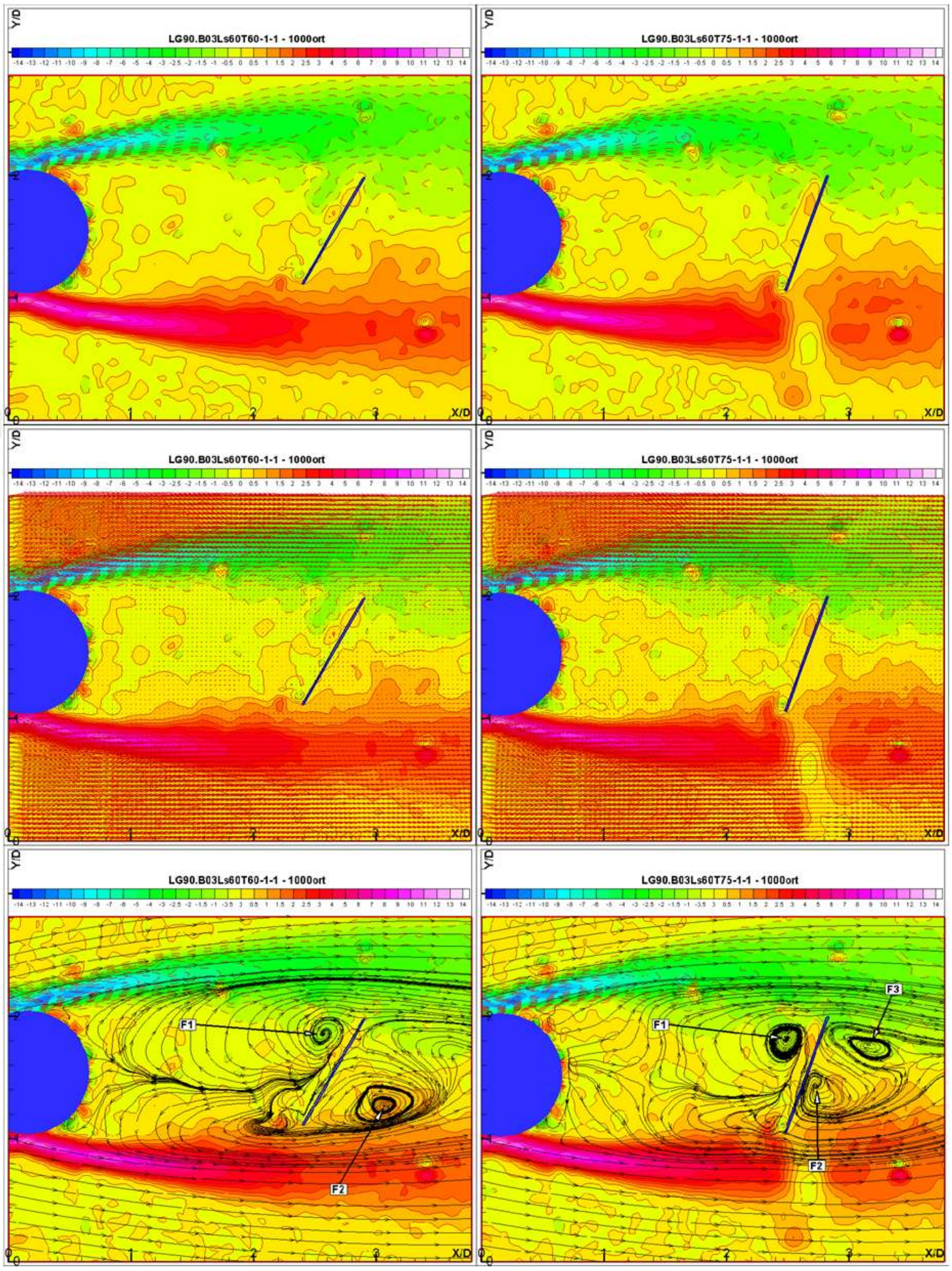

Figure 4.46. Vortex formations for porosity β: 0.3. Rotation angles of splitter plate due to its median are 60^0 and 75^0. Splitter plate length (ls*) is 1. The gap between splitter plate midpoint and cylinder (lg**) is 1.5.

The average value of dimensionless distances on X-axis ($(X/D)_{F2}$) and Y-axis ($(Y/D)_{F2}$) for focus point of the F2 are equal to 3.06614 and 1.2757. After the peak value reached, the turbulent kinetic energy contours dissipate gradually in the flow direction. Negative values for vorticity contours represented with dashed lines. It is also observed that in the turbulent flow regime, the size of the foci F2 becomes wider with the splitter plate, F1 foci lose strength due to momentum loss as a result of the splitter plate. The peak value of turbulence kinetic energy (TKE) is 0.125 for 75 degrees. Downstream of the cylinder, a counter-clockwise rotating focus F1 and a clockwise rotating focus F2 is detected for Reynolds number of 5000 as expected. The position and the strength of the foci vary depending on splitter plate porosity. The average value of dimensionless distances on X-axis ($(X/D)_{F1}$) and Y-axis ($(Y/D)_{F1}$) for focus point of the F1 are equal to 2.49175 and 1.8129 The average value of dimensionless distances on X-axis ($(X/D)_{F2}$) and Y-axis ($(Y/D)_{F2}$) for focus point of the F2 are equal to 2.72729 and 1.42446. The average value of dimensionless distances on X-axis ($(X/D)_{F3}$) and Y-axis ($(Y/D)_{F3}$) for focus point of the F3 are equal to 3.17358 and 1.76744. After the peak value reached, the turbulent kinetic energy contours dissipate gradually in the flow direction. Negative values for vorticity contours represented with dashed lines. It is also observed that in the turbulent flow regime, the size of the foci F2 divide into two foci named as F2 and F3 and their central points shift on downward side of the splitter plate. After the peak value reached, the turbulent kinetic energy contours dissipate gradually in the flow direction. Negative values for vorticity contours represented with dashed lines. It is also observed that in the turbulent flow regime, the size of the foci F2 becomes wider with the splitter plate, and their central points shift downwards along the flow axis. F1 foci loses strength due to momentum loss as a result of splitter plate.

Figure 4.47 shows the vorticity contours, time-averaged velocity vector map, and, the streamline patterns in the downstream base of the cylinder cross sectional plane for Reynolds number of 5000. All values are normalized due to cylinder diameter.

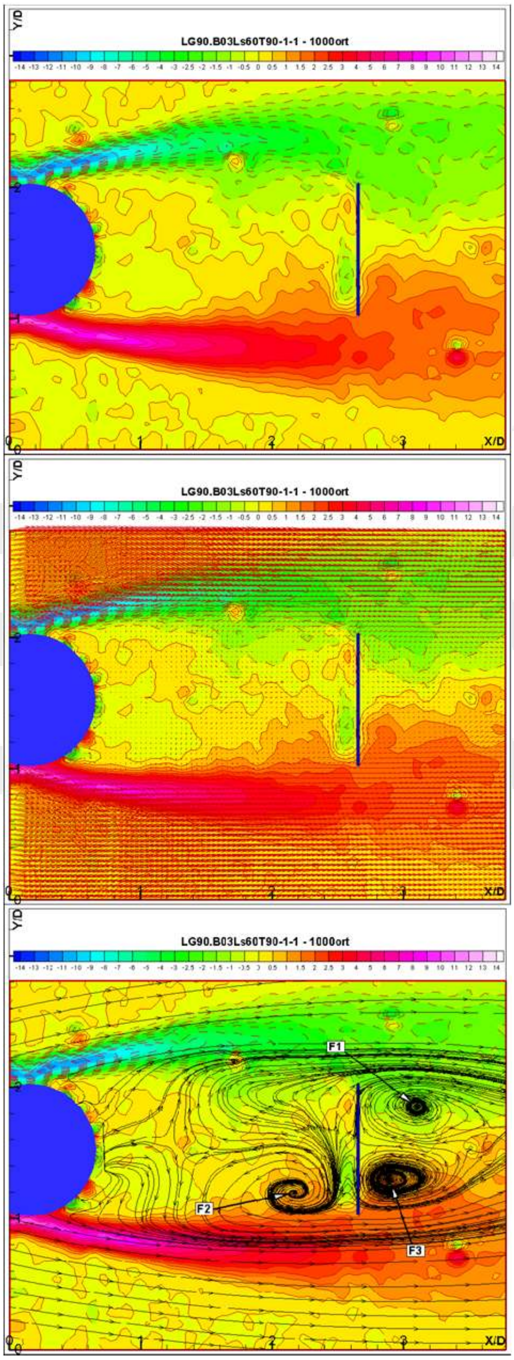

Figure 4.47. Vortex formations for porosity β: 0.3. Rotation angles of splitter plate due to its median is 90^0. Splitter plate length (ls*) is 1. The gap between splitter plate midpoint and cylinder (lg**) is 1.5.

For the cylinder with the splitter plate, for porosity value β equals to 0.3 and splitter plate length value equals to 1. the gap between splitter plate midpoint and cylinder (lg**) is equal to 1.5 times cylinder diameter. Flow contours extended in flow direction. The rotation angle of splitter plate due to its median is 90 degrees. The peak value of turbulence kinetic energy (TKE) is 0.121 for 95 degrees. Downstream of the cylinder, a counter-clockwise rotating focus F1 and a clockwise rotating focus F2 is detected for Reynolds number of 5000 as expected. The position and the strength of the foci vary depending on splitter plate porosity. The average value of dimensionless distances on X-axis ($(X/D)_{F1}$) and Y-axis ($(Y/D)_{F1}$) for focus point of the F1 are equal to 3.1116 and 1.85422 The average value of dimensionless distances on X-axis ($(X/D)_{F2}$) and Y-axis ($(Y/D)_{F2}$) for focus point of the F2 are equal to 2.17356 and 1.19305. The average value of dimensionless distances on X-axis ($(X/D)_{F3}$) and Y-axis ($(Y/D)_{F3}$) for focus point of the F3 are equal to 2.88845 and 1.30462. After the peak value reached, the turbulent kinetic energy contours dissipate gradually in the flow direction.

Negative values for vorticity contours represented with dashed lines. It is also observed that in the turbulent flow regime, the size of the foci F2 divide into two foci named as F2 and F3 and their central points shift on the downward side of the splitter plate. After the peak value reached, the turbulent kinetic energy contours dissipate gradually in the flow direction. Negative values for vorticity contours represented with dashed lines. It is also observed that in the turbulent flow regime, the size of the foci F2 becomes wider with the splitter plate, and their central points shift downwards along the flow axis. F1 foci lose strength due to momentum loss as a result of the splitter plate.

Figure 4.48 shows the vorticity contours, time-averaged velocity vector map, and, the streamline patterns in the downstream base of the cylinder cross-sectional plane for Reynolds number of 5000. All values are normalized due to cylinder diameter. For the cylinder with the splitter plate, for porosity value β equals to 0.5 and splitter plate length value equals to 1.

The gap between splitter plate midpoint and cylinder (lg**) is equal to 1.5 times cylinder diameter. Flow contours extended in flow direction. Rotation angles of splitter plate due to its median are 0 and 15 degrees in order columns. The peak value of turbulence kinetic energy (TKE) is 0.106 for 0 degrees. Downstream of the cylinder, a counter-clockwise rotating focus F1 and a clockwise rotating focus F2 is detected for Reynolds number of 5000 as expected. The position and the strength of the foci vary depending on splitter plate porosity. The average value of dimensionless distances on X-axis ($(X/D)_{F1}$) and Y-axis ($(Y/D)_{F1}$) for focus point of the F1 are equal to 2.25249 and 2.02686. The average value of dimensionless distances on X-axis ($(X/D)_{F2}$) and Y-axis ($(Y/D)_{F2}$) for focus point of the F2 are equal to 2.30114 and 1.12404. After the peak value reached, the turbulent kinetic energy contours dissipate gradually in the flow direction. Negative values for vorticity contours represented with dashed lines. It is also observed that in the turbulent flow regime, the size of the foci F2 becomes wider with the splitter plate, F1 foci lose strength due to momentum loss as a result of the splitter plate. The peak value of turbulence kinetic energy (TKE) is 0.102 for 15 degrees. Downstream of the cylinder, a counter-clockwise rotating focus F1 and a clockwise rotating focus F2 is detected for Reynolds number of 5000 as expected. The position and the strength of the foci vary depending on splitter plate porosity. The average value of dimensionless distances on X-axis ($(X/D)_{F1}$) and Y-axis ($(Y/D)_{F1}$) for focus point of the F1 are equal to 2.16116 and 2.00712 The average value of dimensionless distances on X-axis ($(X/D)_{F2}$) and Y-axis ($(Y/D)_{F2}$) for focus point of the F2 are equal to 2.02892 and 1.11453. The average value of dimensionless distances on X-axis ($(X/D)_{F3}$) and Y-axis ($(Y/D)_{F3}$) for focus point of the F3 are equal to 2.83886 and 1.15586. After the peak value reached, the turbulent kinetic energy contours dissipate gradually in the flow direction.

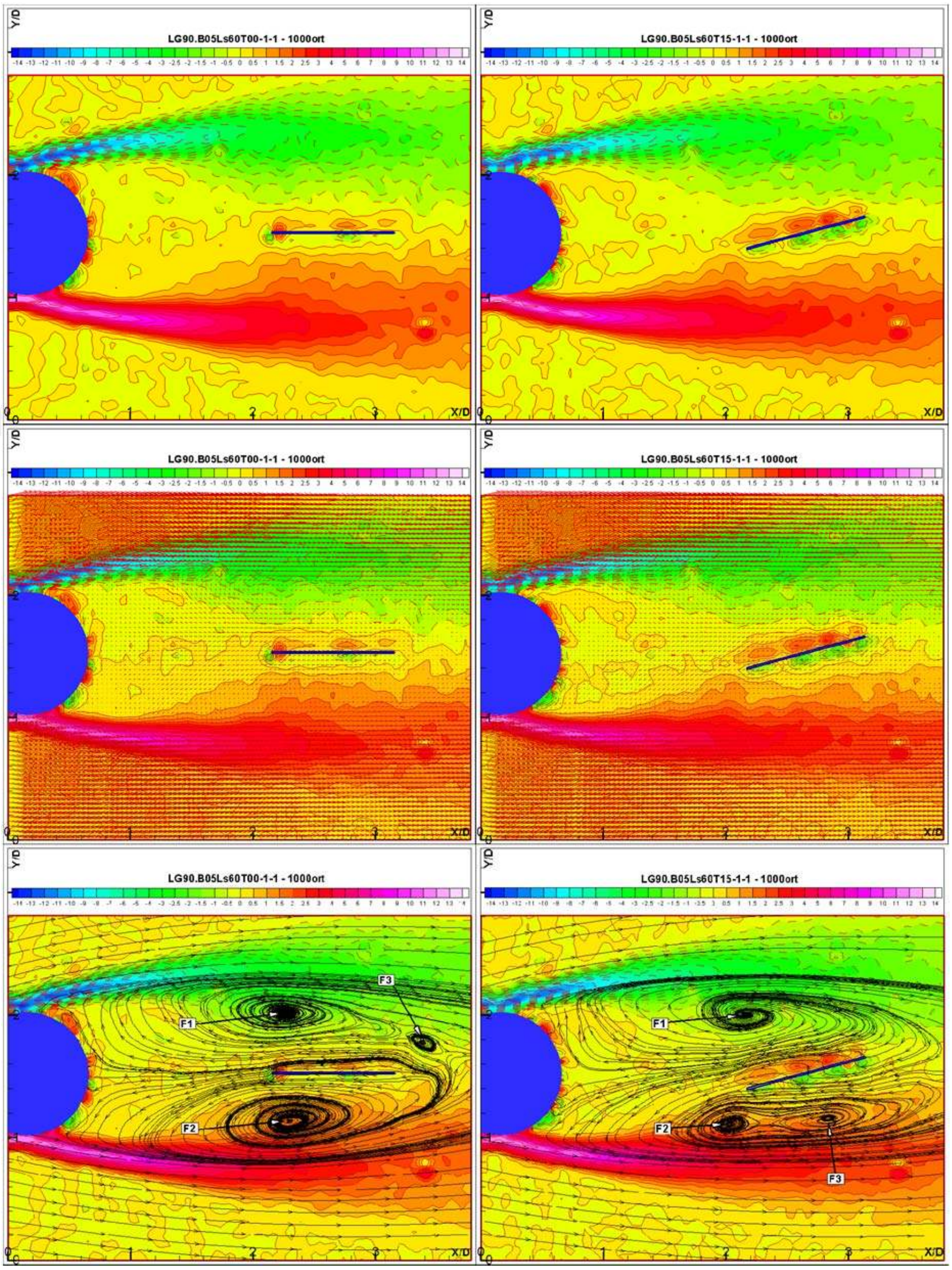

Figure 4.48. Vortex formations for porosity β: 0.5. Rotation angles of splitter plate due to its median are 0^0 and 15^0. Splitter plate length (ls*) is 1. The gap between splitter plate midpoint and cylinder (lg**) is 1.5.

Negative values for vorticity contours represented with dashed lines. It is also observed that in the turbulent flow regime, the size of the foci F2 divide into two foci named as F2 and F3 and their central points shift on the downward side of the splitter plate. After the peak value reached, the turbulent kinetic energy contours dissipate gradually in the flow direction. Negative values for vorticity contours represented with dashed lines. It is also observed that in the turbulent flow regime, the size of the foci F2 becomes wider with the splitter plate, and their central points shift downwards along the flow axis. F1 foci lose strength due to momentum loss as a result of the splitter plate.

Figure 4.49 shows the vorticity contours, time-averaged velocity vector map, and, the streamline patterns in the downstream base of the cylinder cross-sectional plane for Reynolds number of 5000. All values are normalized due to cylinder diameter. For the cylinder with the splitter plate, for porosity value β equals to 0.5 and splitter plate length value equals to 1. the gap between splitter plate midpoint and cylinder (lg**) is equal to 1.5 times cylinder diameter. Flow contours extended in flow direction. Rotation angles of splitter plate due to its median are 30 and 45 degrees in order columns. The peak value of turbulence kinetic energy (TKE) is 0.101 for 30 degrees. Downstream of the cylinder, a counter-clockwise rotating focus F1 and a clockwise rotating focus F2 is detected for Reynolds number of 5000 as expected. The position and the strength of the foci vary depending on splitter plate porosity. The average value of dimensionless distances on X-axis ($(X/D)_{F1}$) and Y-axis ($(Y/D)_{F1}$) for focus point of the F1 are equal to 2.47935 and 1.94927. The average value of dimensionless distances on X-axis ($(X/D)_{F2}$) and Y-axis ($(Y/D)_{F2}$) for focus point of the F2 are equal to 2.49175 and 1.17652. The average value of dimensionless distances on X-axis ($(X/D)_{F3}$) and Y-axis ($(Y/D)_{F3}$) for focus point of the F3 are equal to 3.17772 and 1.76744. The average value of dimensionless distances on X-axis ($(X/D)_{F4}$) and Y-axis ($(Y/D)_{F4}$) for focus point of the F4 are equal to 2.91325 and 1.22198. After the peak value reached, the turbulent kinetic energy contours dissipate gradually in the flow direction. Negative values for vorticity contours represented with dashed lines. It is also observed that in the turbulent flow regime, the size of the foci F2 becomes narrowed and F3, F4, and F5 foci appeared behind the splitter plate. F1 foci lose strength due to momentum loss as a result of the splitter plate. The peak value of turbulence kinetic energy (TKE) is 0.106 for 45 degrees. Downstream of the cylinder, a counter-clockwise rotating focus F1 and a clockwise rotating focus F2 is detected for Reynolds number of 5000 as expected. The position and the strength of the foci vary depending on splitter plate porosity. The average value of dimensionless distances on X-axis ($(X/D)_{F1}$) and Y-axis ($(Y/D)_{F1}$) for focus point of the F1 are equal to 2.66117 and 1.9658. The average value of dimensionless distances on X-axis ($(X/D)_{F2}$) and Y-axis ($(Y/D)_{F2}$) for focus point of the F2 are equal to 2.90085 and 1.24264. The average value of dimensionless distances on X-axis ($(X/D)_{F3}$) and Y-axis ($(Y/D)_{F3}$) for focus point of the F3 are equal to 3.0992 and 1.85009. After the peak value reached, the turbulent kinetic energy contours dissipate gradually in the flow direction. Negative values for vorticity contours represented with dashed lines. It is also observed that in the turbulent flow regime, the size of the foci F2 divide into two foci named as F2 and F3 and their central points shift on downward side of the splitter plate. After the peak value reached, the turbulent kinetic energy contours dissipate gradually in the flow direction. Negative values for vorticity contours represented with dashed lines. It is also observed that in the turbulent flow regime, the size of the foci F2 becomes wider with the splitter plate, and their central points shift downwards along the flow axis. F1 foci lose strength due to momentum loss as a result of the splitter plate.

Figure 4.50 shows the vorticity contours, time-averaged velocity vector map, and, the streamline patterns in the downstream base of the cylinder cross-sectional plane for Reynolds number of 5000. All values are normalized due to cylinder diameter. For the cylinder with the splitter plate, for porosity value β equals to 0.5 and splitter plate length value equals to 1. The gap between splitter plate midpoint and cylinder (lg**) is equal to 1.5 times cylinder diameter.

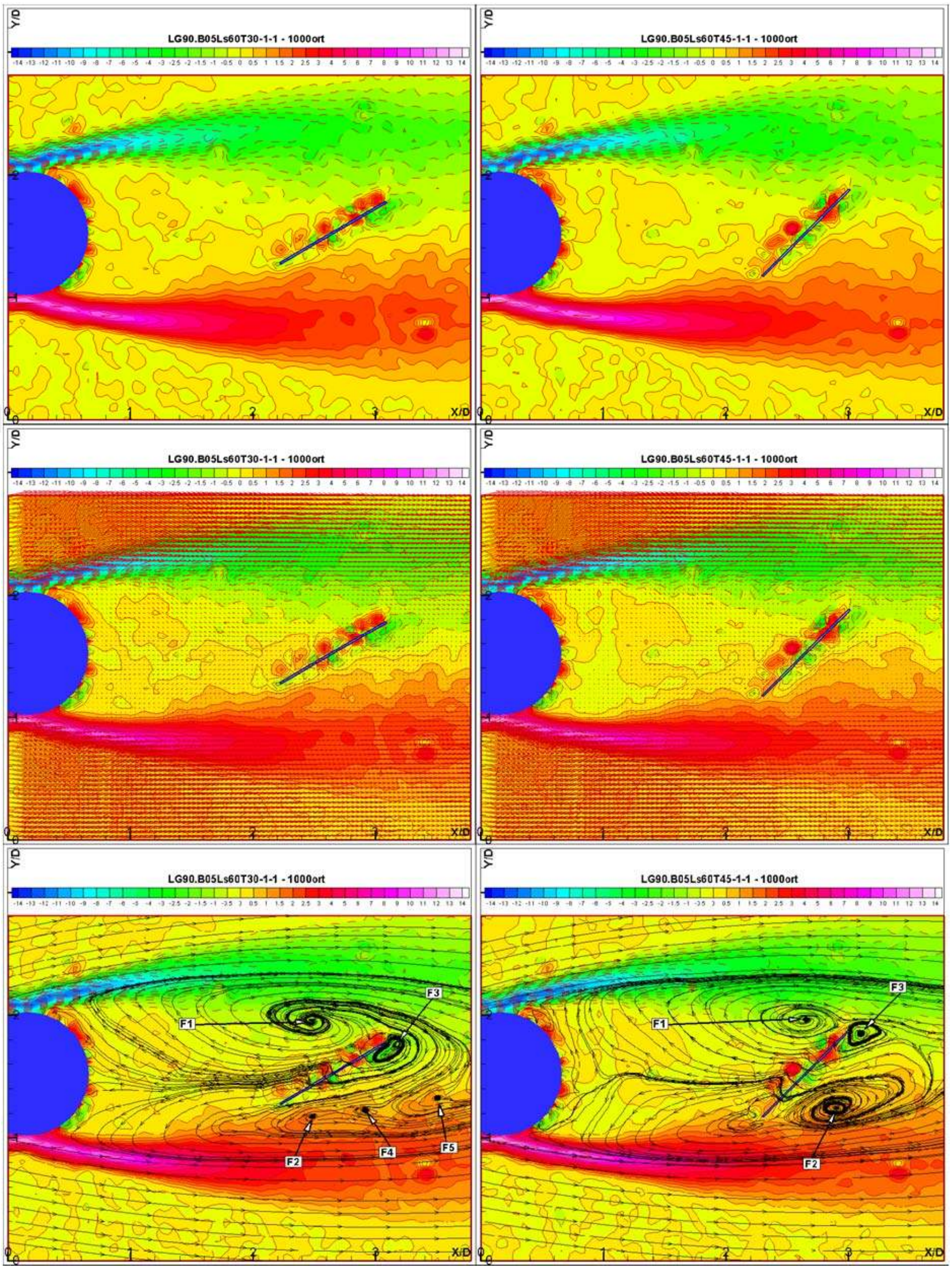

Figure 4.49. Vortex formations for porosity β: 0.5. Rotation angles of splitter plate due to its median are 30^0 and 45^0. Splitter plate length (ls*) is 1. The gap between splitter plate midpoint and cylinder (lg**) is 1.5.

Flow contours extended in the flow direction. Rotation angles of splitter plate due to its median are 60 and 90 degrees in order columns. The peak value of turbulence kinetic energy (TKE) is 0.102 for 60 degrees. Downstream of the cylinder, a counter-clockwise rotating focus F1 and a clockwise rotating focus F2 is detected for Reynolds number of 5000 as expected. The position and the strength of the foci vary depending on splitter plate porosity. The average value of dimensionless distances on X-axis ($(X/D)_{F1}$) and Y-axis ($(Y/D)_{F1}$) for focus point of the F1 are equal to 2.45456 and 1.92034. The average value of dimensionless distances on X-axis ($(X/D)_{F2}$) and Y-axis ($(Y/D)_{F2}$) for focus point of the F2 are equal to 2.2655 and 1.12435. The average value of dimensionless distances on X-axis ($(X/D)_{F3}$) and Y-axis ($(Y/D)_{F3}$) for focus point of the F3 are equal to 2.9587 and 1.82943. The average value of dimensionless distances on X-axis ($(X/D)_{F4}$) and Y-axis ($(Y/D)_{F4}$) for focus point of the F4 are equal to 0.92972 and 1.41206. After the peak value reached, the turbulent kinetic energy contours dissipate gradually in the flow direction. Negative values for vorticity contours represented with dashed lines. It is also observed that in the turbulent flow regime, the size of the foci F2 becomes narrowed and F3, F4 foci appeared behind the splitter plate. F1 foci lose strength due to momentum loss as a result of the splitter plate. The peak value of turbulence kinetic energy (TKE) is 0.124 for 90 degrees. Downstream of the cylinder, a counter-clockwise rotating focus F1 and a clockwise rotating focus F2 is detected for Reynolds number of 5000 as expected. The position and the strength of the foci vary depending on splitter plate porosity. The average value of dimensionless distances on X-axis ($(X/D)_{F1}$) and Y-axis ($(Y/D)_{F1}$) for focus point of the F1 are equal to 2.16942 and 1.89968. The average value of dimensionless distances on X-axis ($(X/D)_{F2}$) and Y-axis ($(Y/D)_{F2}$) for focus point of the F2 are equal to 2.46282 and 1.24264. The average value of dimensionless distances on X-axis ($(X/D)_{F3}$) and Y-axis ($(Y/D)_{F3}$) for focus point of the F3 are equal to 2.86366 and 1.75918. The average value of dimensionless distances on X-axis ($(X/D)_{F4}$) and Y-axis ($(Y/D)_{F4}$) for focus point of the F4 are equal to 3.17358 and 1.34181.

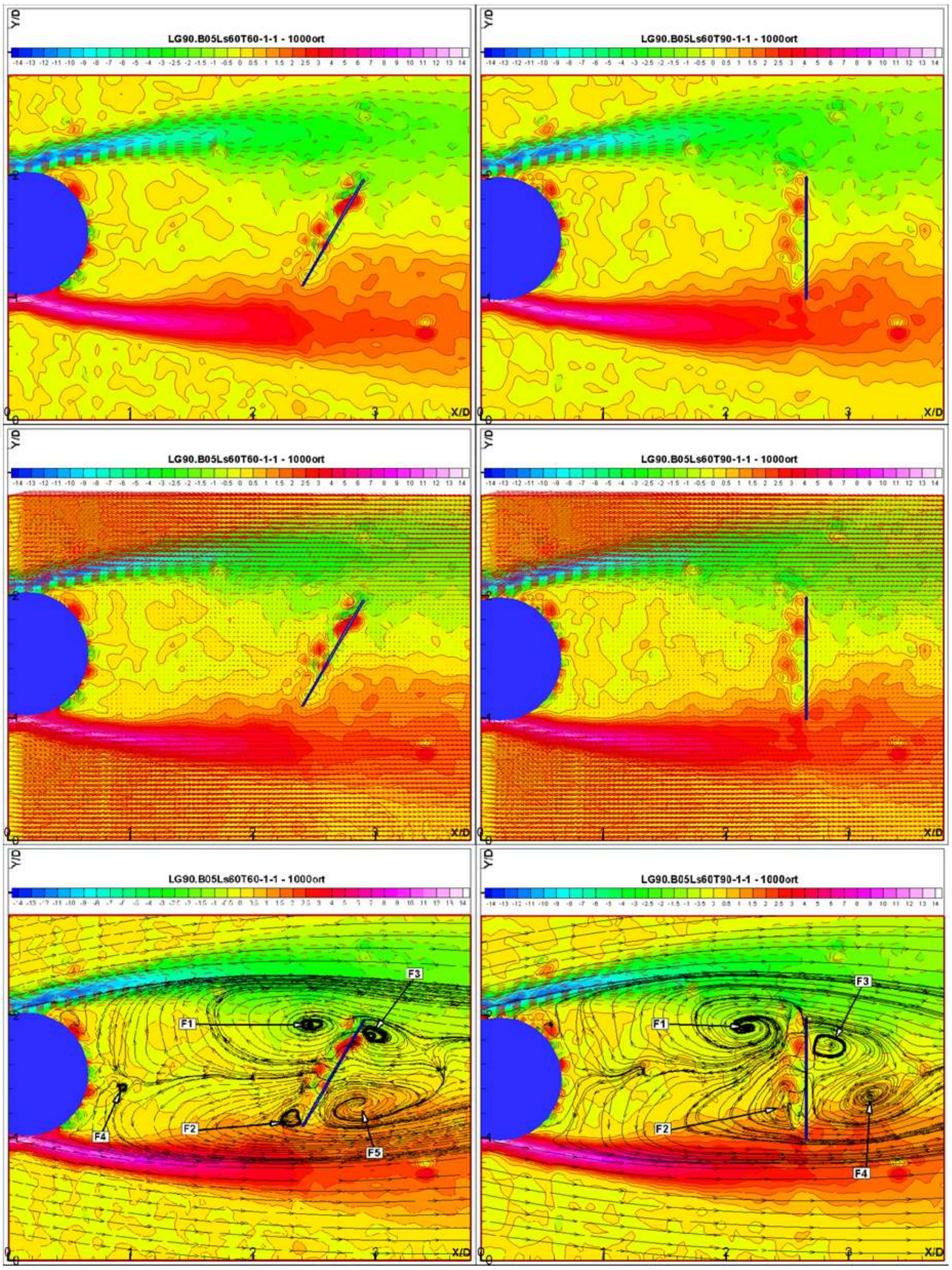

Figure 4.50. Vortex formations for porosity β: 0.5. Rotation angles of splitter plate due to its median are 60^0 and 90^0. Splitter plate length (ls*) is 1. The gap between splitter plate midpoint and cylinder (lg**) is 1.5.

After the peak value reached, the turbulent kinetic energy contours dissipate gradually in the flow direction. Negative values for vorticity contours represented with dashed lines. It is also observed that in the turbulent flow regime, the size of the foci F2 loose strength and two new foci named as F2 and F3 appeared on downward side of the splitter plate. After the peak value reached, the turbulent kinetic energy contours dissipate gradually in the flow direction. Negative values for vorticity contours represented with dashed lines.

Figure 4.51 shows the vorticity contours, time-averaged velocity vector map, and, the streamline patterns in the downstream base of the cylinder cross-sectional plane for Reynolds number of 5000. All values are normalized due to cylinder diameter. For the cylinder with the splitter plate, for porosity value β equals to 0.7 and splitter plate length value equals to 1. the gap between splitter plate midpoint and cylinder (lg**) is equal to 1.5 times cylinder diameter. Flow contours extended in flow direction. Rotation angles of splitter plate due to its median are 0 and 15 degrees in order columns. The peak value of turbulence kinetic energy (TKE) is 0.108 for 0 degrees. Downstream of the cylinder, a counter-clockwise rotating focus F1 and a clockwise rotating focus F2 is detected for Reynolds number of 5000 as expected. The position and the strength of the foci vary depending on splitter plate porosity. The average value of dimensionless distances on X-axis ($(X/D)_{F1}$) and Y-axis ($(Y/D)_{F1}$) for focus point of the F1 are equal to 2.15518 and 2.02146. The average value of dimensionless distances on X-axis ($(X/D)_{F2}$) and Y-axis ($(Y/D)_{F2}$) for focus point of the F2 are equal to 2.24167 and 1.13485. After the peak value reached, the turbulent kinetic energy contours dissipate gradually in the flow direction. Negative values for vorticity contours represented with dashed lines. It is also observed that in the turbulent flow regime, the size of the foci F2 becomes wider along the splitter plate. F1 foci lose strength due to momentum loss as a result of the splitter plate. The peak value of turbulence kinetic energy (TKE) is 0.114 for 15 degrees.

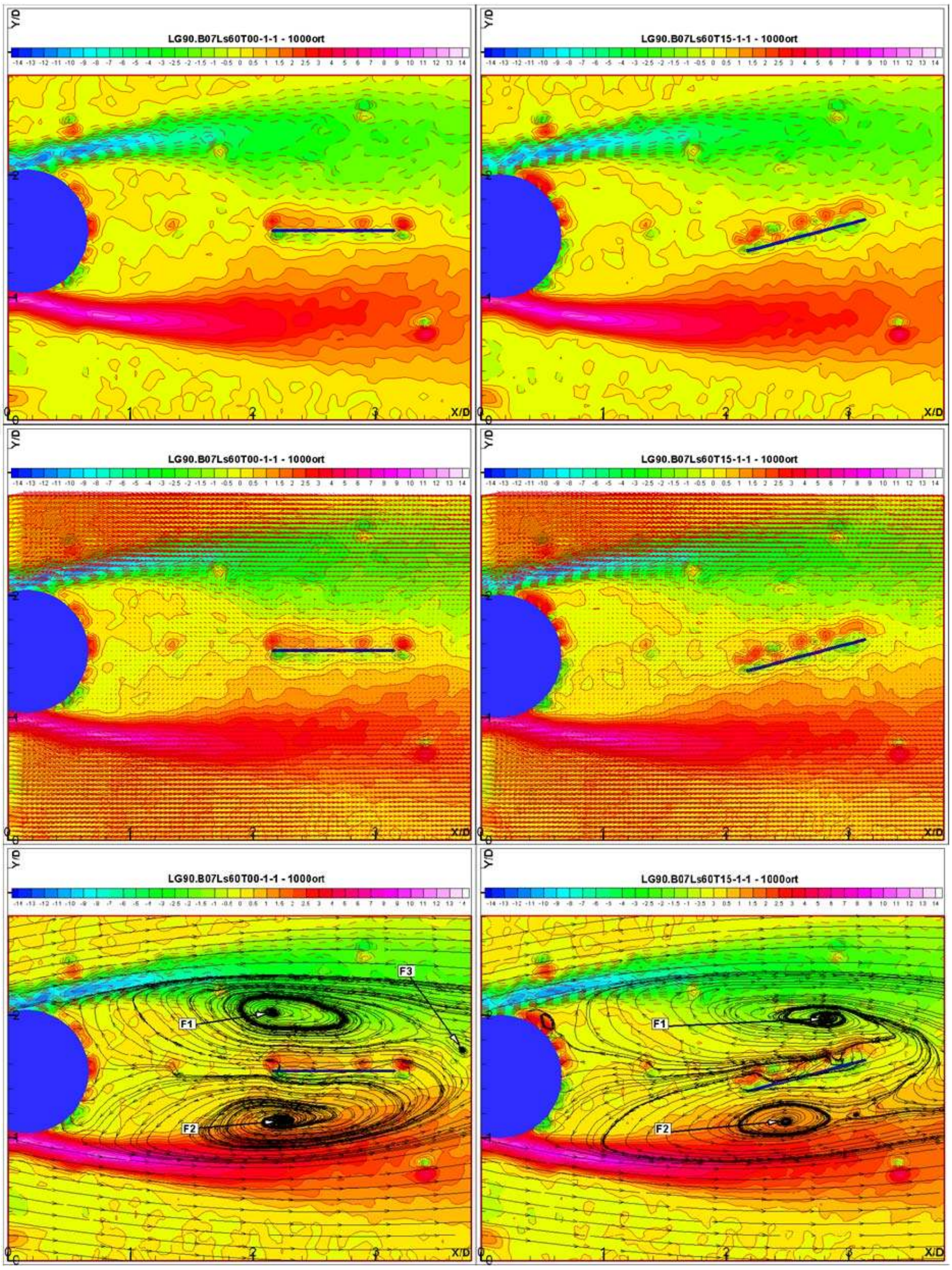

Figure 4.51. Vortex formations for porosity β: 0.7. Rotation angles of splitter plate due to its median are 0^0 and 15^0. Splitter plate length (ls*) is 1. The gap between splitter plate midpoint and cylinder (lg**) is 1.5.

Downstream of the cylinder, a counter-clockwise rotating focus F1 and a clockwise rotating focus F2 is detected for Reynolds number of 5000 as expected. The position and the strength of the foci vary depending on splitter plate porosity. The average value of dimensionless distances on X-axis ($(X/D)_{F1}$) and Y-axis ($(Y/D)_{F1}$) for focus point of the F1 are equal to 2.83473 and 1.97406. The average value of dimensionless distances on X-axis ($(X/D)_{F2}$) and Y-axis ($(Y/D)_{F2}$) for focus point of the F2 are equal to 2.47935 and 1.13106. After the peak value reached, the turbulent kinetic energy contours dissipate gradually in the flow direction. Negative values for vorticity contours represented with dashed lines. It is also observed that in the turbulent flow regime, the size of the foci F2 loose strength. After the peak value reached, the turbulent kinetic energy contours dissipate gradually in the flow direction. Negative values for vorticity contours represented with dashed lines.

Figure 4.52 shows the vorticity contours, time-averaged velocity vector map, and, the streamline patterns in the downstream base of the cylinder cross-sectional plane for Reynolds number of 5000. All values are normalized due to cylinder diameter. For the cylinder with the splitter plate, for porosity value β equals to 0.7 and splitter plate length value equals to 1. the gap between splitter plate midpoint and cylinder (lg**) is equal to 1.5 times cylinder diameter. Flow contours extended in flow direction. Rotation angles of splitter plate due to its median are 30 and 45 degrees in order columns. The peak value of turbulence kinetic energy (TKE) is 0.122 for 30 degrees. Downstream of the cylinder, a counter-clockwise rotating focus F1 and a clockwise rotating focus F2 is detected for Reynolds number of 5000 as expected. The position and the strength of the foci vary depending on splitter plate porosity. The average value of dimensionless distances on X-axis ($(X/D)_{F1}$) and Y-axis ($(Y/D)_{F1}$) for focus point of the F1 are equal to 2.25207 and 1.9368. The average value of dimensionless distances on X-axis ($(X/D)_{F2}$) and Y-axis ($(Y/D)_{F2}$) for focus point of the F2 are equal to 2.85126 and 1.20545.

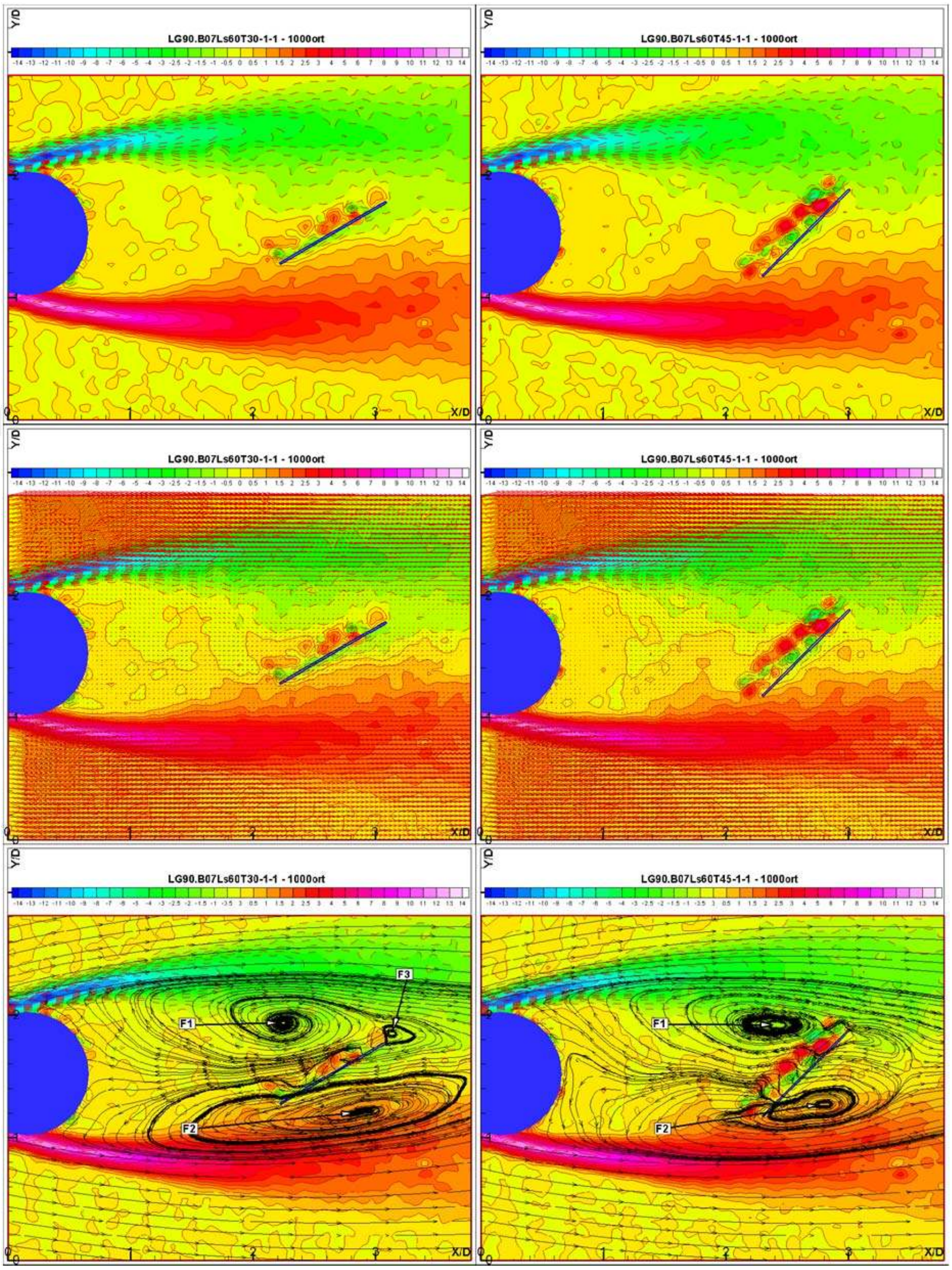

Figure 4.52. Vortex formations for porosity β: 0.7. Rotation angles of splitter plate due to its median are 30^0 and 45^0. Splitter plate length (ls*) is 1. The gap between splitter plate midpoint and cylinder (lg**) is 1.5.

The average value of dimensionless distances on X-axis ($(X/D)_{F3}$) and Y-axis ($(Y/D)_{F3}$) for focus point of the F3 are equal to 3.13226 and 1.84596. After the peak value reached, the turbulent kinetic energy contours dissipate gradually in the flow direction. Negative values for vorticity contours represented with dashed lines. It is also observed that in the turbulent flow regime, the size of the foci F2 becomes narrowed and F3 foci appeared behind the splitter plate. F1 foci lose strength due to momentum loss as a result of the splitter plate. The peak value of turbulence kinetic energy (TKE) is 0.114 for 45 degrees. Downstream of the cylinder, a counter-clockwise rotating focus F1 and a clockwise rotating focus F2 is detected for Reynolds number of 5000 as expected. The position and the strength of the foci vary depending on splitter plate porosity. The average value of dimensionless distances on X-axis ($(X/D)_{F1}$) and Y-axis ($(Y/D)_{F1}$) for focus point of the F1 are equal to 2.4091 and 1.91621. The average value of dimensionless distances on X-axis ($(X/D)_{F2}$) and Y-axis ($(Y/D)_{F2}$) for focus point of the F2 are equal to 2.81407 and 1.27156. After the peak value reached, the turbulent kinetic energy contours dissipate gradually in the flow direction. Negative values for vorticity contours represented with dashed lines. After the peak value reached, the turbulent kinetic energy contours dissipate gradually in the flow direction. Negative values for vorticity contours represented with dashed lines.

Figure 4.53 shows the vorticity contours, time-averaged velocity vector map, and, the streamline patterns in the downstream base of the cylinder cross-sectional plane for Reynolds number of 5000. All values are normalized due to cylinder diameter. For the cylinder with the splitter plate, for porosity value β equals to 0.7 and splitter plate length value equals to 1. the gap between splitter plate midpoint and cylinder (lg**) is equal to 1.5 times cylinder diameter. Flow contours extended in flow direction. Rotation angles of splitter plate due to its median are 60 and 75 degrees in order columns. The peak value of turbulence kinetic energy (TKE) is 0.126 for 60 degrees. Downstream of the cylinder, a counter-clockwise rotating focus F1 and a clockwise rotating focus F2 are detected for Reynolds number of 5000 as expected. The position and the strength of the foci vary depending on splitter plate porosity. The average value of dimensionless distances on X-axis ($(X/D)_{F1}$) and Y-axis ($(Y/D)_{F1}$) for focus point of the F1 are equal to 2.49588 and 1.93274. The average value of dimensionless distances on X-axis ($(X/D)_{F2}$) and Y-axis ($(Y/D)_{F2}$) for focus point of the F2 are equal to 2.01653 and 1.19718. The average value of dimensionless distances on X-axis ($(X/D)_{F3}$) and Y-axis ($(Y/D)_{F3}$) for focus point of the F3 are equal to 3.10333 and 1.85422. The average value of dimensionless distances on X-axis ($(X/D)_{F4}$) and Y-axis ($(Y/D)_{F4}$) for focus point of the F4 are equal to 3.10333 and 1.85422. After the peak value reached, the turbulent kinetic energy contours dissipate gradually in the flow direction. Negative values for vorticity contours represented with dashed lines. It is also observed that in the turbulent flow regime, the size of the foci F2 becomes narrowed and F3, F4 foci appeared behind the splitter plate. F1 foci lose strength due to momentum loss as a result of the splitter plate. The peak value of turbulence kinetic energy (TKE) is 0.112 for 75 degrees. Downstream of the cylinder, a counter-clockwise rotating focus F1 and a clockwise rotating focus F2 are detected for Reynolds number of 5000 as expected. The position and the strength of the foci vary depending on splitter plate porosity. The average value of dimensionless distances on X-axis ($(X/D)_{F1}$) and Y-axis ($(Y/D)_{F1}$) for focus point of the F1 are equal to 2.54133 and 1.90794. The average value of dimensionless distances on X-axis ($(X/D)_{F2}$) and Y-axis ($(Y/D)_{F2}$) for focus point of the F2 are equal to 2.23141 and 1.24677. The average value of dimensionless distances on X-axis ($(X/D)_{F3}$) and Y-axis ($(Y/D)_{F3}$) for focus point of the F3 are equal to 3.25623 and 1.87075. The average value of dimensionless distances on X-axis ($(X/D)_{F4}$) and Y-axis ($(Y/D)_{F4}$) for focus point of the F4 are equal to 3.12813 and 1.35421. After the peak value reached, the turbulent kinetic energy contours dissipate gradually in the flow direction. Negative values for vorticity contours represented with dashed lines. It is also observed that in the turbulent flow regime, the size of the foci F2 loose strength and two new foci named as F3 and F4 appeared on downward side of the splitter plate.

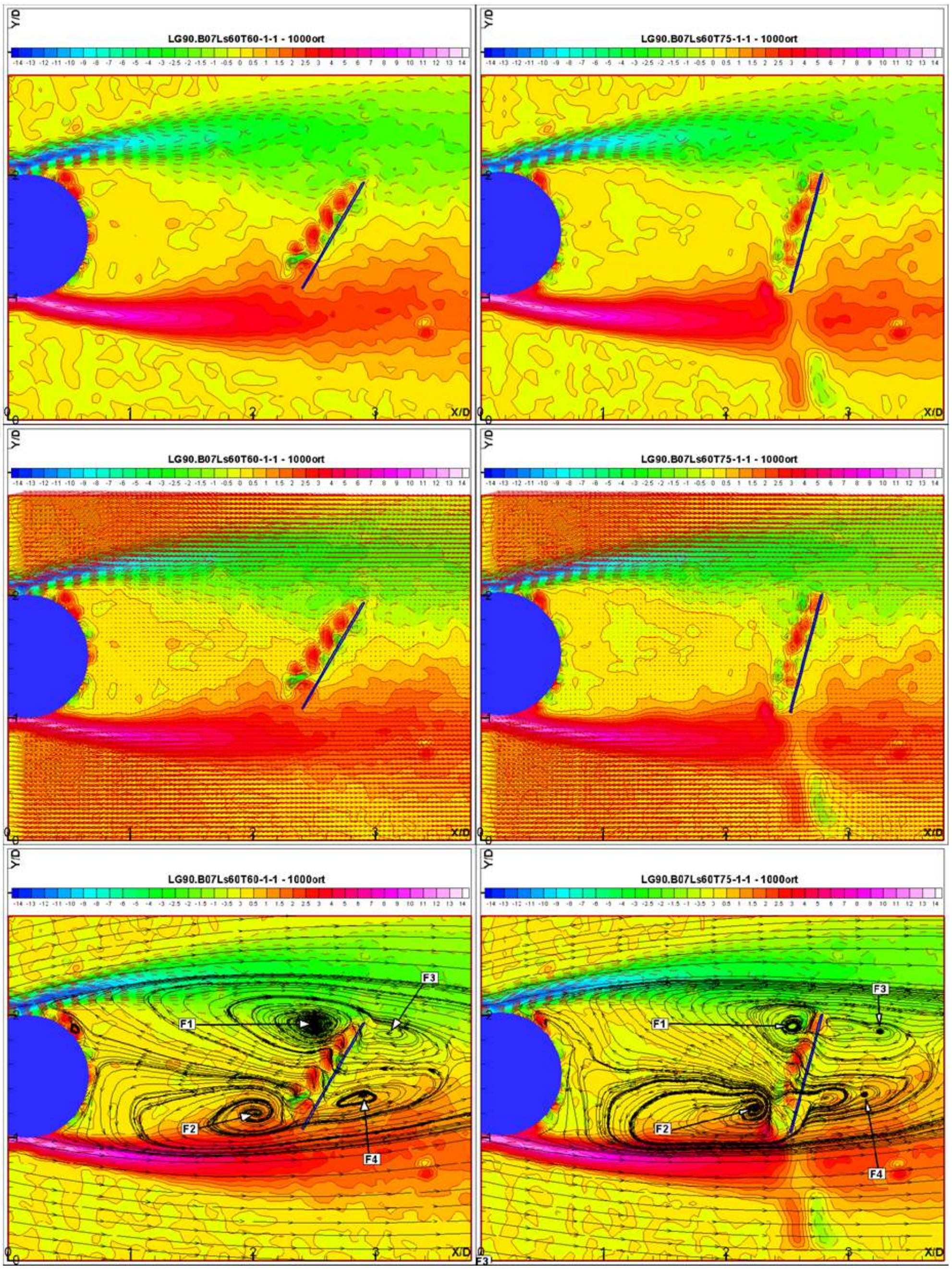

Figure 4.53. Vortex formations for porosity β: 0.7. Rotation angles of splitter plate due to its median are 60^0 and 75^0. Splitter plate length (ls*) is 1. The gap between splitter plate midpoint and cylinder (lg**) is 1.5.

After the peak value reached, the turbulent kinetic energy contours dissipate gradually in the flow direction. Negative values for vorticity contours represented with dashed lines.

Figure 4.54 shows the vorticity contours, time-averaged velocity vector map, and, the streamline patterns in the downstream base of the cylinder cross-sectional plane for Reynolds number of 5000. All values are normalized due to cylinder diameter. For the cylinder with the splitter plate, for porosity value β equals to 0.7 and splitter plate length value equals to 1. the gap between splitter plate midpoint and cylinder (lg**) is equal to 1.5 times cylinder diameter. Flow contours extended in flow direction. Rotation angles of splitter plate due to its median is 90 degrees. The peak value of turbulence kinetic energy (TKE) is 0.097 for 90 degrees. Downstream of the cylinder, a counter-clockwise rotating focus F1 and a clockwise rotating focus F2 are detected for Reynolds number of 5000 as expected. The position and the strength of the foci vary depending on splitter plate porosity. The average value of dimensionless distances on X-axis ($(X/D)_{F1}$) and Y-axis ($(Y/D)_{F1}$) for focus point of the F1 are equal to 2.37191 and 1.88728. The average value of dimensionless distances on X-axis ($(X/D)_{F2}$) and Y-axis ($(Y/D)_{F2}$) for focus point of the F2 are equal to 2.30579 and 1.18892. The average value of dimensionless distances on X-axis ($(X/D)_{F3}$) and Y-axis ($(Y/D)_{F3}$) for focus point of the F3 are equal to 2.76448 and 1.84183. The average value of dimensionless distances on X-axis ($(X/D)_{F4}$) and Y-axis ($(Y/D)_{F4}$) for focus point of the F4 are equal to 2.9463 and 1.25917. After the peak value reached, the turbulent kinetic energy contours dissipate gradually in the flow direction. Negative values for vorticity contours represented with dashed lines. It is also observed that in the turbulent flow regime, the size of the foci F2 becomes narrowed and F3, F4 foci appeared behind the splitter plate. F1 foci lose strength due to momentum loss as a result of the splitter plate. After the peak value reached, the turbulent kinetic energy contours dissipate gradually in the flow direction. Negative values for vorticity contours represented with dashed lines.

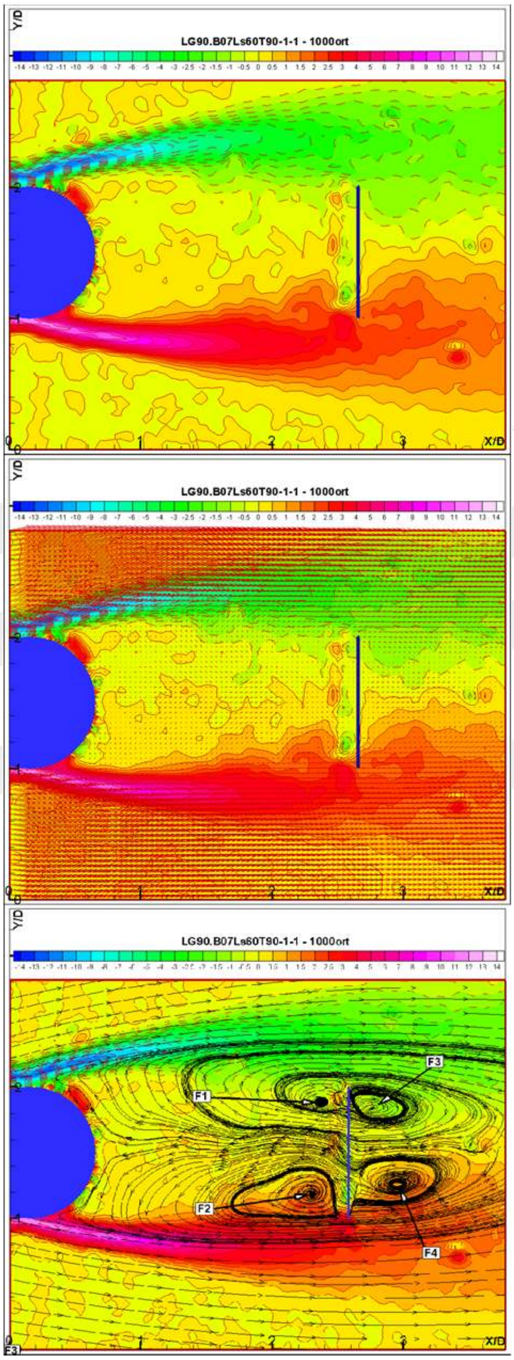

Figure 4.54. Vortex formations for porosity β: 0.7. The rotation angle of splitter plate due to its median is 90^0. Splitter plate length (ls*) is 1. The gap between splitter plate midpoint and cylinder (lg**) is 1.5.

Figure 4.55 shows that a decrease in turbulent kinetic energy is obtained by the θ increase except in only $\theta=90^0$. The peak values of turbulent kinetic energy for splitter plate aligned due to different angle values of θ =0;15;30;45;60;75 are reduced by 16%, 20%, 14%, 20%, 28% and 16% in order, for the porosity value β=0.3. Formation point of the peak value of turbulent kinetic energy in the flow direction for splitter plate length aligned due to angle value of θ =90 is increased by %4 for the porosity value β=0.3. (Figure 4.56)

Figure 4.57 shows that a decrease in turbulent kinetic energy is obtained by the θ increase. The peak values of turbulent kinetic energy for splitter plate aligned due to different angle values of θ =0;15;30;45;60;75;90 are reduced by 5%, 13%, 25%, 18%, 26%, 17% and 9% in order, for the porosity value β=0.5.

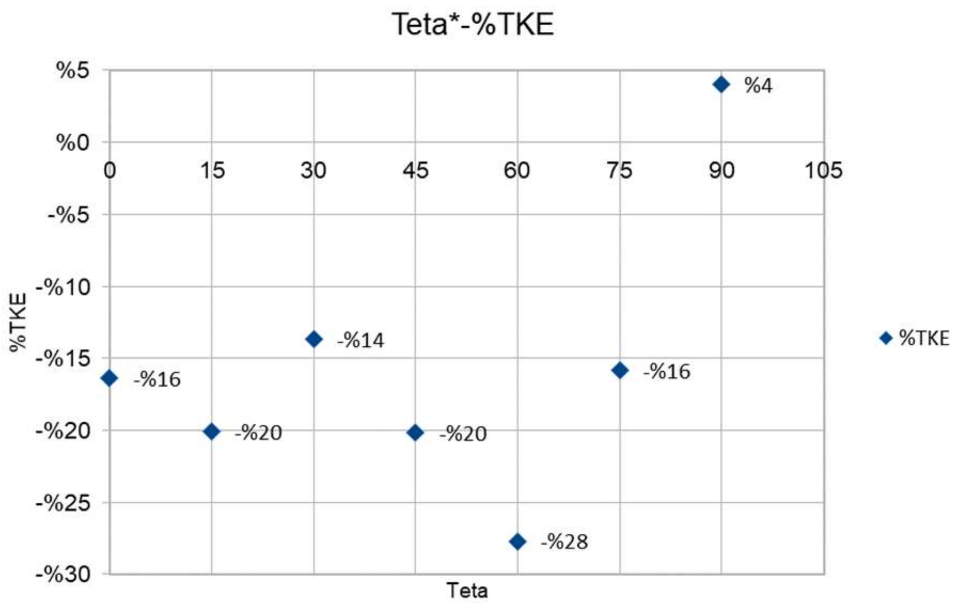

Figure 4.55. TKE variation due to different rotation angle values of 0,15,30,45,60,75 and 90 degrees for porosity (β) 0.3. The splitter plate length (ls*) is 1. Gap between splitter plate midpoint and cylinder (lg**) is 1.5.

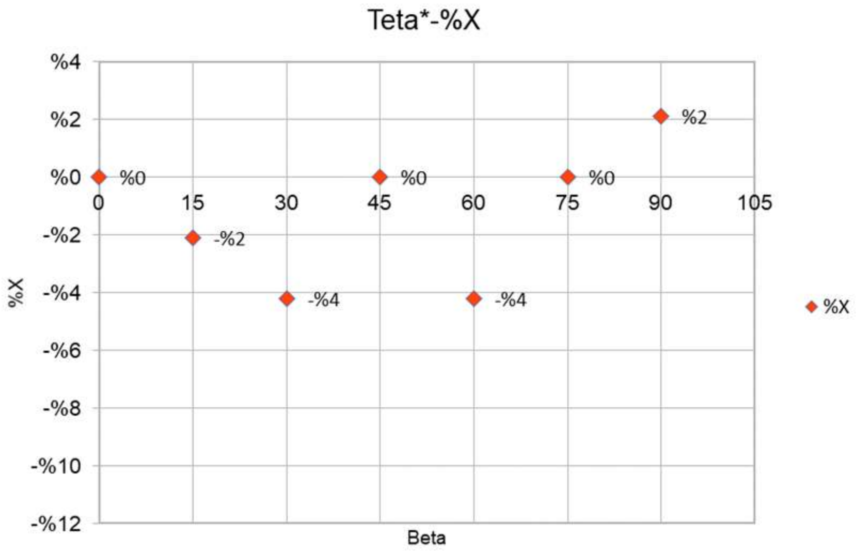

Figure 4.56. Position of max. TKE due to different rotation angle values of 0,15,30,45,60,75 and 90 degrees for porosity (β) 0.3. Splitter plate (ls*) is 1. Gap between splitter plate midpoint and cylinder (lg**) is 1.5

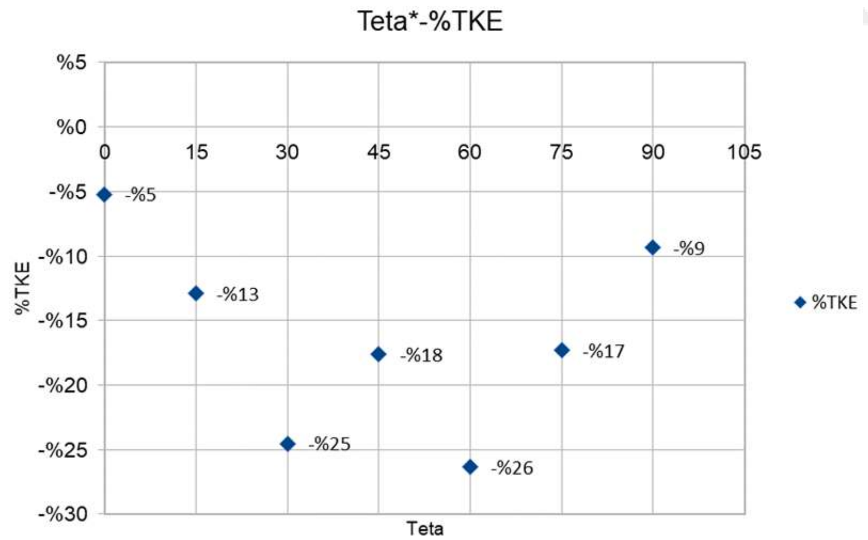

Figure 4.57. TKE variation due to different rotation angle values of 0,15,30,45,60,75 and 90 degrees for porosity (β) 0.5. Splitter plate length (ls*) is 1. Gap between splitter plate midpoint and cylinder (lg**) is 1.5.

Formation point of peak value of turbulent kinetic energy in the flow direction for the θ values (0;15;30;45;60;75;90) are reduced by 9%, 2%, 6%, 3%, 6%, 9%, 2% in order, for porosity value β=0.5 (Figure 4.58).

Figure 4.59 shows that a decrease in turbulent kinetic energy is obtained by the θ increase. The peak values of turbulent kinetic energy for splitter plate aligned due to different angle values of θ =0;15;30;45;60;75;90 are reduced by 12%, 2%, 20%, 16%, 16%, %16 and %4 in order, for the porosity value β=0.7. Formation point of peak value of turbulent kinetic energy in the flow direction for the θ values (0;15;30;45;75;90) are reduced by 2%, 4%, 11%, 0%, 8%, 11% in order, for porosity value β=0.7. Only for θ equals 60 degrees, the formation point of the peak value of turbulent kinetic energy in the flow direction is increased by 2% (Figure 4.60).

Seven different the splitter plate angle values (θ =0; 15; 30; 45; 60; 75; 90) and three different porosity values (β=0.30; 0.50; 0.70) were investigated and the splitter plate length (ls) and the gap between splitter plate midpoint and cylinder (lg^{**}) were kept to constant during the experiments as ls=D and lg^{**}=1.5D. It is observed that vortex formation delayed with increasing the splitter plate angle. As splitter plate angle increase, turbulent kinetic energy reduced in most situation. Also, the formation point of the peak value of turbulent kinetic energy in the flow direction reduced nearly in all situations except θ =90, β=0.30 and θ =60, β=0.70 situations.

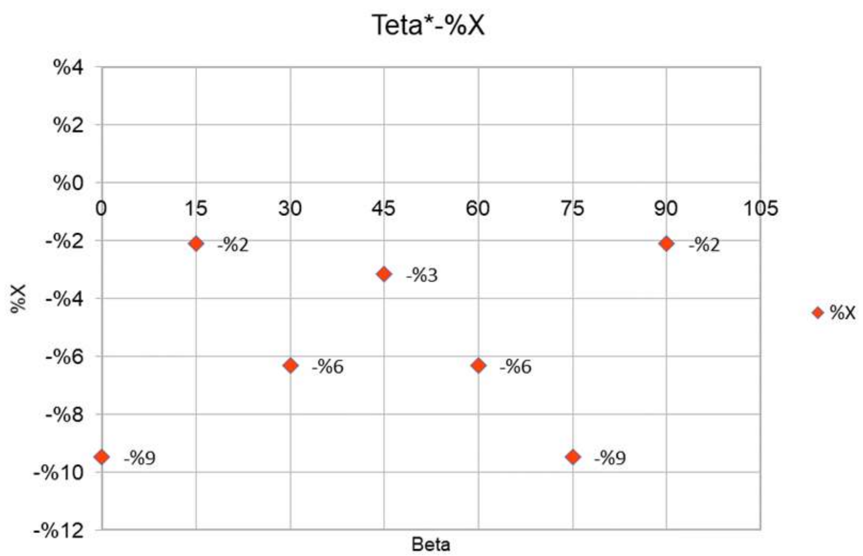

Figure 4.58. Position of max. TKE due to different rotation angle values of 0,15,30,45,60,75 and 90 degrees for porosity (β) 0.5. Splitter plate (ls*) is 1. The gap between splitter plate midpoint and cylinder (lg**) is 1.5.

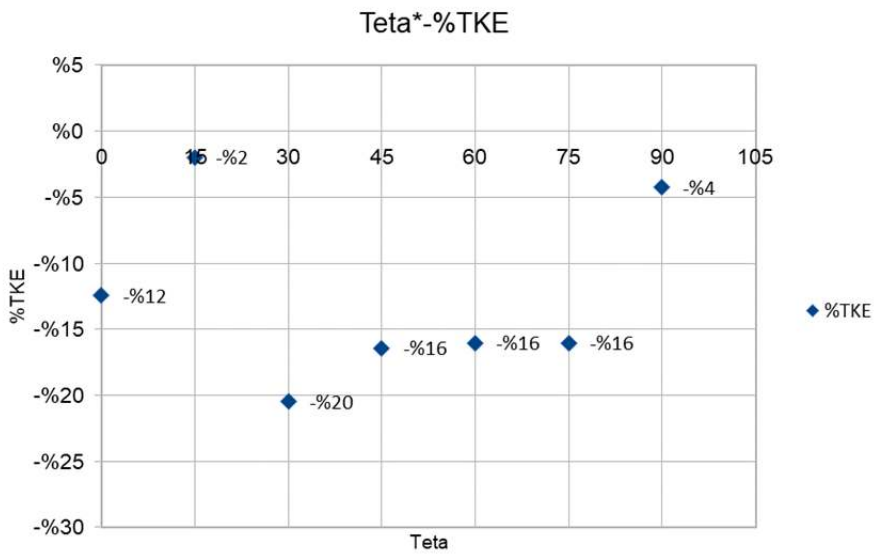

Figure 4.59. TKE variation due to different rotation angle values of 0,15,30,45,60,75 and 90 degrees for porosity (β) 0.7. Splitter plate length (ls*) is 1. The gap between splitter plate midpoint and cylinder (lg**) is 1.5.

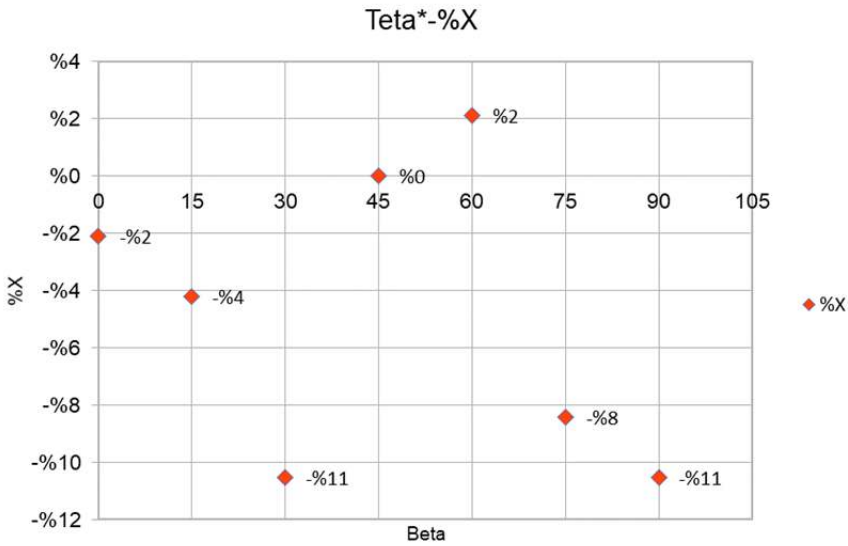

Figure 4.60. Position of max. TKE due to different rotation angle values of 0,15,30,45,60,75 and 90 degrees for porosity (β) 0.7. Splitter plate (ls*) is 1. The gap between splitter plate midpoint and cylinder (lg**) is 1.5.

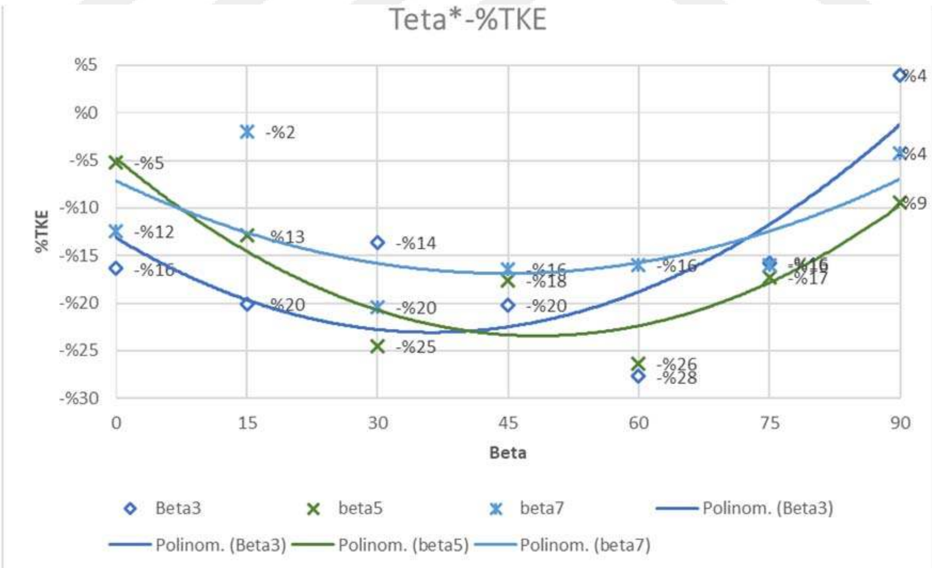

Figure 4.61. TKE variation due to different rotation angle values of 0,15,30,45,60,75 and 90 degrees for porosity values (β) of 0.3, 0.5, 0.7 . Splitter plate (ls*) is 1. Gap between splitter plate midpoint and cylinder (lg**) is 1.5.

It is obviously seen that as the splitter plate angle (θ) changes, turbulent kinetic energy is reduced. For θ=30 degrees, TKE reducing is maximized. The effect of the splitter plate angle is obviously seen in these investigations, but the effect of the porosity is not observed.

Flow control is achieved for β=0.30 and $\theta=90^0$. The peak magnitude of TKE is reduced up to 28%, although the location of the peak magnitude of TKE is decreased by 4%.

The effect of the splitter plate angle is obviously seen in these investigations, but the effect of the porosity is not observed.

5. CONCLUSIONS AND RECOMMENDATIONS

To define the effect of splitter plates with different porosities to flow structure in the wake region of a bare cylinder were investigated. For this purpose, peak value of turbulent kinetic energy and formation point of peak value of turbulent kinetic energy were compared due to bare cylinder case. 251 different cases are inspected by PIV system. Most valuable ones are evaluated in three different cases due to TKE formation: 1) Flow control of a circular cylinder by permeable splitter plate with different porosities and gap values. 2) Flow control of a circular cylinder by permeable splitter plate with different porosities and length values. 3) Flow control of a circular cylinder by permeable splitter plate with different porosities and angle values. The findings of these examinations are compiled under the following headings: a)Effect of gap b) Effect of Splitter Plate Length c) Effect of Splitter Plate Porosity d) Effect of Splitter Plate Angle

5.1. Effect of Gap

It is obviously seen that as the gap between splitter plate and the cylinder increase, turbulent kinetic energy reduced and as the gap between splitter plate and the cylinder increases, Formation point of the peak value of turbulent kinetic energy in the flow direction reduced. Flow control is achieved for the gap lg*=2 and β=0.7. The peak magnitude of TKE is reduced up to 35%, although the location of the peak magnitude of TKE is decreased compared to the bare cylinder for the gap lg*=2 and β=0.7.

It is obviously seen that as the splitter plate porosity (β) changes, turbulent kinetic energy is reduced. But a linear correlation is not observed.

5.2. Effect of Splitter Plate Length

Three different the splitter plate length values (ls*=1, 2 and 3) were investigated and the splitter plate angle and the gap between splitter plate and cylinder were kept to constant during the experiments as lg*=1. As splitter plate length increase, turbulent kinetic energy reduced in all situation. Also, the formation point of the peak value of turbulent kinetic energy in the flow direction increased nearly in all situations except ls*=1, β=0.50, lg*=1 and ls*=1, β=0.70, lg*=1 situations. Flow control is achieved for the gap ls*=3 and β=0.3. The peak magnitude of TKE is reduced up to 42%, although the location of the peak magnitude of TKE is increased by 25%.

It is obviously seen that as the splitter plate porosity (β) changes, turbulent kinetic energy is reduced. But a linear correlation is not observed.

5.3. Effect of Splitter Plate Porosity

The porosities of the splitter plate were taken as β=0.3, 0.5 and 0.7. Four different gaps where between the cylinder and the splitter plate (lg*=0.5, 1, 1.5 and 2) were investigated and the splitter plate angle and length were kept to constant during the experiments as ls*=1. The effect of the porosity is not observed in these investigations.

To define the porosity effect, TKE variation due to porosity values 0.3/0.5/0.7, with constant values of ls and lg, is investigated. The effect of splitter plate length is obviously seen in these investigations, but the effect of the porosity is not observed. The effect of the porosity is not observed in these investigations.

Seven different the splitter plate angle values (θ =0; 15; 30; 45; 60; 75; 90) and three different porosity values (β=0.30; 0.50; 0.70) were investigated and the splitter plate length (ls*) and the gap between splitter plate midpoint and cylinder (lg^{**}) were kept to constant during the experiments as ls*=1 and lg^{**}=1.5.

It is obviously seen that as the splitter plate porosity (β) changes, turbulent kinetic energy is reduced. But a linear correlation is not observed.

5.4. Effect of Splitter Plate Angle

Seven different the splitter plate angle values (θ =0; 15; 30; 45; 60; 75; 90) and three different porosity values (β=0.30; 0.50; 0.70) were investigated and the splitter plate length (ls*) and the gap between splitter plate midpoint and cylinder (lg^{**}) were kept to constant during the experiments as ls*=1 and lg^{**}=1.5. It is observed that vortex formation delayed with increasing the splitter plate angle. As splitter plate angle increase, turbulent kinetic energy reduced in most situation. Also, the formation point of peak value of turbulent kinetic energy in the flow direction reduced nearly in all situations except θ =90, β=0.30 and θ =60, β=0.70 situations.

It is obviously seen that as the splitter plate angle (θ) changes, turbulent kinetic energy is reduced. For θ=30 degrees, TKE reducing is maximized. The effect of the splitter plate angle is obviously seen in these investigations, but the effect of the porosity is not observed.

Flow control is achieved for β=0.30 and $\theta=90^0$. The peak magnitude of TKE is reduced up to 28%, although the location of the peak magnitude of TKE is decreased by 4%.

It is obviously seen that as the splitter plate porosity (β) changes, turbulent kinetic energy is reduced. But a linear correlation is not observed.

5.5. Recommendations

The aim of present work is investigating the flow characteristic of vertical cylinder with different splitter plate applications. Effects of gap between cylinder and splitter plate and splitter plate length are obvious. Also, porosity influences TKE formation, but more studies must be conducted on defining the minimum hole diameter for porosity calculations to prevent skin effects on the splitter plate. Thirdly, active vortex suppression techniques such as vibrating of splitter plate and flow suction and blowing due to splitter plate angle can be undertaken for further improvement on vortex shedding.

Splitter plate angle has an obvious effect on TKE formation. TKE-Teta curve has a bowl type curve which has the bottom at 45 degrees. This finding was determined for the first time in this study. More studies must be conducted

REFERENCES

Akilli, H., Sahin, B., & Filiz Tumen, N. (2005). Suppression of vortex shedding of circular cylinder in shallow water by a splitter plate. *Flow Measurement and Instrumentation*, *16*, 211–219. https://doi.org/10.1016/j.flowmeasinst.2005.04.004

Bao, Y., & Tao, J. (2013). The passive control of wake flow behind a circular cylinder by parallel dual plates. *Journal of Fluids and Structures*, *37*(FEBRUARY), 201–219. https://doi.org/10.1016/j.jfluidstructs.2012.11.002

Blevins, R. D. (1985). The effect of sound on vortex shedding from cylinders. *J. of Fluid Mech.*, (161), 217–237.

Cardell, G. S. (1993). *Flow Past a Circular Cylinder with a Permeable Wake Splitter Plate*. *Phd Thesis*. California Institute of Technology.

Chakrabarty, S. G., Yadav, A. H., & Wagh, K. N. (2013). Experimental Analysis of Heat Transfer and Pressure Drop Behaviour of a Circular Cylinder with Passive Flow Control Technique. *International Journal of Application or Innovation in Engineering & Management (IJAIEM)*, *2013*(Ratmig).

CHEN, D.; JIRKA, H. (1997). Absolute and convective instabilities of plane turbulent wakes in a shallow water layer. *Journal of Fluid Mechanics*, (338), 157–172.

Chen, W. L., Xin, D. B., Xu, F., Li, H., Ou, J. P., & Hu, H. (2013). Suppression of vortex-induced vibration of a circular cylinder using suction-based flow control. *Journal of Fluids and Structures*, *42*, 25–39. https://doi.org/10.1016/j.jfluidstructs.2013.05.009

E. Guilmineau, P. Q. (2002). A numerical simulation of vortex shedding from an oscillating circular cylinder. *J. Fluid Struct.*, (16), 773–794.

Favier, J., Dauptain, A., Basso, D., & Bottaro, A. (2009). Passive separation control using a self-adaptive hairy coating. *Journal of Fluid Mechanics*, *627*, 451–483. https://doi.org/10.1017/S0022112009006119

Fujisawa, N. (2001). Feedback control of vortex shedding from a circular cylinder by rotational oscillations. *J. Fluid Struct.*, (15), 23–37.

Gao, Y., Wang, M., Zong, Z., Zou, L., & Peng, G. (2017). *Effect of Splitter Plate Length on Hydrodynamic Performance Around Cylinder at High Reynolds Numbers*. *Shanghai Jiaotong Daxue Xuebao/Journal of Shanghai Jiaotong University* (Vol. 51). https://doi.org/10.16183/j.cnki.jsjtu.2017.04.019

Ghadimi, P., Kermani, S., Razughi, S., & Zamanian, R. (2013). Aerodynamic and Acoustical Analysis of Flow around a Circular Cylinder in a Channel and Parametric Study on the Effects of a Splitter Plate on the Generated Vibration and Noise, *1*(1), 1–5. https://doi.org/10.12691/amp-1-1-1

Gozmen, B., Akilli, H., & Sahin, B. (2013). Passive control of circular cylinder wake in shallow flow. *Measurement: Journal of the International Measurement Confederation*. https://doi.org/10.1016/j.measurement.2012.11.008

Gozmen, B., Fırat, E., Akilli, H., & Sahin, B. (2013). Flow control behind a circular cylinder via a porous cylinder in deep water. *EPJ Web of Conferences*, *1035*(45). https://doi.org/10.1051/epjconf/20134501035

Istiarto, I. (2001). *Flow Around a Cylinder in a Scoured Channel Bed*. ÉCOLE POLYTECHNIQUE FÉDÉRALE DE LAUSANNE POUR.

Kwon, K., & Choi, H. (1996). Control of laminar vortex shedding behind a circular cylinder using splitter plates. *Physics of Fluids*, *8*(2), 479–486. https://doi.org/10.1063/1.868801

Lecordier, J. C., L. Hamma, P. P. (1991). The control vortex shedding behind heated cylinders at low Reynolds numbers. *Exp. in Fluids*, (10), 224–229.

Lee, J., & You, D. (2013). Study of vortex-shedding-induced vibration of a flexible splitter plate behind a cylinder. *Physics of Fluids*, *25*(11). https://doi.org/10.1063/1.4819346

Lienhard, J. H. (1966). Synopsis of lift, drag, and vortex frequency data for rigid circular cylinders. *Bulletin 300*.

Oruc, V., Akar, M. A., Akilli, H., & Sahin, B. (2013). Suppression of asymmetric flow behavior downstream of two side-by-side circular cylinders with a splitter plate in shallow water. *Measurement: Journal of the International Measurement Confederation*, *46*(1), 442–455. https://doi.org/10.1016/j.measurement.2012.07.020

Ozdil, N. F. (2013). *Investigation of Flow Characteristics Around In-Line Horizontal Cylinders In Shallow Waters*. *Phd Thesis*.

Roshko, A. (1954a). *On the development of turbulent wakes from vortex streets*.

Roshko, A. (1954b). On the drag and shedding frequency of two-dimensional bluff bodies. *NACA Technical Note 3169*, (July 1954), 1–30. https://doi.org/10.1.1.477.979

S. Reza-zadeh. (2013). Investigation of fluid flow around a cylinder with EHD actuation on inclined plates behind the cylinder, 212–217.

Soumya, S., & Prakash, K. A. (2017). Effect of splitter plate on fluid flow characteristics past a triangular cylinder. *IOP Conf. Series: Journal of Physics: Conf. Series*, *822*. https://doi.org/10.1088/1742-6596/822/1/012054

T. Weier, G. Gerbeth, G. Mutschke, E. Platacis, O. L. (1998). Experiments on cylinder wake stabilization in an electrolyte solution by means of electromagnetic forced localized on the cylinder surface. *Exp. Therm Fluid Sci.*, (16), 84–91.

Tabatabaeian S., M. Mirzaei, A. Sadighzadeh, V. Damideh, Shadaram, A. (2015). Experimental Study of the Flow Field around a Circular Cylinder Using Plasma Actuators. *J. Applied Fluid Mechanics*, *8*(2), 291–299.

Teksin, S., & Yayla, S. (2016). Effects of Flexible Splitter Plate in the Wake of a Cylindrical Body. *Journal of Applied Fluid Mechanics*, *9*(6), 3053–3059.

Tritton, D. J. (1987). *Physical fluid dynamics*. Oxford: Oxford University Press.

Xiao, Q., Sun, K., Liu, H., & Hu, J. (2011). Computational study on near wake interaction between undulation body and a D-section cylinder. *Ocean Engineering*, *38*(4), 673–683. https://doi.org/10.1016/j.oceaneng.2010.12.017

CURRICULUM VITAE

Serdar ŞAHİN was born in Mersin, 1977. In 1995, he enrolled at İstanbul Technical University to study mechanical engineering. In 1999, he graduated with a Bachelor of Science degree in mechanical engineering from the Department of Mechanical Engineering. He began his MSc studies at the Department of Mechanical Engineering of İstanbul Technical University. He completed Master of Science degree in this department in 2002. Between 1999-2019 he worked for industry.